A STUDY OF THE BASE FLOW OF AN IDEAL DISSOCIATING GAS

A THESIS

Presented to

The Faculty of the Graduate Division

by

Robert Kirkland Sigman

In Partial Fulfillment

of the Requirements for the Degree

Doctor of Philosophy

in the School of Aerospace Engineering

Georgia Institute of Technology

October, 1969

In presenting the dissertation as a partial fulfillment of the requirements for an advanced degree from the Georgia Institute of Technology, I agree that the Library of the Institute shall make it available for inspection and circulation in accordance with its regulations governing materials of this type. I agree that permission to copy from, or to publish from, this dissertation may be granted by the professor under whose direction it was written, or, in his absence, by the Dean of the Graduate Division when such copying or publication is solely for scholarly purposes and does not involve potential financial gain. It is understood that any copying from, or publication of, this dissertation which involves potential financial gain will not be allowed without written permission.

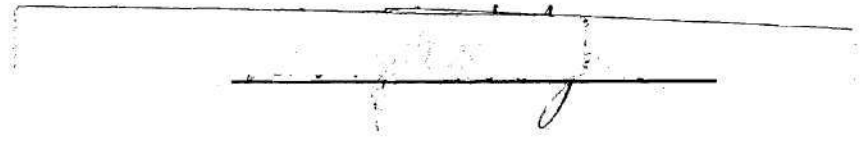

7/25/68

A STUDY OF THE BASE FLOW OF AN IDEAL DISSOCIATING GAS

Approved:

Chairman

Date approved by Chairman: Oct. 1, 1969

ACKNOWLEDGMENTS

I would like to express my deepest appreciation to Dr. James C. Wu for his suggestion of this problem and for his guidance throughout the course of this investigation. To Dr. Wu and the members of my committee, Dr. Arnold L. Ducoffe and Professor James E. Hubbartt, I owe special thanks for their many hours of discussion during the preparation of this thesis. I would also like to thank Dr. Robin B. Gray who provided the encouragement to pursue my graduate academic career.

The advice of my fellow graduate students is also gratefully acknowledged. The numerous discussions with Dr. T. Taz Bramlette and Dr. Danny L. Hartley concerning the theoretical aspects of this thesis were invaluable. To Dr. Jerry A. Sills and Dr. Kenton D. Whitehead for their suggestions concerning the numerical methods and assistance in programming, many thanks are given. I would like to thank Mr. Terry Wright and Mr. Charles E. Hammond for their advice in the correction of the manuscript. I also express my gratitude to Mrs. Marolyn M. Varney for patience and skill in typing the body of this thesis and to Mr. A. Michael Varney for his supervision of the typing.

The financial assistance of the National Aeronautics and Space Administration, the National Science Foundation, and the Georgia Institute of Technology are gratefully acknowledged.

Finally, I wish to thank my mother for her inspiration and assistance throughout my life. Her years of unselfish sacrifice are greatly appreciated.

TABLE OF CONTENTS

LIST OF TABLES

LIST OF ILLUSTRATIONS

Figure Page

LIST OF SYMBOLS

a	speed of sound
A	constant in coordinate transformation defined in equation (140)
A^*	$\sqrt{M_f^2 - 1}$
$A_1(i,j)$, $A_2(i,j)$	coefficients in the momentum difference equations
A_{ij}	coefficient in the compatibility relations
B^2	$\left(M_{e\infty}^2-1\right) / \left(M_{f\infty}^2-1\right)$
B^*	$\rho^* U^{*2}$
B_{ij}	coefficient in the compatibility relations
C	nondimensional product of density and viscosity
C_f	constant in Freeman's form of the rate equation
C_p	generalized specific heat at constant pressure
$C_1(i,j)$, $C_2(i,j)$	coefficients in the species conservation difference equations
d_m	column vector representing the right-hand side of equation (164)
D^*	dimensionless coefficient defined in equation (29)
D_{12}	coefficient of diffusion
D_{ij}	coefficient in the compatibility relations
$E_{c\infty}$	Eckert number, $U_\infty^2 / R_m T_\infty$

E_∞	Eckert number, $U_\infty^2/C_{p_\infty} T_\infty$
$E_1(i,j)$, $E_2(i,j)$	coefficients in the energy difference equation
F_1, F_2	integrals of the velocity defined in Appendix B
F_{ij}	term defined in equation (32)
g_1	dimensionless form of F_1 and F_2
g_2	dimensionless form of F_1 and F_2
g_{ij}	dummy dependent variables
h	enthalpy
k	coefficient of conductivity, defined in equation (117)
K_1, K_2	integration constants
ℓ	reference length
Le	the Lewis number, Pr/Sc
L{ }	Laplace transform operator
m	mass flow rate
M	Mach number
$\hat{M}$	molecular weight
n	exponential dependence of the rate constant on temperature
N	there are 2N + 1 vertical grid points at each station in the shear layer
O, O_2	oxygen atoms and molecules, respectively
p	static pressure
Pr	the Prandtl number, $\mu C_p/k$

q	Laplace variable
R	nondimensional specific heat at constant pressure
Rey	the Reynolds number, $\rho U\ell/\mu$
R_m	gas constant based on the molecular weight
s	distance along a streamline
Sc	the Schmidt number, $\mu/\rho D_{12}$
T	static temperature
u	x-component of velocity
U	total velocity
v	y-component of velocity
V	velocity parameter defined in equation (124)
x	distance along axis fixed at the corner and aligned with the freestream
x_s	distance along the dividing streamline
y	distance normal to x
y_s	distance normal to x_s
Y^*	transformed normal coordinate defined by equation (119)
z	similarity parameter, $\psi^*/\sqrt{s^*}$
z_k	similarity parameter, $\eta_c/\sqrt{Sc}$
z_{ij}	dummy dependent variable
Z_{mn}	array consisting of the coefficients in the species conservation equation
α	degree of dissociation, ρ_A/ρ
α_m	column vector representing the unknown values of α at station i + 1
β	dummy variable

β_f	frozen shock wave angle
γ	ratio of specific heats, C_p/C_v
Γ	dimensionless parameter defined in equation (68)
$\Delta\eta$, $\Delta\xi$	incremental distances between characteristics
Δs^*	incremental distance along a streamline
$\Delta\zeta$	increment in the normal direction
ε	temperature characteristic of intermolecular attraction
ζ	transformed normal coordinate defined by equation (140)
η	distance along a left running characteristic curve
η_{bl}	Blasius' similarity variable, $Y^*/\sqrt{s^*}$
η_c	Chapman's similarity variable, $\eta_{bl}/\sqrt{C}$
θ	flow deflection angle
θ_d	characteristic temperature for dissociation
κ	coefficient of thermal conductivity
μ	coefficient of viscosity
μ_f	frozen Mach angle
ξ	distance along a right running characteristic
ρ	density
ρ_d	characteristic density for dissociation
σ	zero energy collision diameter
τ	relaxation time
ψ	stream function
ω	rate of production of atoms
$\Omega^{(1,1)^*}$	reduced collision integral for diffusion

$\Omega^{(2,2)*}$	reduced collision integral for viscosity and thermal conductivity

Superscripts

*	refers to non-dimensionalized variable
'	denotes a small disturbance quantity
-	indicates a mean variable
~	denotes a distance nondimensionalized by the freestream velocity and relaxation time

Subscripts

A	refers to atomic species
b	indicates values on the constant-pressure boundary
B	refers to the base or recirculation region
dsl	denotes values on the dividing streamline
e	indicates equilibrium values
f	indicates frozen values
i	step index in the streamwise direction
m,n	dummy subscripts used in the derivation of the characteristic equations
j	step index in the normal direction
M	indicates molecular species
r	indicates special coefficients of the energy equation for equilibrium flow
s	refers to the stagnation region
ssl	denotes values on the stagnating streamline
st	indicates stagnation conditions
∞	denotes freestream conditions
1	indicates values computed by frozen Prandtl Meyer theory
2	denotes values in the inviscid flow immediately preceding the frozen shock

3	denotes values immediately behind the frozen shock

Special Symbol

$\equiv$	is defined as

SUMMARY

An analytical investigation of the effects of finite rate dissociation and recombination reactions on the base pressure for supersonic, two-dimensional, laminar flow is presented. The Chapman-Korst flow model and the ideal dissociating gas model are used. The problem considered has negligible initial boundary layer thickness. The reattachment region of the flow is assumed to be chemically frozen and isentropic. The recompression of the inviscid flow is assumed to be governed by the frozen oblique shock relations. The resulting model requires detailed investigation of two regions -- the inviscid, nonequilibrium expansion into a constant-pressure region and the laminar free shear layer with finite rate reactions.

The exterior inviscid expansion into a constant-pressure region is treated by the method of characteristics. All flow properties along the constant-pressure boundary are found to vary monotonically, in contrast to the overexpansion observed in the nonequilibrium expansion around a convex corner. The compression waves generated by the chemical reactions in the expansion fan reflect from the constant-pressure boundary as expansion waves, thus eliminating the possibility of a recombination shock wave. As a matter of general interest, a linearized theory for the inviscid expansion is also presented.

The laminar, constant-pressure mixing region is investigated by means of an implicit finite difference method. The nonequilibrium boundary layer equations are first transformed to the incompressible

form by means of a Howarth type of transformation and then to a finite coordinate range, in the normal direction, by means of a hyperbolic tangent transformation.

The results indicate that finite reaction rates do not significantly influence the velocity. The temperature and degree of dissociation profiles for finite rate flow are found to be bounded by the solutions for frozen and equilibrium flow.

Chapman's analysis of the laminar free shear layer is extended to the case of frozen flow with unity Lewis number. The finite difference solutions for frozen flow with constant Prandtl number, Schmidt number, and density viscosity product agree well with the results of the extended Chapman theory. However, these results do not compare well with the finite difference solutions with variable properties.

The two regions are coupled and several base pressure problems are investigated. The closed base solutions are obtained by interpolation of the base bleed. The results are summarized in the following statements.

1. Finite rate reactions in the inviscid exterior flow tend to cause an increase in the base pressure. This agrees with the prediction of Resler that the base pressure on a body in equilibrium flow is greater than the base pressure on a body in frozen flow.

2. If the recirculation region is hot (on the order of the freestream stagnation temperature), chemical recombination increases the dividing streamline temperature, thus decreasing the dividing streamline kinetic energy. This tends to increase the resulting base pressure.

3. If the recirculation region is cool, the dividing streamline temperature is decreased due to dissociation and the kinetic energy is increased. The base pressure for this condition tends to decrease as the flow varies from frozen to equilibrium flow.

CHAPTER I

INTRODUCTION

Background and Review of Recent Literature

The development of rockets and re-entry vehicles has produced a number of new aerothermodynamic problems and revived interest in many unsolved problems. A criterion of re-entry vehicle design, that the vehicle be able to survive the intense heating while decelerating through the atmosphere, leads to the use of a blunt body whose form drag is much greater than its friction drag. In problems where the heat transfer is not of primary concern, such as artillery shells and supersonic wings with finite trailing edges; the reduction of drag is often important. All of these problems share two important similarities: they involve supersonic velocities, and they have a region of separated flow over the base.

Much interest has centered lately on the real gas effects associated with the base flow. The trail of ionized gas created by a re-entry body gives a characteristic radar return which can be used to identify the body. The analysis of the high heat transfer rates encountered in clustered rocket engines requires a knowledge of the high temperature flow in the base region.

Nash[1] and Lykoudis[2] have presented reviews of the investigations into base flow and other associated separated flow phenomena. Lykoudis presents more than 180 references which were available in January of 1965. Of the 19 base flow references cited in this thesis,

8 have been completed since 1965, giving some idea of the effort directed toward this problem.

Chapman[3] pointed out the indeterminate character of an entirely inviscid solution to the supersonic base flow problem and concluded that the effect of viscosity must be considered to obtain a unique solution. He introduced a physical model of the near wake, and gave a qualitative description of the effect of viscosity on the base flow.

Shortly thereafter, two methods of analysis for the base flow, the Crocco-Lees method and the Chapman-Korst method, were introduced. The former method is based on the Crocco-Lees[4] theory for the interaction between dissipative and nearly isentropic streams. By considering an overall picture of the base flow, the Crocco-Lees theory attempts to describe the balance which must exist between the external inviscid flow and the internal dissipative flow governed by the transport of momentum between the two flows. The dissipative mixing is described by semi-empirical integral quantities which are adjusted to account for laminar or turbulent dissipation.

The Chapman-Korst method is based on the independent works of Chapman, et al.[5] and Korst, et al.[6] which advanced a simplified model of the supersonic base flow for laminar and turbulent flows, respectively. The base or recirculation region and the exterior inviscid flow are assumed to be separated by a thin viscous shear layer. The Chapman-Korst approach allows the flow to be subdivided into its constituent parts. These parts are then analyzed to discover their role in determining the base pressure. A unique solution to the problem is obtained by a suitable matching of these regions.

The supersonic, laminar flow over the upper half of a two-dimensional base is illustrated in Figure 1. The flow is symmetric about the centerline and thus only half of the flow need be considered.

The flow over the forebody is regarded as steady, uniform, and supersonic, except near the body where a thin boundary layer is formed. At the corner, the flow expands and separates into a region of constant pressure. Since there is a subsonic region in the attached boundary layer, it is possible for the base region to exert an influence on the flow upstream of the corner. Theoretical investigations by Weiss and Nelson[7] and experimental results of Hama[8] indicate that the expansion process is influenced for several boundary layer thicknesses upstream. This influence causes a larger initial turning angle of the inner boundary of the separated flow compared to the values computed neglecting the upstream influence. At hypersonic Mach numbers, this overexpansion results in the formation of a separation shock wave. Investigations by Weiss and Weinbaum[9] have shown, however, that for initially small supersonic Mach numbers, the departure from Prandtl-Meyer theory is not severe.

Except for cases involving large amounts of bleed into or from the base, the recirculation region is a region of relatively low velocity flow. Therefore, most investigators have assumed it to be a semi-infinite region of stagnant fluid and thus also a region of constant pressure. Attempts have been made by Viviand and Berger[10], Weiss[11], and others to account for the conservation of angular momentum in this region with an approximate solution to the Navier-Stokes equations. This consideration results in the correct dependence

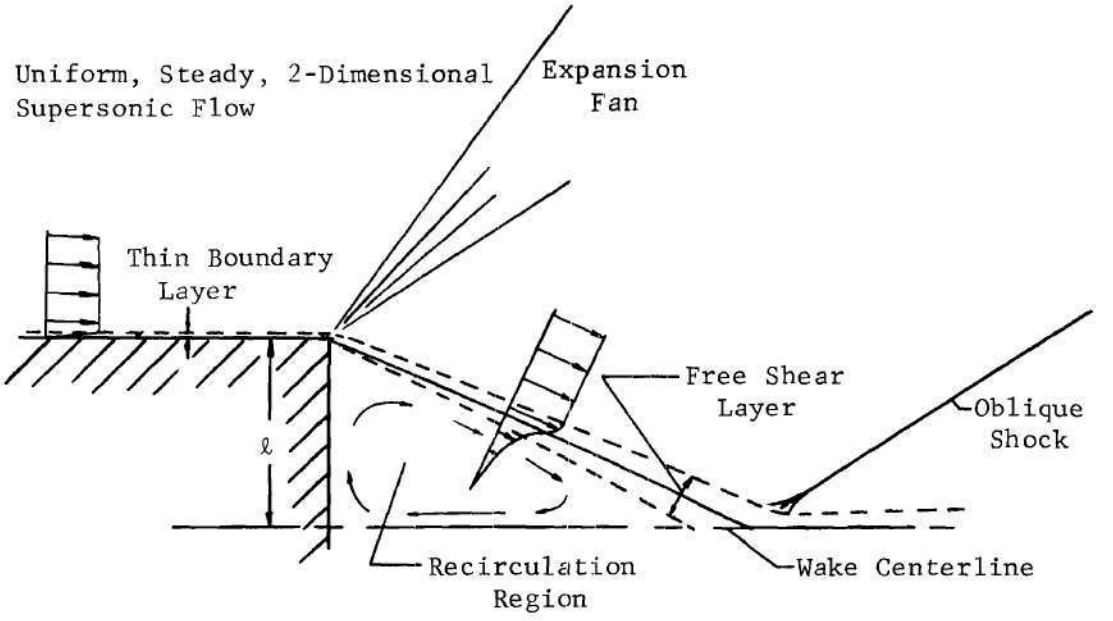

a. Closed Base

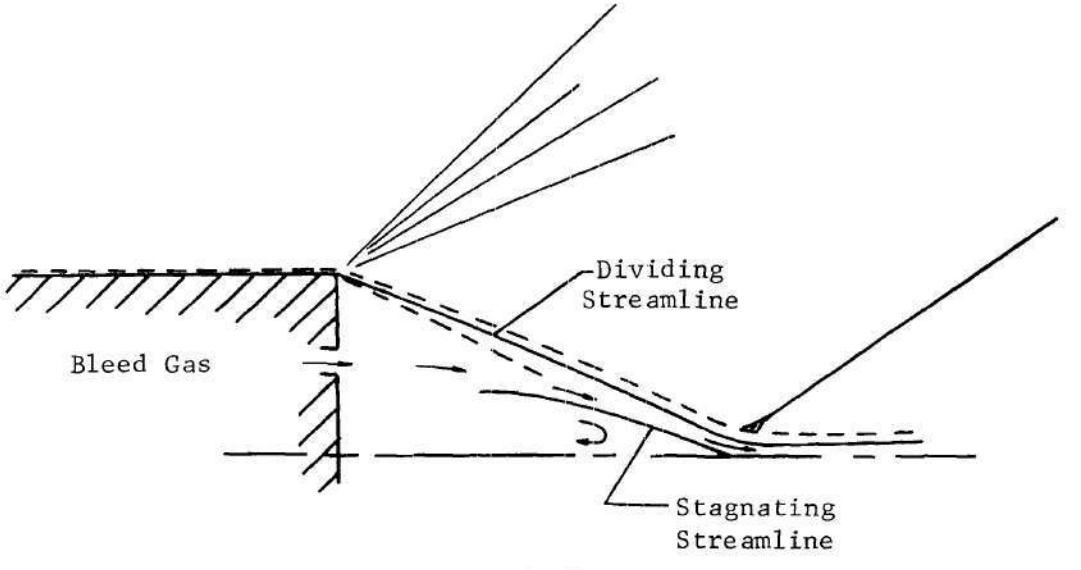

b. Base Bleed

Figure 1. Physical Model of the Base Flow

on the Reynolds number at lower Reynolds numbers. Weiss[11] has concluded that for Reynolds numbers (based on the forebody length) larger than 10^4, the flow takes on a shear layer character and for Reynolds numbers greater than 10^6, an essentially inviscid core is formed and there is no longer a Reynolds number dependence.

For high Reynolds numbers, the expanded exterior inviscid flow is separated from the recirculating region by a thin viscous shear layer. A dividing streamline, which defines the inner boundary of the fluid originating upstream, emerges from the corner. The shear layer mixing occurs at a constant pressure, the value of which is determined by the adjacent inviscid stream. This fact has been substantiated by the experiments of Chapman, et al.[5] and Charwat and Yakura[12] for moderate supersonic Mach numbers and Reynolds numbers of 10^5 and larger.

The free shear layer has received much attention, since it occurs in other separated flow phenomena such as flow over cavities. Chapman[13] has obtained a similar solution for the asymptotic limit as the ratio of the initial boundary layer thickness to the shear layer length approaches zero. By assuming the product of density and viscosity coefficient to be constant, the momentum and energy equations are uncoupled, resulting in a constant velocity along the dividing streamline. Chapman also reports a solution for variable $\rho\mu$ resulting in a dependency of the dividing streamline velocity on the Mach number.

Denison and Baum[14], Sills[15], and Lew[16] have employed finite difference methods to investigate the development of a free shear layer with an initial Blasius flat plate profile. Denison and Baum use the

Crocco coordinate system and the assumptions of unity Prandtl number and constant $\rho\mu$, while Sills has employed a finite range transformation, and the assumptions of constant $\rho\mu$ and constant but arbitrary Prandtl number. Although the solutions in references [14] and [15] approach Chapman's solution as the ratio of the flat plate length to the shear layer length approaches zero, the authors conclude that, for most practical applications, the length of the near wake is much too short for the Chapman profile to be appropriate.

As the exterior inviscid flow approaches the wake centerline, it is turned back parallel to the centerline. Chapman[5] assumes that the recompression is accomplished by a gradual turning so that the shock wave does not form near the neck, and the exterior recompression can be treated as isentropic. Korst[6], however, considers the turning to be abrupt and thus governed by the oblique shock wave relations.

Both Chapman and Korst assume that the recompression of the shear layer occurs isentropically. The stagnating streamline (See Figure 1b.) is defined as the streamline which separates the recirculating flow from the flow which passes downstream. The fluid above the stagnating streamline has sufficient kinetic energy to negotiate the pressure rise, while that below the stagnating streamline is reversed and contained in the recirculating region. Since for steady flow the mass in the recirculating region is conserved, the mass flow between the dividing streamline and the stagnating streamline must be the rate of mass bleed into the base. A unique base pressure solution corresponds to the solution which satisfies both of the above requirements, i.e., the conservation of mass in the recirculating region and

the conservation of mechanical energy on the stagnating streamline.

Both experimental evidence and physical reasoning indicate that the reattachment actually occurs in a region of continuous positive pressure gradient. Because of the viscous interaction, the pressure at reattachment is less than the maximum. Nash[17], in his investigation of turbulent reattachment, has concluded that the neglect of the initial boundary layer combined with the reattachment pressure assumption lead to cancelling errors.

Lykoudis[2] has pointed out that the effects of finite rate chemistry are relevant since at higher attitudes where the flow is laminar, the flow will not, in general, be in equilibrium. Consideration of high temperature gasdynamic effects has been confined primarily to ionized far wake studies. Lew[16] has proposed research into dissociating base flows, but as yet none has been reported.

Purpose of the Research

This thesis is concerned with the effects of finite rate dissociation-recombination reactions on the base pressure. The flow is analyzed by using relatively simple models -- the ideal dissociating gas model and the Chapman-Korst flow model.

The exterior inviscid flow is investigated by the method of characteristics for reacting flows. A linearized theory is developed and compared with the method of characteristics.

Non-similar solutions for the laminar shear layer are obtained by a finite difference method. The effects of variable properties and finite reaction rates on the velocity, species concentration, and temperature profiles are investigated. A comparison is made between

frozen, finite rate, and equilibrium profiles.

Finally, the base pressure is computed and compared with the results of Chapman's solution.

CHAPTER II

FLOW MODEL AND ANALYTICAL APPROACH

As previously noted, one advantage of the Chapman-Korst model is that it divides the flow field into regions which are analyzed independently. It is now possible to analyze these regions to determine which regions are influenced by finite rate chemistry, in particular, dissociation-recombination reactions.

Flow conditions will be chosen to illustrate the effects of finite reaction rates. Experiments of Chapman, et al.[5] indicate that the stability of shear layers increases with an increase in Mach number, and at a Mach number of 4, they can remain laminar for Reynolds numbers of the order 10^6. For this investigation, the flow will be restricted to relatively high Reynolds numbers ($10^4 < \text{Rey} < 10^6$), moderate supersonic Mach numbers ($2 < M_\infty < 4$), and shear layers, which are assumed to be laminar.

The initial boundary layer thickness is assumed to be vanishingly thin and upstream influence is neglected.

The expansion of the uniform, two-dimensional, supersonic flow of a perfect gas into a constant-pressure region is a simple problem. There is no characteristic length in the problem and the flow consists of two uniform parallel flows joined by a Prandtl-Meyer fan. The problem is, in fact, identical to the problem of the flow over a convex corner. For flows with finite rate reactions, however, a relaxation length enters through the fluid properties and the problem is extremely

complex. The flow downstream of the corner is not uniform, and the boundary of the flow is curved.

The boundary conditions for the shear layer must now include the temperature and degree of dissociation gradients of the inviscid flow. Although the mixing is at a constant pressure, flow similarity is not preserved since a relaxation length is involved.

The recirculating region is assumed to be stagnant. The gas in this region is in equilibrium.

A frozen shock recompression of the exterior inviscid flow is assumed. Correspondingly, the length of the reattachment region is small and the recompression of the stagnating streamline is also assumed to be frozen.

The solution to the base pressure problem can no longer be expressed in closed form. With a given base pressure, the exterior inviscid flow is computed. This solution gives the boundary conditions for the shear layer as well as the recompression shock strength immediately adjacent to the shear layer. The shear layer is then computed until the reattachment point is reached. The stagnation pressure profile for the shear layer is calculated, and the stagnating streamline is identified as the streamline with a stagnation pressure equal to the static pressure in the inviscid flow behind the shock. A base bleed rate is obtained by calculating the mass flow rate between the dividing streamline and the stagnating streamline. By performing a number of computations using different base pressure values, a solution for the case of zero bleed is obtained by interpolation.

Based on the postulated flow model, the solutions for the inviscid

expansion and the shear layer development must be obtained and then coupled to obtain the base pressure. The solutions of these two problems are discussed in the following two chapters. It is noted that in addition to being intermediate steps in the solution to the base pressure problem, these two problems have additional applications so that the methods presented are of further interest.

CHAPTER III

INVISCID EXPANSION OF A DISSOCIATING GAS INTO A CONSTANT-PRESSURE REGION

In this chapter the problem of the supersonic expansion of an inviscid dissociating gas into a region of constant pressure is considered. A numerical solution of this problem is obtained by the method of characteristics. A linearized solution is obtained which is valid for weak expansions. The features of the flow field are discussed and a comparison is made between the two theories.

Formulation of the Problem

The conservation equations for the steady, two-dimensional, continuum flow of an inviscid, adiabatic, dissociating gas are [18] the continuity equation,

$$\frac{\partial(\rho u)}{\partial x} + \frac{\partial(\rho v)}{\partial y} = 0 \ , \tag{1}$$

the momentum equations,

$$\rho u \frac{\partial u}{\partial x} + \rho v \frac{\partial u}{\partial y} + \frac{\partial p}{\partial x} = 0 \tag{2}$$

$$\rho u \frac{\partial v}{\partial x} + \rho v \frac{\partial v}{\partial y} + \frac{\partial p}{\partial y} = 0 \ , \tag{3}$$

the energy equation,

$$\rho u \frac{\partial}{\partial x}\left(h + \frac{1}{2} U^2\right) + \rho v \frac{\partial}{\partial y}\left(h + \frac{1}{2} U^2\right) = 0 \ , \tag{4}$$

the species conservation equation,

$$u \frac{\partial \alpha}{\partial x} + v \frac{\partial \alpha}{\partial y} = \omega \ , \tag{5}$$

an equation of state,

$$h = h(p, \rho, \alpha) \ , \tag{6}$$

and an equilibrium relation,

$$\alpha_e = \alpha_e(p, \rho) \ . \tag{7}$$

For the present problem, an orthogonal x-y coordinate system is fixed at the corner. The initially uniform freestream is considered to be in chemical equilibrium, with the velocity in the x-direction.

Method of Characteristics

For supersonic flow, the set of non-linear equations, (1) through (7), can be solved numerically, using an extension of the well-known method of characteristics of perfect fluid dynamics.

Derivation of the Characteristic Equations for a Dissociating Gas

A convenient definition [18] of the characteristic directions is that they are the special directions along which a system of partial differential equations reduces to a system of ordinary differential equations. Along a streamline, defined by

$$\frac{dy}{dx} = \tan \theta \ , \tag{8}$$

where θ is the angle of inclination of the streamline, three ordinary differential equations can be written. The three equations valid along a streamline are the streamline momentum equation,

$$\rho U dU + dp = 0 \ , \tag{9}$$

the species conservation equation,

$$U d\alpha - \omega ds = 0 \ , \tag{10}$$

and the energy equation,

$$U dU + dh = 0 \ , \tag{11}$$

where ds is a differential element of length along a streamline.

Along the left running characteristic curve, the compatability relation,

$$\sqrt{M_f^2 - 1}\, dp + \rho U^2 d\theta - \frac{\left(\frac{\partial h}{\partial \alpha}\right)_{p,\rho}}{\left(\frac{\partial h}{\partial \rho}\right)_{p,\alpha}} a_f \omega d\eta = 0 \ , \tag{12}$$

where $d\eta$ is a differential element of length along the characteristic, is valid. The left running characteristic direction is defined by

$$\frac{dy}{dx} = \tan(\theta + \mu_f) \ , \tag{13}$$

where

$$\mu_f = \text{Arctan}\left(\frac{1}{\sqrt{M_f^2 - 1}}\right) \ , \tag{14}$$

and M_f is the frozen Mach number based on the frozen sound speed, a_f, defined in Appendix A, equation (A-11). Written in terms of the thermodynamic variables, the frozen sound speed for an ideal dissociating gas is

$$a_f^2 = \frac{(4+\alpha)(1+\alpha)R_m T}{3} \quad . \tag{15}$$

The compatability relation,

$$\sqrt{M_f^2 - 1}\, dp - \rho U^2 d\theta - \frac{\left(\frac{\partial h}{\partial \alpha}\right)_{p,\rho}}{\left(\frac{\partial h}{\partial \rho}\right)_{p,\alpha}} a_f \omega d\xi = 0 \quad , \tag{16}$$

is valid along the right running characteristic curve with incremental distance $d\xi$, and direction defined by

$$\frac{dy}{dx} = \tan(\theta - \mu_f) \quad . \tag{17}$$

The importance of the frozen Mach number in defining two of the characteristic directions was discussed by Wood and Kirkwood[19] and Chu[20]. Since the frozen Mach number is always smaller than the equilibrium Mach number, $M_f > 1$ is a sufficient condition for supersonic flow. This thesis will consider only flows for which $M_f > 1$.

The last term in equations (12) and (16) is indicative of the vorticity created by the chemical reactions. As in the case of a perfect gas with rotation, it is not possible to integrate equations (12) and (16) once and for all. Instead, a step-by-step numerical method must be used.

For an ideal dissociating gas (see Appendix A), the caloric equation of state is

$$h = R_m[(4 + \alpha)T + \alpha\theta_d] \tag{18}$$

and the thermal equation of state is

$$p = \rho(1 + \alpha)R_m T \quad . \tag{19}$$

The derivatives $\left(\frac{\partial h}{\partial \alpha}\right)_{p,\rho}$ and $\left(\frac{\partial h}{\partial \rho}\right)_{p,\alpha}$ required in equations (12) and (16) are thus

$$\left(\frac{\partial h}{\partial \alpha}\right)_{p,\rho} = R_m\left[\theta_d - \frac{3T}{(1+\alpha)}\right] \tag{20}$$

and

$$\left(\frac{\partial h}{\partial \rho}\right)_{p,\alpha} = -R_m(4 + \alpha)\frac{T}{\rho} \quad . \tag{21}$$

The governing equations will be written in dimensionless form by introducing non-dimensional variables based on freestream conditions:

$$\left.\begin{aligned} U^* = \frac{U}{U_\infty} \quad , \qquad \rho^* = \frac{\rho}{\rho_\infty} \quad , \qquad \text{and} \qquad p^* = \frac{p}{\rho_\infty U_\infty^2} \quad ; \\ T^* = \frac{T}{T_\infty} \qquad \text{and} \qquad \theta_d^* = \frac{\theta_d}{T_\infty} \quad ; \\ \text{and} \qquad \xi^* = \frac{\xi}{\ell} \quad , \qquad \eta^* = \frac{\eta}{\ell} \quad , \qquad \text{and} \qquad s^* = \frac{s}{\ell} \quad . \end{aligned}\right\} \tag{22}$$

Since there is no geometric length associated with the problem, a reference length has meaning only in relation to a relaxation length.

It will be shown that ℓ can be expressed in terms of the coefficient of the rate equation.

In dimensionless form, the streamline momentum equation is

$$\rho^* U^* dU^* + dp^* = 0 \ , \tag{23}$$

the species conservation equation is

$$U^* d\alpha - \omega^* ds^* = 0 \ , \tag{24}$$

and the energy equation is

$$U^* dU^* + \frac{1}{E_{c\infty}} \left[(4 + \alpha) dT^* + (\theta_d^* + T^*) d\alpha \right] = 0 \ , \tag{25}$$

where

$$\left.\begin{aligned} E_{c\infty} &= \frac{U_\infty^2}{R_m T_\infty} \\ \text{and} \qquad & \\ \omega^* &= \frac{\omega \ell}{U_\infty} \ . \end{aligned}\right\} \tag{26}$$

Similarly, the compatability relations (12) and (16), are written in dimensionless form as follows:

$$A^* dp^* + B^* d\theta - D^* d\eta^* = 0 \tag{27}$$

$$A^* dp^* - B^* d\theta - D^* d\xi^* = 0 \tag{28}$$

where

$$A^* = \sqrt{M_f^2 - 1} \ ,$$

$$B^* = \rho^* U^{*2} \ ,$$

and

$$D^* = \frac{-\rho^* \omega^*}{(4+\alpha)(1+\alpha) M_{f_\infty}} \left(\frac{a_f}{a_{f_\infty}}\right) \{(1+\alpha)\theta_d^* - 3T^*\} . \qquad (29)$$

Computational Procedure

The set of differential equations (23), (24), (25), (27), and (28) is solved by a numerical approach in the form of a finite difference scheme. In the finite difference approximation of the differential equations, average quantities are used for the terms in the coefficients. For example, equation (23) is written

$$\bar{\rho}^*_{mn} \bar{U}^*_{mn} (U^*_n - U^*_m) + (p^*_n - p^*_m) = 0 \ ,$$

where the subscripts m and n denote two neighboring points on a streamline, with the properties at the point m known and properties at n to be determined. The barred quantities are the linearly averaged values

$$\bar{g}_{mn} = \frac{g_m + g_n}{2} \ ,$$

where g is any flow quantity. For example,

$$\bar{\rho}^*_{mn} = \frac{\rho^*_m + \rho^*_n}{2} \ .$$

The set of finite difference equations is solved using an

iterative method. For the first iteration, the values of g_n are taken to be equal to g_m. For subsequent iterations, the values of g_n obtained from the preceding iteration are used. The iteration continues until the coefficients change less than one tenth of one per cent between iterations.

Referring to Figure 2, the flow properties at points 1, 2, and 3 are known, and the flow quantities at point 4 (intersection point of the ξ and η characteristics through points 3 and 2, respectively) are to be determined.

From the geometry of Figure 2, the coordinates of point 4 are approximated by

$$\left.\begin{aligned} x_4^* &= x_2^* + \Delta\xi^* \cos(\bar{\theta}_{24} - \bar{\mu}_{f24}) = x_3^* + \Delta\eta^* \cos(\bar{\theta}_{34} + \bar{\mu}_{f34}) \\ y_4^* &= y_2^* + \Delta\xi^* \sin(\bar{\theta}_{24} - \bar{\mu}_{f24}) = y_3^* + \Delta\eta^* \sin(\bar{\theta}_{34} + \bar{\mu}_{f34}) \end{aligned}\right\} . \quad (30)$$

This set of equations is solved for the incremental distances along the characteristics, $\Delta\xi^*$ and $\Delta\eta^*$, yielding:

$$\left.\begin{aligned} \Delta\xi^* &= \frac{(y_3^*-y_2^*)\cos(\bar{\theta}_{34}+\bar{\mu}_{f34}) - (x_3^*-x_2^*)\sin(\bar{\theta}_{34}+\bar{\mu}_{f34})}{\cos(\bar{\theta}_{34}+\bar{\mu}_{f34})\sin(\bar{\theta}_{24}-\bar{\mu}_{f24}) - \cos(\bar{\theta}_{24}-\bar{\mu}_{f24})\sin(\bar{\theta}_{34}+\bar{\mu}_{f34})} \\ \Delta\eta^* &= \frac{(y_3^*-y_2^*)\cos(\bar{\theta}_{24}-\bar{\mu}_{f24}) - (x_3^*-x_2^*)\sin(\bar{\theta}_{24}-\bar{\mu}_{f24})}{\cos(\bar{\theta}_{34}+\bar{\mu}_{f34})\sin(\bar{\theta}_{24}-\bar{\mu}_{f24}) - \cos(\bar{\theta}_{24}-\bar{\mu}_{f24})\sin(\bar{\theta}_{34}+\bar{\mu}_{f34})} \end{aligned}\right\} \quad (31)$$

Using these values of $\Delta\xi^*$ and $\Delta\eta^*$, the coordinates of point 4 are determined by equations (30).

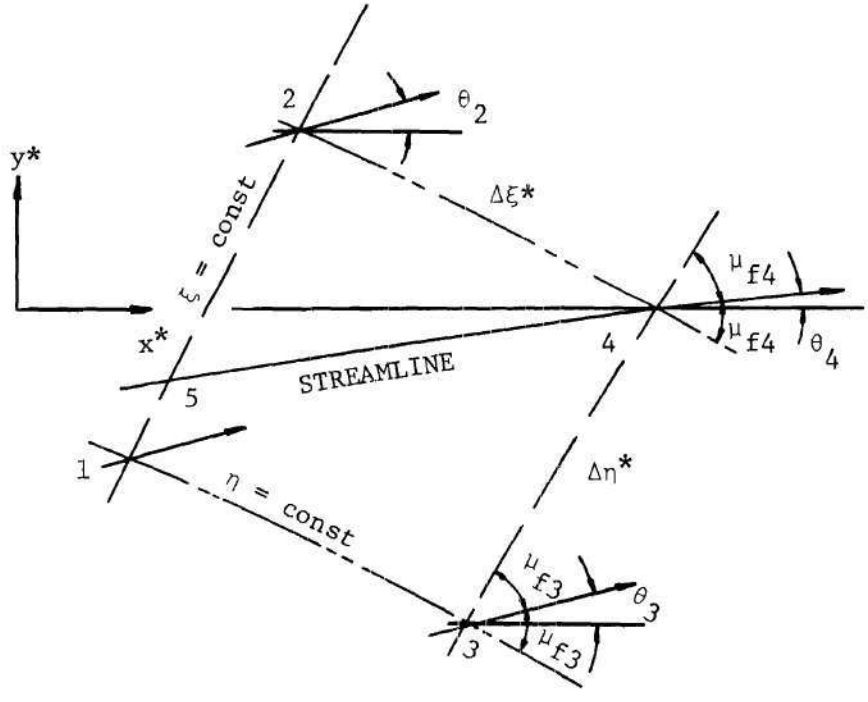

Figure 2. Finite Difference Grid for the Method of Characteristics

Written in finite difference form, the compatability relations (27) and (28) become

$$\left.\begin{aligned} \bar{A}^*_{24}p^*_4 - \bar{B}^*_{24}\theta_4 &= \bar{D}^*_{24}\Delta\xi^* + \bar{A}_{24}p^*_2 - \bar{B}_{24}\theta_2 \equiv \bar{F}^*_{24} \\ \bar{A}^*_{34}p^*_4 + \bar{B}^*_{34}\theta_4 &= \bar{D}^*_{34}\Delta\eta^* + \bar{A}_{34}p^*_3 + \bar{B}_{34}\theta_3 \equiv \bar{F}^*_{34} \end{aligned}\right\} \tag{32}$$

where $\bar{F}^*_{24}$ and $\bar{F}^*_{34}$ are known to the first approximation.

The pressure and flow deflection are obtained by solving equations (32), yielding:

$$p^*_4 = \frac{\bar{F}^*_{24}\bar{B}^*_{34} + \bar{F}^*_{34}\bar{B}^*_{24}}{\bar{A}^*_{24}\bar{B}^*_{34} + \bar{A}^*_{34}\bar{B}^*_{24}} \tag{33}$$

and

$$\theta_4 = \frac{\bar{F}^*_{34}\bar{A}^*_{24} - \bar{F}^*_{24}\bar{A}^*_{34}}{\bar{A}^*_{24}\bar{B}^*_{34} + \bar{A}^*_{34}\bar{B}^*_{24}} \ . \tag{34}$$

With θ_4 known, the coordinates of point 5 are determined from the intersection of the streamline 4-5 with the line 2-1 (or 1-3). Properties at 5 are obtained by linear interpolation based on the known values at points 1 and 2 (or 1 and 3). The incremental streamline length is found from

$$\Delta s^* = \left[(x^*_5 - x^*_4)^2 + (y^*_5 - y^*_4)^2 \right]^{\frac{1}{2}} .$$

With p^*_4 known, the velocity at point 4 is obtained by writing the

streamline momentum equation (23) in finite difference form and solving for U_4^* explicitly:

$$U_4^* = U_5^* - \frac{1}{\bar{\rho}_{45}^* \bar{U}_{45}^*} \left(p_4^* - p_5^* \right) . \tag{35}$$

The temperature is obtained from the energy equation (25),

$$T_4^* = T_5^* + \frac{1}{(4+\bar{\alpha}_{45})} \left[\frac{E_{c\infty}}{\bar{\rho}_{45}^*} \left(p_4^* - p_5^* \right) - \left(\theta_d^* + \bar{T}_{45}^* \right) \left(\alpha_4 - \alpha_5 \right) \right] , \tag{36}$$

where α_4 is the result of the previous iteration.

Equation (24) is solved for α_4 as follows:

$$\alpha_4 = \alpha_5 + \frac{\bar{\omega}_{45}^*}{\bar{U}_{45}^*} \Delta s^* , \tag{37}$$

where the averaged temperature used in the calculation of $\bar{\omega}_{45}^*$ is based on the present iterate of T_4^*. In this thesis, Freeman's form of the rate equation (discussed in Appendix A) is used. In non-dimensional form, this is

$$\omega^* = \left(\frac{\ell C_f \rho_\infty T_\infty^n}{U_\infty} \right) T^{*n} \rho^* \left[\left(1 - \alpha \right) e^{-\frac{\theta_d^*}{T^*}} - \frac{\rho^*}{\rho_d^*} \alpha^2 \right] . \tag{38}$$

Thus a convenient reference length can be written:

$$\ell = \frac{U_\infty}{C_f \rho_\infty T_\infty^n} . \tag{39}$$

Initial and Boundary Conditions

The initial conditions are specified on the frozen wave head (Figure 3), which is inclined to the freestream at the Mach angle based on the freestream frozen Mach number. The properties along this line are specified as the freestream properties.

The boundary conditions at the corner are used to construct the expansion fan. The flow at the corner is frozen since $\Delta s^* = 0$, and flow properties are obtained from the Prandtl-Meyer and isentropic relations with the degree of dissociation frozen at the freestream value.

For a frozen Mach number, M_f, the flow deflection is given by the Prandtl-Meyer relation:

$$\theta_f - \theta_\infty = \sqrt{\frac{\gamma+1}{\gamma-1}} \left[\tan^{-1}\left(\sqrt{\frac{\gamma-1}{\gamma+1}} \sqrt{M_f^2 - 1} \right) - \tan^{-1}\left(\sqrt{\frac{\gamma-1}{\gamma+1}} \sqrt{M_{f\infty}^2 - 1} \right) \right] \quad (40)$$

$$- \left[\tan^{-1}\left(\sqrt{M_f^2 - 1} \right) - \tan^{-1}\left(\sqrt{M_{f\infty}^2 - 1} \right) \right] .$$

The isentropic relations give the temperature,

$$T_f^* = \frac{1 + \frac{\gamma-1}{2} M_{f\infty}^2}{1 + \frac{\gamma-1}{2} M_f^2} , \quad (41)$$

the pressure,

$$\frac{p_f^*}{p_\infty^*} = T_f^{* \frac{\gamma}{\gamma-1}} , \quad (42)$$

and the density,

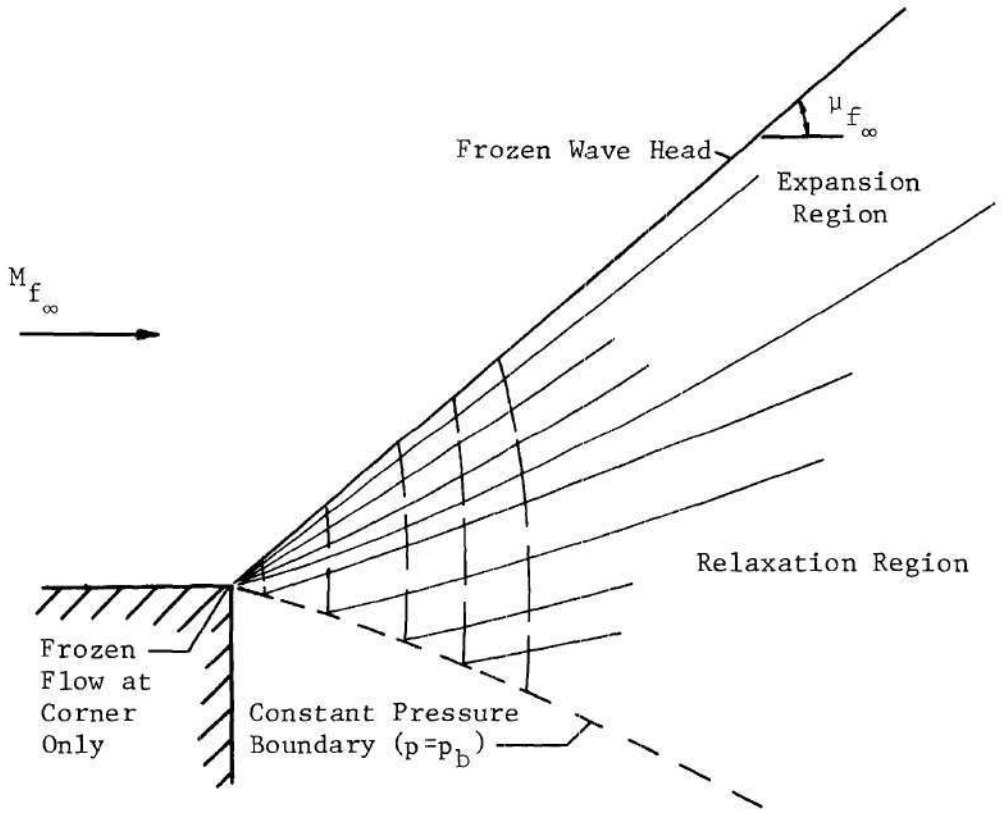

Figure 3. Flow Regions for the Supersonic Expansion into a Constant-Pressure Region

$$\rho_f^* = T_f^{*\frac{1}{\gamma-1}} , \tag{43}$$

where the expression for γ, derived in Appendix A, is

$$\gamma = \frac{4+\alpha_\infty}{3} .$$

The frozen Mach number immediately downstream of the corner is related to p_b^* by

$$M_{fb} = \left\{ \frac{2}{\gamma-1} \left[\left(\frac{p_b^*}{p_\infty^*} \right)^{\frac{1-\gamma}{\gamma}} \left(1 + \frac{\gamma-1}{2} M_{f\infty}^2 \right) - 1 \right] \right\}^{1/2} . \tag{44}$$

At the corner, the flow properties are multi-valued and are divided into segments based on a linear division of the Mach number between $M_{f\infty}$ and M_{fb}. The flow quantities for each segment are obtained from equations (40) through (43) based on the frozen Mach number at each division.

Downstream of the corner, the pressure is constant along the streamline which forms the boundary of the flow. The coordinates of a point on the boundary, x_4^* and y_4^*, are given by

$$\left.\begin{aligned} x_4^* &= x_5^* + \Delta s^* \cos\bar{\theta}_{45} = x_2^* + \Delta\xi^* \cos(\bar{\theta}_{24} - \bar{\mu}_{f24}) \\ y_4^* &= y_5^* + \Delta s^* \sin\bar{\theta}_{45} = y_2^* + \Delta\xi^* \sin(\bar{\theta}_{24} - \bar{\mu}_{f24}) \end{aligned}\right\} , \tag{45}$$

where the subscript 5 indicates the preceding point on the boundary streamline, and 2 is the adjacent point on the right running

characteristic passing through 4. Solving for the incremental distances yields

$$\left.\begin{aligned} \Delta s^* &= \frac{(y_5^*-y_2^*)\cos(\bar{\theta}_{24}-\bar{\mu}_{f24}) - (x_5^*-x_2^*)\sin(\bar{\theta}_{24}-\bar{\mu}_{f24})}{\sin\bar{\theta}_{45}\cos(\bar{\theta}_{24}-\bar{\mu}_{f24}) - \cos\bar{\theta}_{45}\sin(\bar{\theta}_{24}-\bar{\mu}_{f24})} \\ \Delta\xi^* &= \frac{(x_5^*-x_2^*)\sin\bar{\theta}_{45} - (y_5^*-y_2^*)\cos\bar{\theta}_{45}}{\sin\bar{\theta}_{45}\cos(\bar{\theta}_{24}-\bar{\mu}_{f24}) - \cos\bar{\theta}_{45}\sin(\bar{\theta}_{24}-\bar{\mu}_{f24})} \end{aligned}\right\} . \quad (46)$$

Using the known value of p_b^*, the flow deflection, θ_4, is computed from the first of equations (32),

$$\theta_4 = \frac{\bar{A}_{24}^* p_b^* - \bar{F}_{24}^*}{\bar{B}_{24}^*} . \quad (47)$$

Since the pressure is constant along the boundary streamline, by equation (35), the velocity is constant. The temperature is given by

$$T_4^* = T_5^* + \frac{(\theta_d^* + \bar{T}_{45}^*)}{(4+\bar{\alpha}_{45})}\left(\alpha_4 - \alpha_5\right) , \quad (48)$$

and the degree of dissociation is given by

$$\alpha_4 = \alpha_5 + \frac{\bar{\omega}_{45}^*}{U_5^*}\Delta s^* . \quad (49)$$

The set of equations (45) through (49) is iterated until the non-

linear coefficients change less than one tenth of one per cent between iterations.

This investigation is concerned primarily with the resulting flow properties along the constant-pressure boundary. As shown in Figure 3, the general difference scheme is used to advance the calculations of the right running waves from the initial frozen wave head through the expansion and relaxation region until it intersects the constant-pressure boundary.

Results and Discussion

A test case for frozen flow was run on the Burroughs B 5500 computer to check the computer program. The resulting flow field agreed with simple wave theory.

Since the expansion of a dissociating gas into a constant-pressure region has not been previously reported, there is no existing solution for comparison with the present results. Flow around a convex corner has been reported (see, for example [21] and [22]), however, and a comparison of the flow features between the two problems will be made.

The flow patterns for the two problems are shown in Figure 4. In the problem of flow around a convex corner, the pressure at the corner drops from p^*_∞ to p^*_{wf}. Downstream of the corner, the pressure along the wall rises and overshoots the final value, which it then approaches from above. The temperature and degree of dissociation along the wall show a monotonic increase and decrease respectively. Feldman[23] has suggested that the compression waves reflected from the solid wall may coalesce to form a recombination shock wave. Appleton's[21] investigations, using an ideal dissociating gas, showed

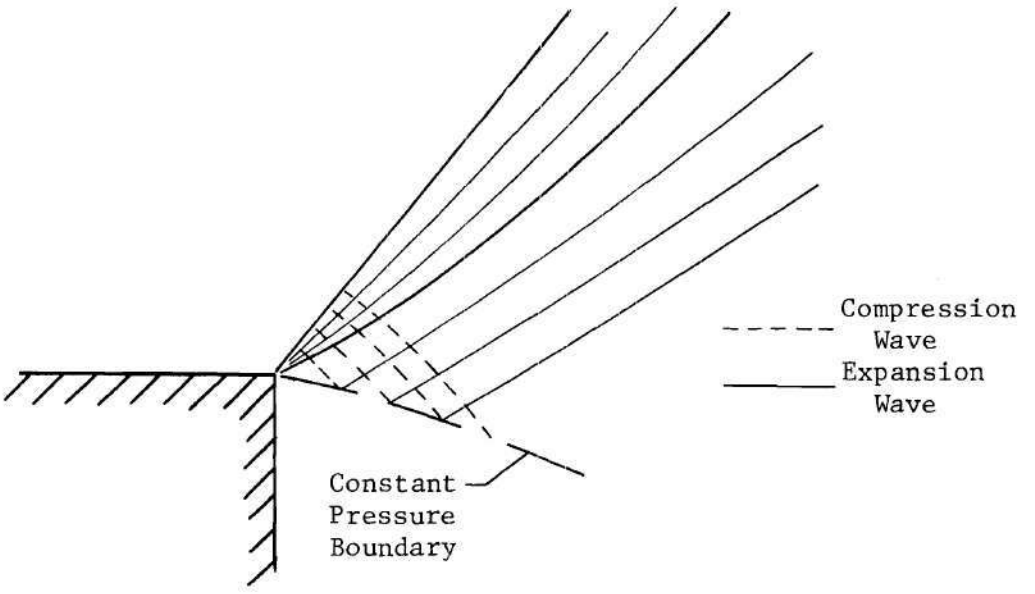

a. Nonequilibrium Expansion into a Constant-Pressure Region

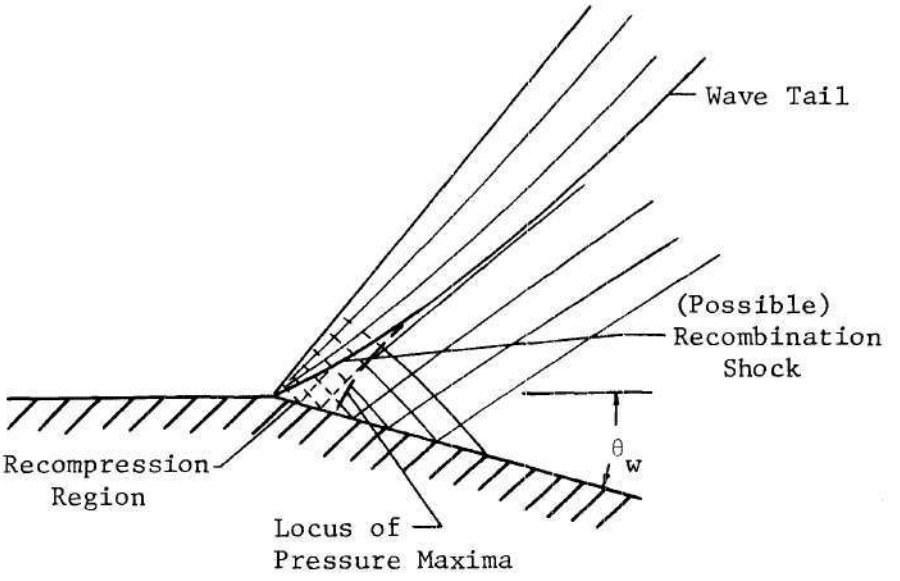

b. Nonequilibrium Expansion Around a Convex Corner

Figure 4. Illustration of the Nonequilibrium Expansion Problems

no trace of a recombination shock, but later works by Glass and Takano [22] revealed the presence of a weak shock. The gas model used by Glass and Takano assumes the vibrational modes to be in equilibrium at the local temperature, and they suggest that this assumption is probably responsible for the shock.

A solution was obtained for the expansion of oxygen from 4.746 to 1.414 atmospheres. The initial uniform freestream has a Mach number of 2.58, a temperature of 3720° K, and a corresponding degree of dissociation of 0.1816. The initial frozen flow deflection was 15.81 degrees. These initial conditions were used by Glass and Takano[22] for the expansion around a 15° corner.

The temperature and degree of dissociation along the constant-pressure boundary are shown in Figures 5 and 6, respectively. Following the frozen expansion, the temperature increases monotonically. The degree of dissociation decreases monotonically.

The flow deflection, shown in Figure 7, decreases monotonically. No overshoot of the flow deflection corresponding to the pressure overshoot of the fixed wall problem of references [21] and [22] was observed. For the constant-pressure boundary problem, the right running compression waves resulting from the chemical relaxation reflect from the constant-pressure boundary as left running expansion waves. No recombination shock appears.

The frozen Mach number along the constant-pressure boundary is shown in Figure 8. The velocity is constant along the boundary so that the Mach number is influenced by the degree of dissociation and the temperature. These effects are opposing (Figures 5 and 6, and equation

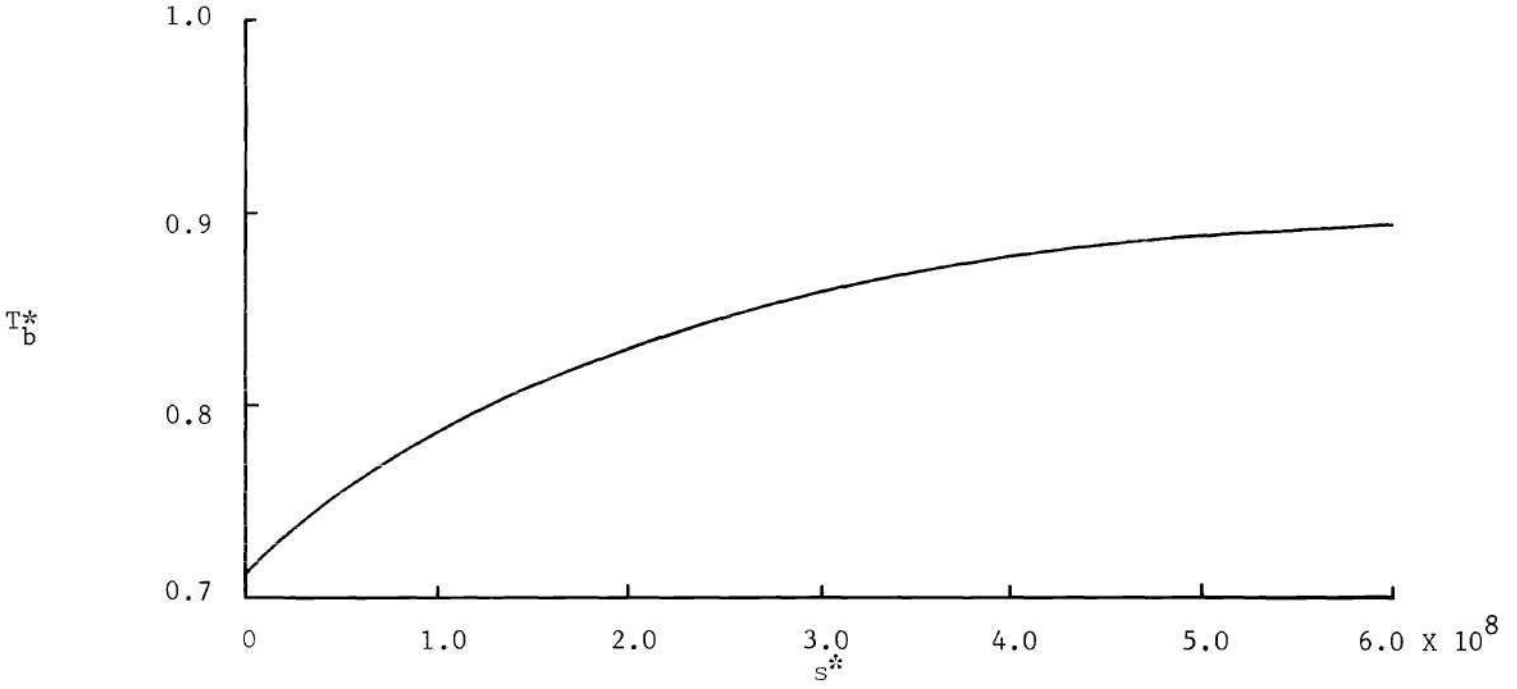

Figure 5. Non-Dimensional Temperature Along the Constant-Pressure Boundary

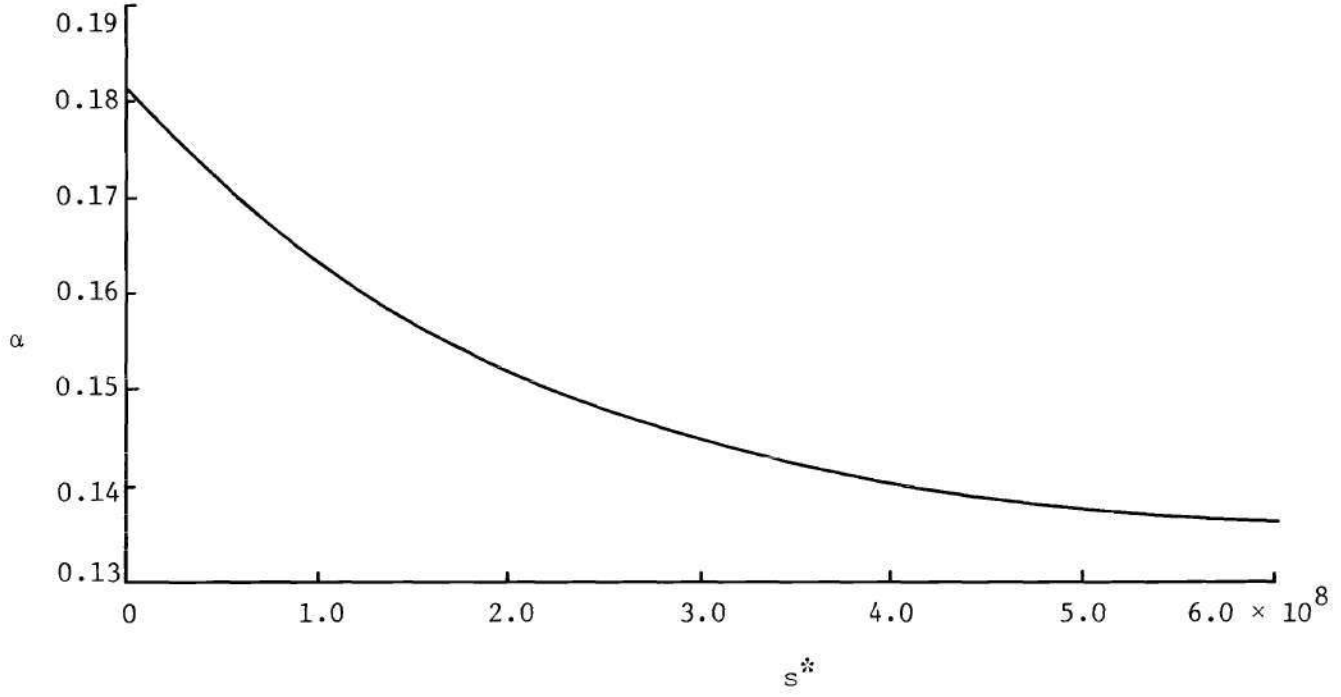

Figure 6. Degree of Dissociation Along the Constant-Pressure Boundary

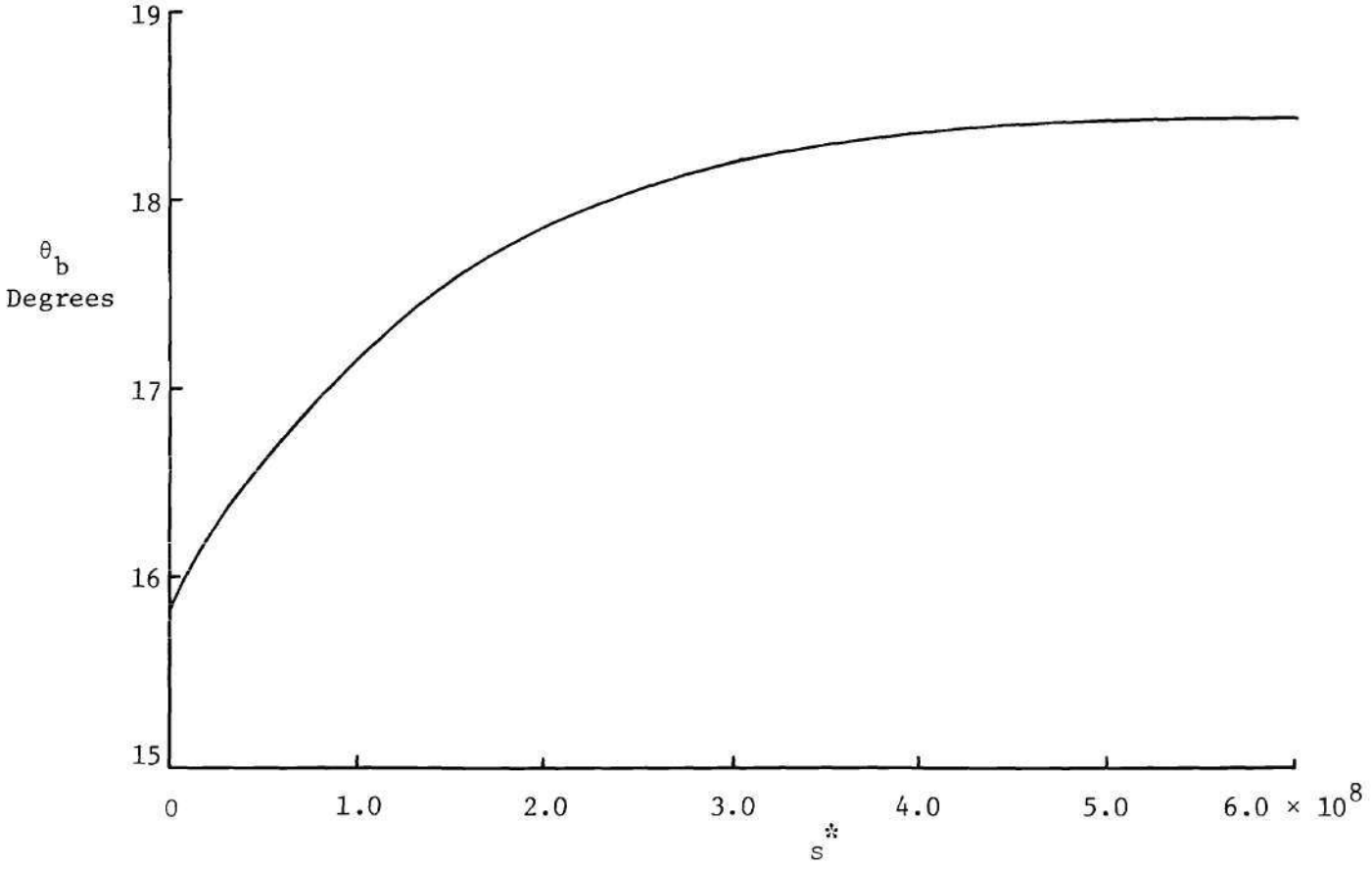

Figure 7. Flow Deflection Along the Constant-Pressure Boundary

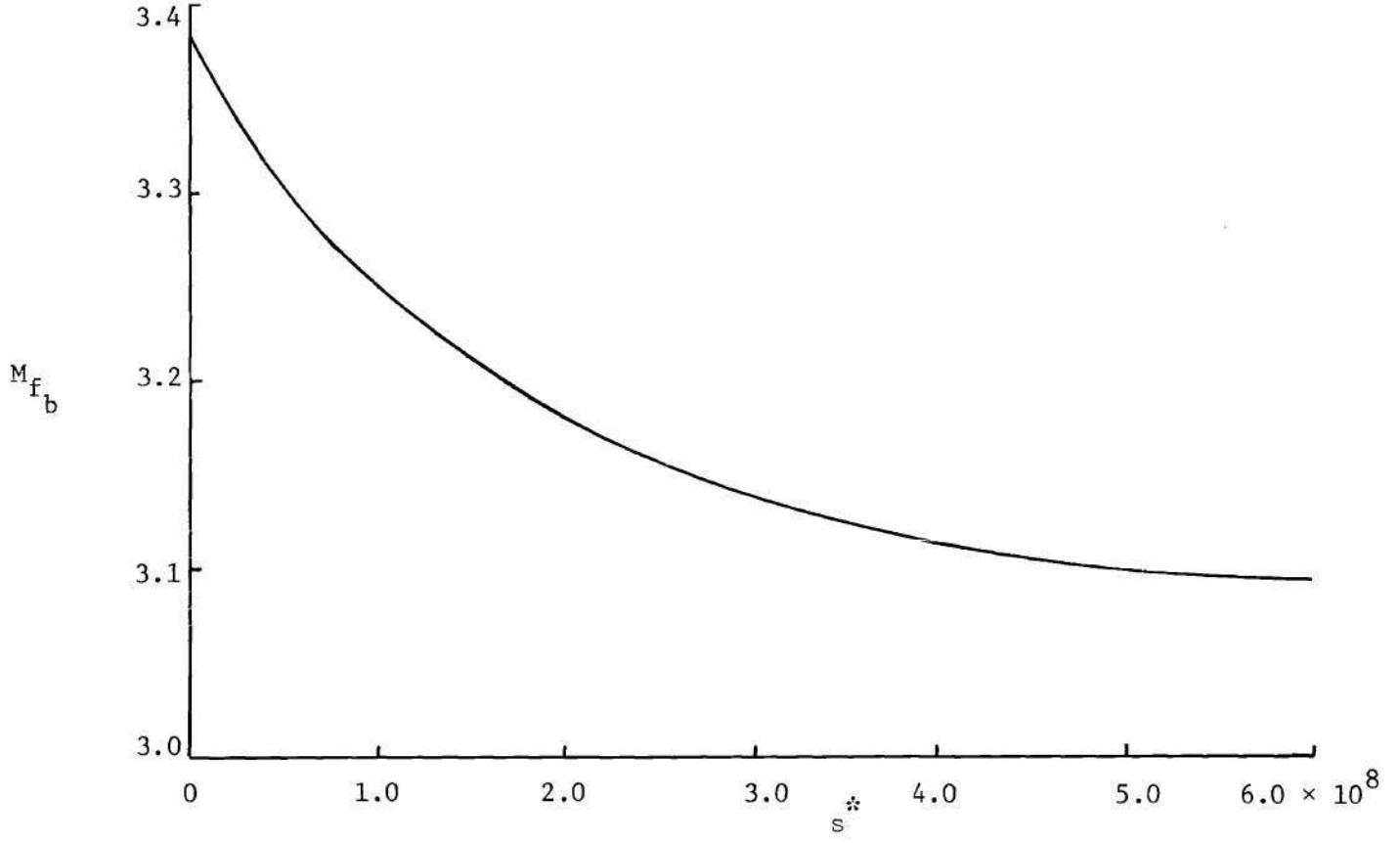

Figure 8. Frozen Mach Number Along the Constant-Pressure Boundary

(15)), but the temperature effect dominates and the frozen Mach number decreases from the initially frozen value.

Linearized Theory

Clarke[24] has derived the linearized equations for a dissociating gas. By employing a Laplace transform method, he has obtained an exact solution to the linearized equations for the expansion around a convex corner.

In this section, the linearized equations and boundary conditions for the two-dimensional, supersonic expansion of a dissociating gas into a constant-pressure region are derived. The problem is solved by a Laplace transform method.

Derivation of the Linearized Equations for a Dissociating Gas

The basic equations, sometimes called the acoustic equations, are derived here for reference in the solution. The method of derivation is similar to that of Vincenti and Kruger[18].

The equations of motion for the steady, two-dimensional flow of an inviscid, dissociating gas were presented in the previous section as equations (1) through (7). For the derivation of the acoustic equations, it is advantageous to write the energy equation (4) in the following form:

$$\rho u \frac{\partial h}{\partial x} + \rho v \frac{\partial h}{\partial y} - u \frac{\partial p}{\partial x} - v \frac{\partial p}{\partial y} = 0 \ . \tag{50}$$

The linearization procedure begins with the introduction of small disturbance quantities:

$$\left.\begin{aligned} p &= p_\infty(1 + p') & u &= U_\infty(1 + u') \\ T &= T_\infty(1 + T') & v &= U_\infty v' \\ \rho &= \rho_\infty(1 + \rho') & \alpha &= \alpha_\infty + \alpha' \\ h &= h_\infty(1 + h') & \alpha_e &= \alpha_\infty + \alpha_e' \end{aligned}\right\} , \qquad (51)$$

where the subscript ∞ indicates freestream conditions. The local equilibrium degree of dissociation, α_e, is the value that α would have if the flow were in equilibrium at the local values of p and ρ.

The primed quantities represent small disturbances from the undisturbed freestream. The quantities α' and α_e' are both much smaller than α_∞. All other primed quantities and their derivatives are assumed to be much less than unity, so that to a first approximation, the products of prime quantities can be neglected.

If the disturbances are small, it is possible to introduce the small disturbance form of the rate equation,

$$\omega \approx \frac{\alpha_e - \alpha}{\tau} , \qquad (52)$$

where τ is a characteristic time of dissociation defined by

$$\tau = -\frac{1}{\left(\frac{\partial \omega}{\partial \alpha}\right)_{p,\rho}} . \qquad (53)$$

Substituting equations (51) and (52) into equations (1), (2), (3), (50), (5), (6) and (7), and neglecting higher order terms, gives the linearized forms of the continuity equation,

$$\frac{\partial \rho'}{\partial \tilde{x}} + \frac{\partial u'}{\partial \tilde{x}} + \frac{\partial v'}{\partial \tilde{y}} = 0 \ , \tag{54}$$

the momentum equations,

$$\rho_\infty U_\infty^2 \frac{\partial u'}{\partial \tilde{x}} + p_\infty \frac{\partial p'}{\partial \tilde{x}} = 0 \tag{55}$$

$$\rho_\infty U_\infty^2 \frac{\partial v'}{\partial \tilde{x}} + p_\infty \frac{\partial p'}{\partial \tilde{y}} = 0 \ , \tag{56}$$

the energy equation,

$$\rho_\infty h_\infty \frac{\partial h'}{\partial \tilde{x}} - p_\infty \frac{\partial p'}{\partial \tilde{x}} = 0 \ , \tag{57}$$

the species conservation equation,

$$\frac{\partial \alpha'}{\partial \tilde{x}} = \alpha_e' - \alpha' \ , \tag{58}$$

the caloric equation of state,

$$h_\infty h' = p_\infty \left(\frac{\partial h}{\partial p}\right)_{\rho,\alpha} p' + \rho_\infty \left(\frac{\partial h}{\partial \rho}\right)_{p,\alpha} \rho' + \left(\frac{\partial h}{\partial \alpha}\right)_{p,\rho} \alpha' \ , \tag{59}$$

and the equilibrium relation,

$$\alpha_e' = p_\infty \left(\frac{\partial \alpha_e}{\partial p}\right)_\rho p' + \rho_\infty \left(\frac{\partial \alpha_e}{\partial \rho}\right)_p \rho' \ , \tag{60}$$

where

$$\tilde{x} = \frac{x}{U_\infty \tau} \qquad \tilde{y} = \frac{y}{U_\infty \tau} \ . \tag{61}$$

$\tilde{x}$ and $\tilde{y}$ represent the ratios of the flow length to the relaxation length. The limit of frozen flow is represented by $\tilde{x}$ or $\tilde{y}$ approaching zero, and equilibrium flow is represented by $\tilde{x}$ or $\tilde{y}$ approaching infinity.

The species conservation equation (58) is differentiated twice with respect to $\tilde{x}$, giving

$$\frac{\partial^3 \alpha'}{\partial \tilde{x}^3} = \frac{\partial^2 \alpha'_e}{\partial \tilde{x}^2} - \frac{\partial^2 \alpha'}{\partial \tilde{x}^2} \quad . \tag{62}$$

Solving equation (59) for α', differentiating the result with respect to $\tilde{x}$, and eliminating $\frac{\partial \rho'}{\partial \tilde{x}}$ and $\frac{\partial h'}{\partial \tilde{x}}$ by means of equations (54) and (57), gives

$$\frac{\partial \alpha'}{\partial \tilde{x}} = \left[\frac{\left(\frac{\partial h}{\partial p}\right)_{p,\alpha}}{\left(\frac{\partial h}{\partial \alpha}\right)_{p,\rho}}\right]_\infty \left[- p_\infty \left[\frac{\left(\frac{\partial h}{\partial p}\right)_{\rho,\alpha} - \frac{1}{\rho}}{\left(\frac{\partial h}{\partial \rho}\right)_{p,\alpha}} \right]_\infty \frac{\partial p'}{\partial \tilde{x}} + \rho_\infty \left[\frac{\partial u'}{\partial \tilde{x}} + \frac{\partial v'}{\partial \tilde{y}}\right] \right] . \tag{63}$$

Differentiating equation (60) with respect to $\tilde{x}$, substituting for $\frac{\partial \rho'}{\partial \tilde{x}}$ from equation (54) and combining with equation (63) gives

$$\frac{\partial (\alpha_e - \alpha)}{\partial \tilde{x}} = \left\{ \frac{\left[\left(\frac{\partial h}{\partial \rho}\right)_{p,\alpha} + \left(\frac{\partial h}{\partial \alpha}\right)_{p,\rho} \left(\frac{\partial \alpha_e}{\partial \rho}\right)_p\right]}{\left(\frac{\partial h}{\partial \alpha}\right)_{p,\rho}} \right\}_\infty \tag{64}$$

$$\left[p_\infty \left[\frac{\left(\frac{\partial \alpha_e}{\partial p}\right)_\rho \left(\frac{\partial h}{\partial \alpha}\right)_{p,\rho} + \left(\frac{\partial h}{\partial p}\right)_{\rho,\alpha} - \frac{1}{\rho}}{\left(\frac{\partial h}{\partial \rho}\right)_{p,\alpha} + \left(\frac{\partial h}{\partial \alpha}\right)_{p,\rho} \left(\frac{\partial \alpha_e}{\partial \rho}\right)_p} \right]_\infty \frac{\partial p'}{\partial \tilde{x}} \right.$$

$$\left. - \rho_\infty \left[\frac{\partial u'}{\partial \tilde{x}} + \frac{\partial v'}{\partial \tilde{y}}\right] \right] .$$

The frozen sound speed, a_f, given by

$$a_f^2 = -\frac{\left(\frac{\partial h}{\partial \rho}\right)_{p,\alpha}}{\left(\frac{\partial h}{\partial p}\right)_{\rho,\alpha} - \frac{1}{\rho}} , \tag{65}$$

and the equilibrium sound speed, a_e, given by

$$a_e^2 = -\frac{\left(\frac{\partial h}{\partial \rho}\right)_{p,\alpha} + \left(\frac{\partial h}{\partial \alpha}\right)_{p,\rho}\left(\frac{\partial \alpha_e}{\partial \rho}\right)_p}{\left(\frac{\partial h}{\partial p}\right)_{\rho,\alpha} + \left(\frac{\partial h}{\partial \alpha}\right)_{p,\rho}\left(\frac{\partial \alpha_e}{\partial p}\right)_\rho - \frac{1}{\rho}} \tag{66}$$

are substituted into equations (63) and (64), and the velocity derivatives in equations (63) and (64) are eliminated by means of equations (55) and (56). The resulting equations, now in terms of the derivatives of p' only, are differentiated again with respect to $\tilde{x}$ and substituted into equation (62). The result is the acoustic equation in terms of p' only:

$$\Gamma \frac{\partial}{\partial \tilde{x}}\left[\left(M_{f_\infty}^2 - 1\right)\frac{\partial^2 p'}{\partial \tilde{x}^2} - \frac{\partial^2 p'}{\partial \tilde{y}^2}\right] + \left(M_{e_\infty}^2 - 1\right)\frac{\partial^2 p'}{\partial \tilde{x}^2} - \frac{\partial^2 p'}{\partial \tilde{y}^2} = 0 , \tag{67}$$

where

$$\Gamma = \frac{\left(\frac{\partial h}{\partial \rho}\right)_{p,\alpha}}{\left[\left(\frac{\partial h}{\partial \rho}\right)_{p,\alpha} + \left(\frac{\partial h}{\partial \alpha}\right)_{p,\rho}\left(\frac{\partial \alpha_e}{\partial \rho}\right)_p\right]} . \tag{68}$$

Similarly, another equation is derived by differentiating equation (58) once with respect to $\tilde{x}$ and once with respect to $\tilde{y}$. The resulting equation is now in terms of v' only:

$$\Gamma \frac{\partial}{\partial \tilde{x}}\left[\left(M_{f_\infty}^2 - 1\right)\frac{\partial^2 v'}{\partial \tilde{x}^2} - \frac{\partial^2 v'}{\partial \tilde{y}^2}\right] + \left(M_{e_\infty}^2 - 1\right)\frac{\partial^2 v'}{\partial \tilde{x}^2} - \frac{\partial^2 v'}{\partial \tilde{y}^2} = 0 \ . \quad (69)$$

Solution of the Linearized Equations

The problem under consideration is the expansion of a supersonic stream into a region of constant pressure. As before, the term supersonic refers to the frozen Mach number, thus assuring a supersonic equilibrium Mach number also.

The initial conditions are established by the freestream, where all primed quantities are zero. The boundary condition on equation (67) is specified by the pressure in the base region

$$p_b = p_\infty (1 + p_b') \ , \quad (70)$$

where in the linearized analysis, this condition is imposed along $\tilde{y} = 0$. The boundary condition for equation (69) is obtained from the linearized streamline definition. A streamline is defined by

$$v = u \tan \theta \ ,$$

which in linearized form, becomes

$$v' = \theta \ . \quad (71)$$

As a result, equation (69) is written directly in terms of θ.

$$\Gamma \frac{\partial}{\partial \tilde{x}}\left[\left(M_{f_\infty}^2 - 1\right)\frac{\partial^2 \theta}{\partial \tilde{x}^2} - \frac{\partial^2 \theta}{\partial \tilde{y}^2}\right] + \left(M_{e_\infty}^2 - 1\right)\frac{\partial^2 \theta}{\partial \tilde{x}^2} - \frac{\partial^2 \theta}{\partial \tilde{y}^2} = 0 \ . \quad (72)$$

The Laplace transform is defined by

$$L\{\theta\} = \int_0^\infty \theta(\tilde{x}, \tilde{y}) \exp(-q\tilde{x}) d\tilde{x} \quad (73)$$

Applying the transformation to equation (72) gives

$$\frac{d^2}{d\tilde{y}^2}\left(L\{\theta\}\right) - \left(qB_f\right)^2\left[\frac{B^2+q\Gamma}{1+q\Gamma}\right]L\{\theta\} = 0 \ , \tag{74}$$

where

$$\left.\begin{aligned} B_f^2 &= M_{f\infty}^2 - 1 \ , \qquad B_e^2 = M_{e\infty}^2 - 1, \\ \text{and} \qquad B^2 &= \frac{B_e^2}{B_f^2} > 1 \ . \end{aligned}\right\} \tag{75}$$

Of the two exponential solutions to equation (74), the negative exponential is appropriate.

$$L\{\theta\} = K_1 \exp\left(-qB_f\left[\frac{B^2+\Gamma q}{1+\Gamma q}\right]^{\frac{1}{2}}\tilde{y}\right) \ . \tag{76}$$

To evaluate K_1, it is necessary to transform equation (56) and replace v' by θ to obtain

$$L\{\theta\} = -\frac{p_\infty}{\rho_\infty U_\infty^2}\left[\frac{1}{q}\frac{\partial}{\partial\tilde{y}}\left(L\{p'\}\right)\right] \ . \tag{77}$$

Since the two acoustic equations (66) and (72) are identical except for the dependent variables, the solution for the Laplace transform of the pressure disturbance is also given by the negative exponential.

$$L\{p'\} = K_2 \exp\left(-qB_f\left[\frac{B^2+\Gamma q}{1+\Gamma q}\right]^{\frac{1}{2}}\tilde{y}\right) \ . \tag{78}$$

From equation (70), the transformed boundary condition is

$$L\{p'\} = \frac{p'_b}{q} \tag{79}$$

for $\tilde{y} = 0$. Thus,

$$K_2 = \frac{p'_b}{q} .$$

Equation (78) is differentiated with respect to $\tilde{y}$ and substituted into equation (77) to give

$$L\{\theta\} = \frac{p_\infty}{\rho_\infty U_\infty^2}\left(\frac{p'_b}{q} B_f\left[\frac{B^2+\Gamma q}{1+\Gamma q}\right]^{\frac{1}{2}}\right) \exp\left(-qB_f\left[\frac{B^2+\Gamma q}{1+\Gamma q}\right]^{\frac{1}{2}} \tilde{y}\right) . \tag{80}$$

The inverse transformation can be found along the boundary where $\tilde{y} = 0$. Erdlyi, et al.[25] have found the inverse to be

$$\theta_b = \frac{p_\infty p'_b B_f}{\rho_\infty U_\infty^2}\left[\exp\left(-\frac{(B^2+1)}{2}\frac{\tilde{x}}{\Gamma}\right) I_o\left(\frac{1-B^2}{2}\frac{\tilde{x}}{\Gamma}\right)\right. \tag{81}$$

$$\left. + B^2 \int_0^{\frac{\tilde{x}}{\Gamma}} \exp\left(-\frac{(B^2+1)}{2} w\right) I_o\left(\frac{1-B^2}{2} w\right) dw\right],$$

where I_o is the zeroth order modified Bessel function of the first kind.

Γ is simply a weighting function which does not affect the limiting values for frozen and equilibrium flow. Thus for frozen flow ($\tilde{x} = 0$), the flow deflection is

$$\theta_b = \frac{p_\infty p_b'}{\rho_\infty U_\infty^2} \sqrt{M_{f\infty}^2 - 1} , \tag{82}$$

which is recognized as the result of perfect gas linearized theory, where now the Mach number is designated as the frozen Mach number. Clarke[24] has shown that as $\tilde{x}$ approaches infinity, the integral in equation (81) approaches B^{-1}. The equilibrium limit for the flow deflection is therefore given by

$$\theta_b = \frac{p_\infty p_b'}{\rho_\infty U_\infty^2} \sqrt{M_{e\infty}^2 - 1} , \tag{83}$$

which is the classical expression based on the equilibrium Mach number.

In order to obtain the density perturbation, the continuity equation (54) is transformed, giving

$$qL\{\rho'\} = \frac{p_\infty q}{\rho_\infty U_\infty^2} L\{p'\} - \frac{\partial}{\partial \tilde{y}}\Big(L\{\theta\}\Big) . \tag{84}$$

Equation (79) and the derivative of equation (80) are substituted into equation (84) and evaluated at $\tilde{y} = 0$, yielding

$$L\{\rho_b'\} = \frac{p_\infty p_b'}{\rho_\infty U_\infty^2}\left(\frac{1}{q} + \frac{B_f^2}{q}\left[\frac{B^2 + \Gamma q}{1 + \Gamma q}\right]\right) . \tag{85}$$

The inverse transformation is

$$\rho_b' = \frac{p_\infty p_b'}{\rho_\infty U_\infty^2}\left[1 + B_f^2\left[B^2 - (B^2 - 1)\exp\left(-\frac{\tilde{x}}{\Gamma}\right)\right]\right]. \tag{86}$$

The limit for frozen flow ($\tilde{x} = 0$) is given by

$$\rho_b' = \frac{p_\infty p_b'}{\rho_\infty U_\infty^2} M_{f\infty}^2 \quad . \tag{87}$$

Similarly, as $x \to \infty$, equation (85) approaches the equilibrium limit given by

$$\rho_b' = \frac{p_\infty p_b'}{\rho_\infty U_\infty^2} M_{e\infty}^2 \quad . \tag{88}$$

The degree of dissociation is found by integrating the energy equation (57) and substituting the result into the caloric equation of state (59). Dividing the result by $\rho_\infty\left(\frac{\partial h}{\partial \rho}\right)_{p,\alpha}$ gives

$$\alpha' \left[\frac{\left(\frac{\partial h}{\partial \alpha}\right)_{p,\rho}}{\left(\frac{\partial h}{\partial \rho}\right)_{p,\alpha}}\right]_\infty = -p_\infty p_b' \left[\frac{\left(\frac{\partial h}{\partial p}\right)_{\rho,\alpha} - \frac{1}{\rho}}{\left(\frac{\partial h}{\partial \rho}\right)_{p,\alpha}}\right]_\infty - \rho_\infty \rho' \quad . \tag{89}$$

The term in brackets on the right-hand side of equation (89) is defined in equation (65) in terms of the frozen sound speed, so that the right-hand side of equation (89) becomes

$$\frac{p_\infty p_b'}{a_{f\infty}^2} - \rho_\infty \rho' \quad .$$

Using the expression for the frozen sound speed of an ideal dissociating gas, (15), the right-hand side of equation (89) becomes

$$\rho_\infty \left[\frac{3p_b'}{(4+\alpha_\infty)} - \rho_b'\right] \quad .$$

The derivatives $\left(\frac{\partial h}{\partial \alpha}\right)_{p,\rho}$ and $\left(\frac{\partial h}{\partial \rho}\right)_{p,\alpha}$, given in equations (20) and

(21), are evaluated at freestream conditions and substituted into equation (89) to give

$$\alpha_b' = \frac{(1+\alpha_\infty)}{\left[\left(1+\alpha_\infty\right)\frac{\theta_d}{T_\infty} - 3\right]}\left[\frac{3p_b' B_f^2 (B^2-1)}{M_{f\infty}^2}\right]\left[1 - \exp\left(-\frac{\tilde{x}}{\Gamma}\right)\right] . \qquad (90)$$

The perturbation of the degree of dissociation varies from the initially frozen value, $\alpha_b' = 0$, to the limit as $\tilde{x} \to \infty$:

$$\alpha_b' = \frac{(1+\alpha_\infty)}{\left[\left(1+\alpha_\infty\right)\frac{\theta_d}{T_\infty} - 3\right]}\left[\frac{3p_b' B_f^2 (B^2-1)}{M_{f\infty}^2}\right] . \qquad (91)$$

The temperature is obtained by logarithmically differentiating the equation of state (19).

$$T' = p' - \rho' - \frac{\alpha'}{(1+\alpha_\infty)} . \qquad (92)$$

The frozen flow limit is obtained by substituting equation (87) for ρ', p_b' for p', and $\alpha_b' = 0$, to give

$$T_{fb}' = p_b'\left(\frac{\gamma_\infty - 1}{\gamma_\infty}\right) , \qquad (93)$$

where

$$\gamma_\infty = \frac{4+\alpha_\infty}{3} .$$

Substitution of equations (88) and (91) for the density and degree of

dissociation perturbations as $\tilde{x} \to \infty$, gives the equilibrium limit

$$T_b' = p_b' \left[1 - \frac{M_{e\infty}^2}{\gamma_\infty M_{f\infty}^2} - \frac{3B_f^2 (B^2 - 1)}{\left[\left(1+\alpha_\infty \right) \frac{\theta_d}{T_\infty} - 3 \right] M_{f\infty}^2} \right] . \tag{94}$$

Transformation to Physical Coordinates

The relaxation time, τ, was defined in equation (53) as follows:

$$\tau = - \frac{1}{\left(\frac{\partial \omega}{\partial \alpha} \right)_{p,\rho}} .$$

The rate equation in Freeman's form

$$\omega = C_f T^n \rho \left[(1 - \alpha) e^{-\frac{\theta_d}{T}} - \frac{\rho}{\rho_d} \alpha^2 \right] \tag{95}$$

can be differentiated and substituted into equation (53), giving

$$\tau = \left[C_f T^n \rho \left\{ \left[\frac{(1-\alpha)}{(1-\alpha)} \left(n + \frac{\theta_d}{T} \right) + 1 \right] e^{-\frac{\theta_d}{T}} + \frac{\rho}{\rho_d} \left[2\alpha - \frac{n\alpha^2}{(1+\alpha)} \right] \right\} \right]^{-1} . \tag{96}$$

The accuracy of the linearized rate equation (52) depends on the ability to select a suitable mean value for τ. Due to the exponential dependence of τ on temperature, the selection of the reference temperature is critical.

Good results were obtained when τ was evaluated based on the asymptotic downstream value of T', i.e., the limit as $\tilde{x} \to \infty$. This limit is expressed in equation (94).

The derivatives $\left(\frac{\partial h}{\partial \rho} \right)_{p,\alpha}$ and $\left(\frac{\partial h}{\partial \alpha} \right)_{p,\rho}$ are obtained from equations

(20) and (21), and $\left(\frac{\partial \alpha_e}{\partial \rho}\right)_p$ is obtained by differentiating the equilibrium relation

$$\frac{\alpha_e^2}{1-\alpha_e} = \frac{\rho_d}{\rho} e^{-\frac{\theta_d}{T}} . \tag{97}$$

Substituting these derivatives into equation (68), the expression for Γ is

$$\Gamma = \frac{4+\alpha_\infty}{4+\alpha_\infty+\left(1+\frac{\theta_d}{T_\infty}\right)\left(\frac{\theta_d}{T_\infty}-\frac{3}{(1+\alpha_\infty)}\right)\frac{\alpha_\infty(1-\alpha_\infty^2)}{\left[\left(2-\alpha_\infty\right)\left(1+\alpha_\infty\right)+\alpha_\infty\left(1-\alpha_\infty\right)\frac{\theta_d}{T_\infty}\right]}} . \tag{98}$$

Results and Discussion

Calculations were carried out using the linearized theory for the expansion of oxygen from 1 atmosphere to 0.8 atmospheres. The freestream temperature was 4250° K and the frozen Mach number was 1.83. The corresponding equilibrium Mach number was 2.12 so that $B^2 = 1.496$. These conditions were chosen so that Clarke's[24] values for the integral in equation (81) can be used.

Using the same initial and boundary conditions, calculations by the method of characteristics were obtained on the Burroughs B 5500.

The flow deflection, density, temperature, and degree of dissociation perturbations as obtained by linear theory and the method of characteristics are compared in Figures 9 through 12. The agreement is good, in spite of the rather large expansion ratio. The discrepancy in the flow deflection is due primarily to the defect in the perfect

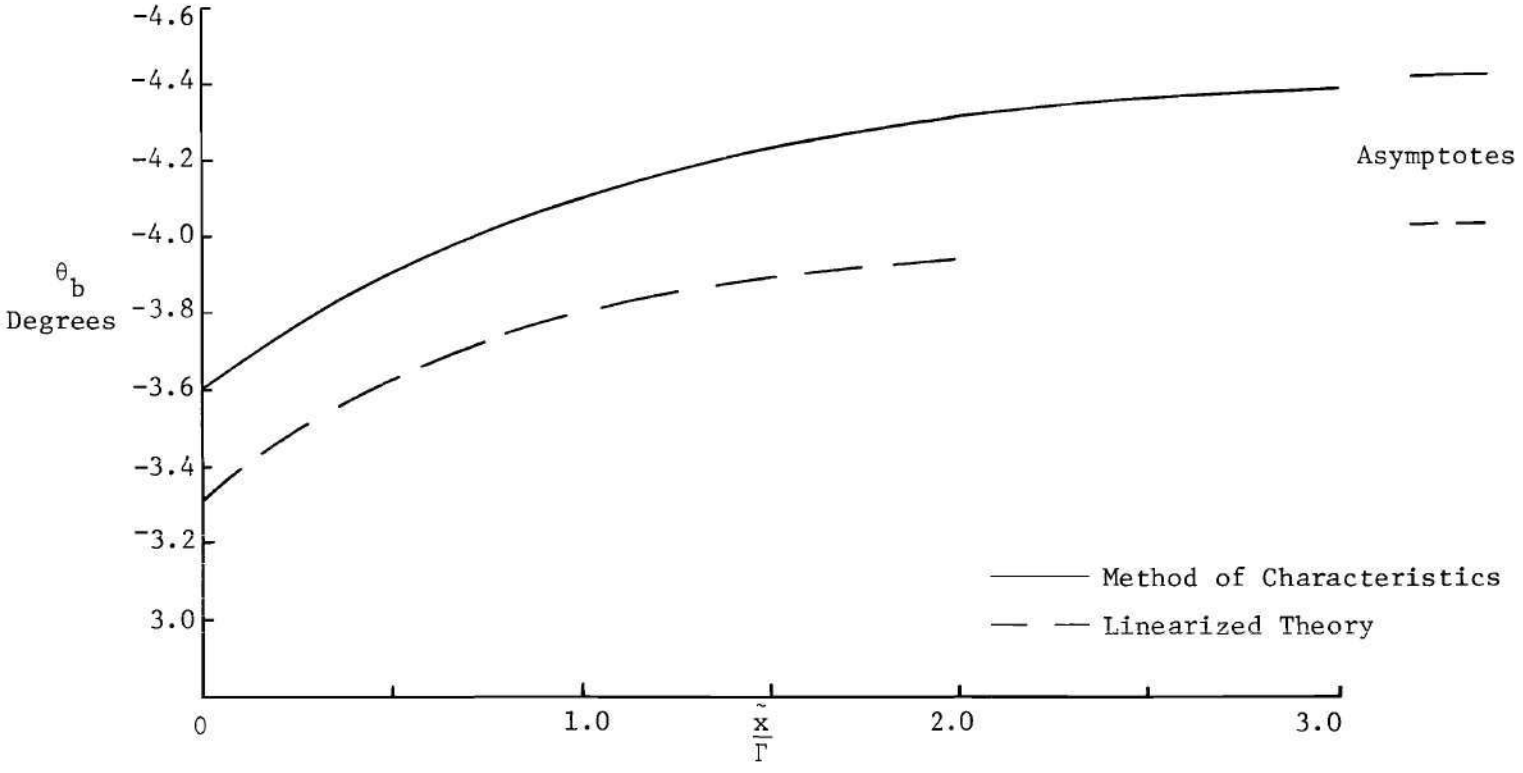

Figure 9. Comparison of the Flow Deflection of the Constant-Pressure Boundary by the Linearized Theory and the Method of Characteristics

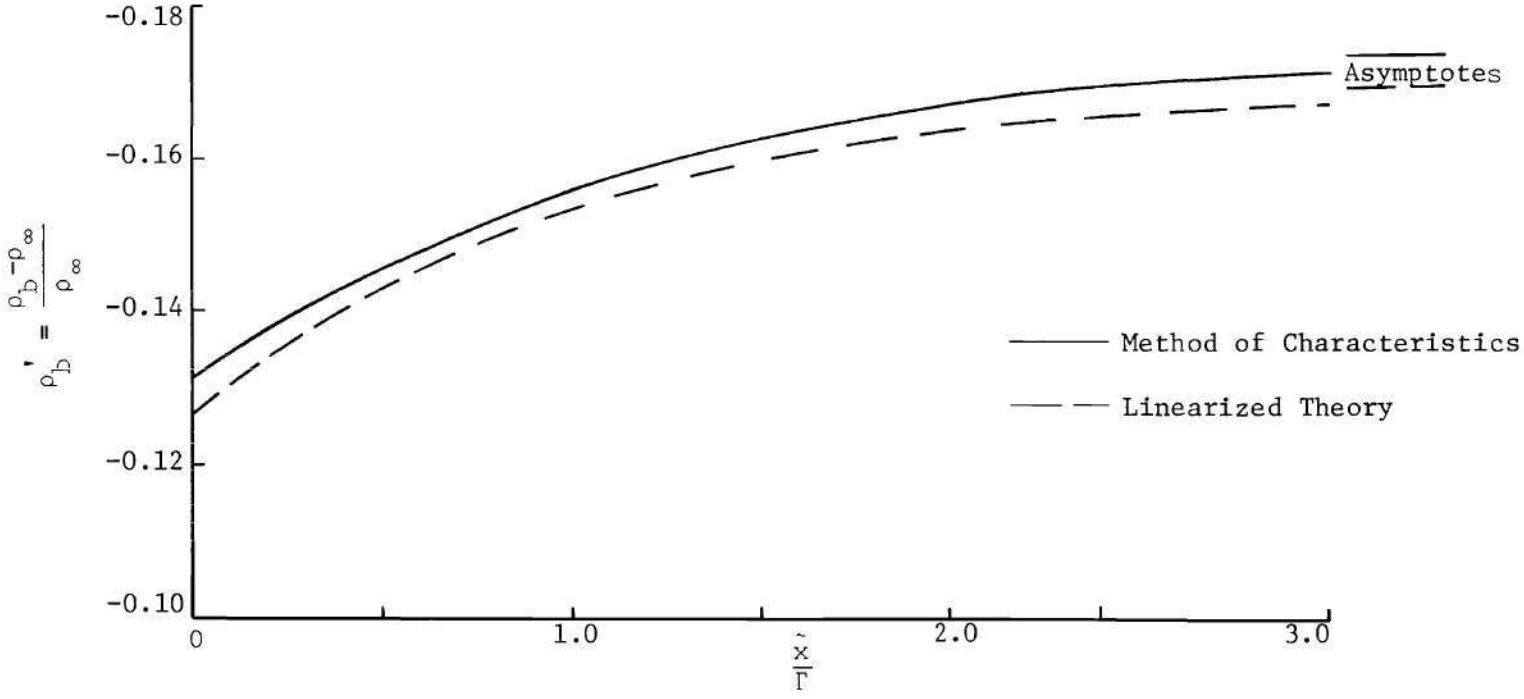

Figure 10. Comparison of the Density Perturbation on the Constant-Pressure Boundary by the Linearized Theory and the Method of Characteristics

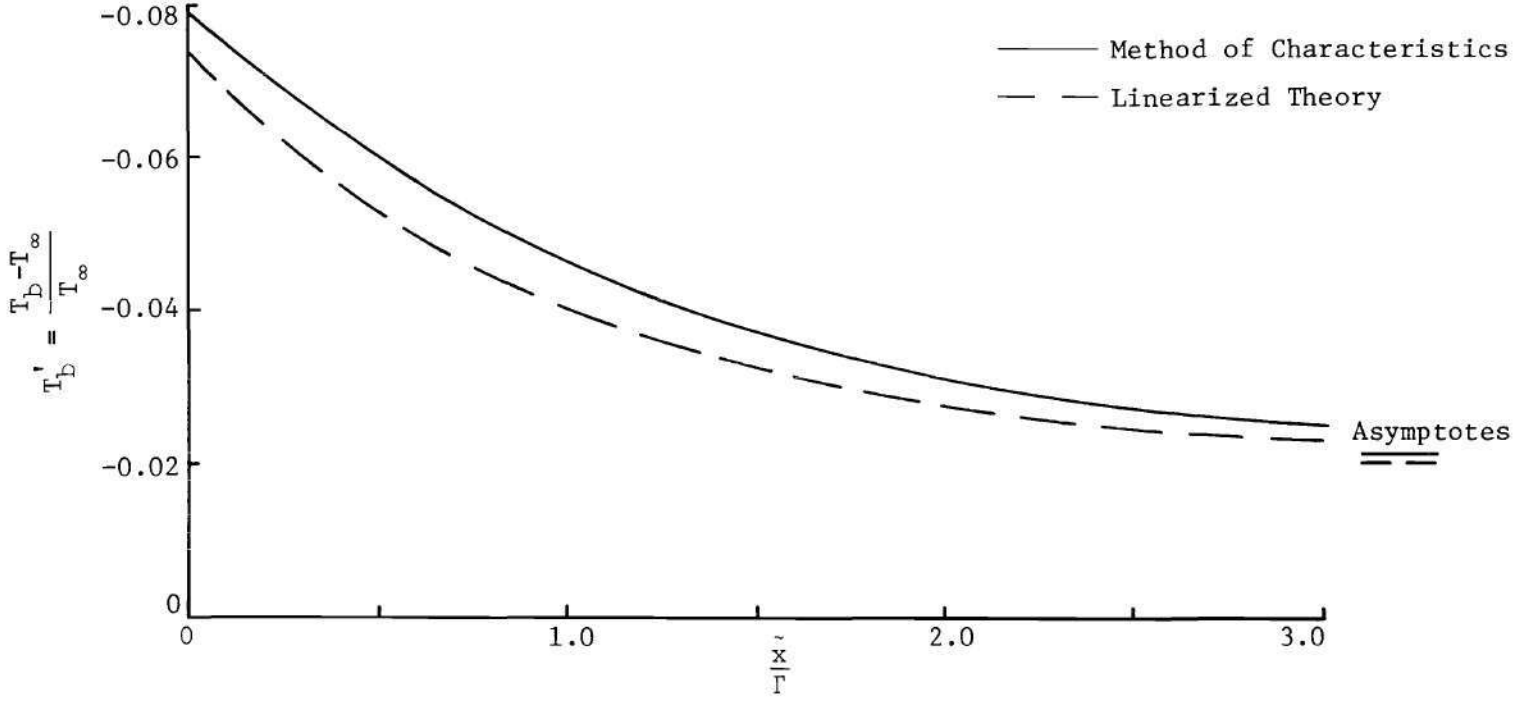

Figure 11. Comparison of the Temperature Perturbation on the Constant-Pressure Boundary by the Linearized Theory and the Method of Characteristics

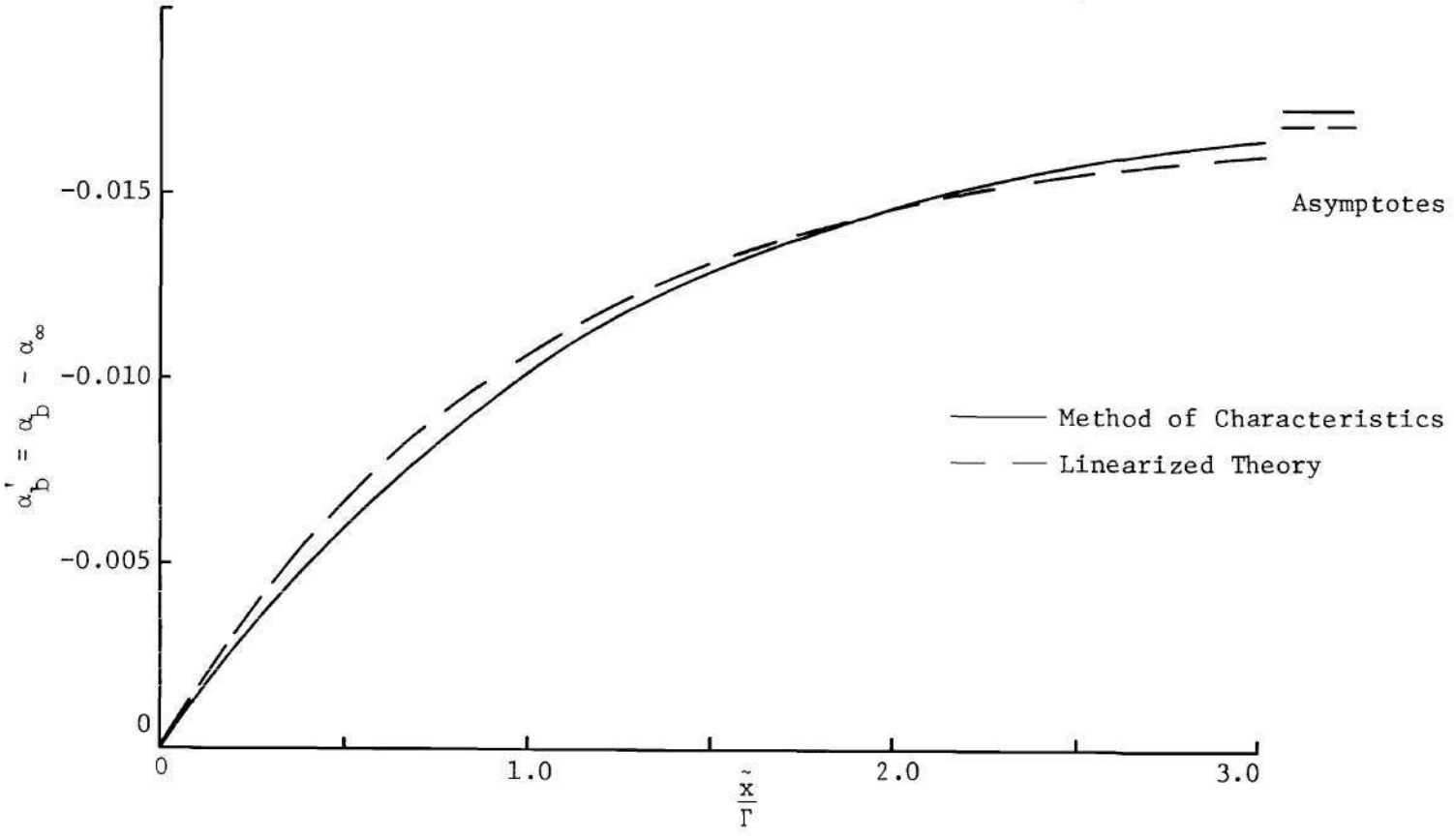

Figure 12. Comparison of the Degree of Dissociation Perturbation on the Constant-Pressure Boundary by the Linearized Theory and the Method of Characteristics

gas limit of the linearized theory, rather than the chemical effects. The results for the flow deflection are replotted in Figure 13, where the results are now plotted as the ratio of the flow deflection to the flow deflection immediately after expansion, θ_b/θ_{bf}, versus the length $\tilde{x}/\Gamma$. Allowing for the classical defects in the linearized theory, the solution appears to give a good description of the relaxation zone after expansion.

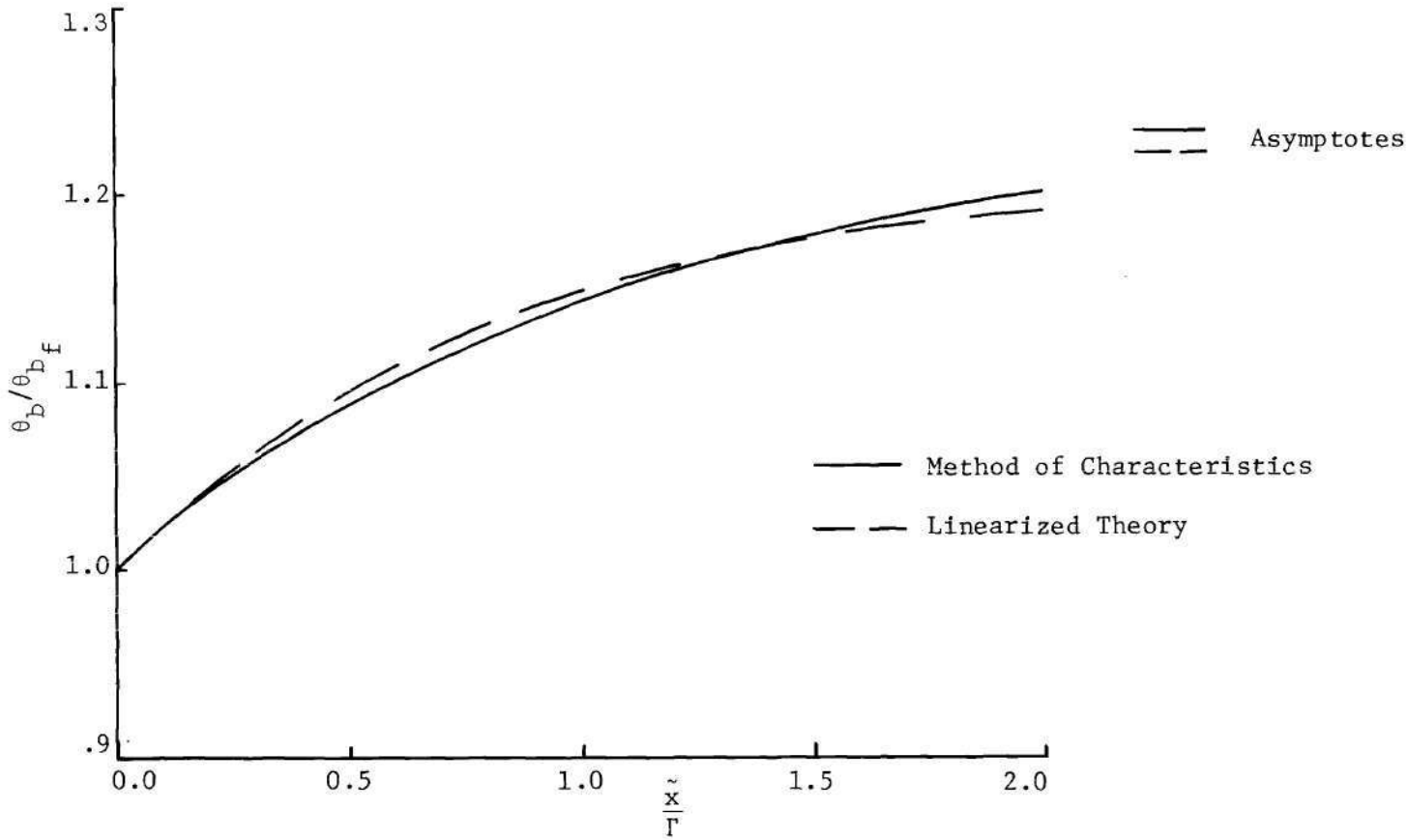

Figure 13. Comparison of the Normalized Flow Deflection of the Constant Pressure Boundary by the Linearized Theory and the Method of Characteristics

CHAPTER IV

LAMINAR MIXING OF A DISSOCIATING GAS

The problem of the nonequilibrium, viscous mixing region is treated in this chapter. First, the governing differential equations are derived and transformed into a form suitable for the finite difference solution. Next, the finite difference system of equations is derived and the stability, convergence, and method of solution are discussed. The extension of Chapman's similar solutions to account for the frozen flow of a dissociated gas, derived in Appendix B, is discussed and compared with the finite difference solutions. Finally, a comparison is made between solutions for finite rate, frozen, and equilibrium flow.

Derivation of the Governing Equations

Neglecting thermal diffusion, the boundary-layer equations for the steady, laminar, constant-pressure, two-dimensional flow of a dissociating gas, with x_s measured along the dividing streamline and y_s measured normal to x_s, are written (see, for example, reference [26]) as follows: the continuity equation,

$$\frac{\partial}{\partial x_s}\left(\rho u\right) + \frac{\partial}{\partial y_s}\left(\rho v\right) = 0 \ , \tag{99}$$

the species conservation equation,

$$\rho u \frac{\partial \alpha}{\partial x_s} + \rho v \frac{\partial \alpha}{\partial y_s} = \frac{\partial}{\partial y_s}\left(\rho D_{12} \frac{\partial \alpha}{\partial y_s}\right) + \rho \omega \ , \tag{100}$$

the momentum equation,

$$\rho u \frac{\partial u}{\partial x_s} + \rho v \frac{\partial u}{\partial y_s} = \frac{\partial}{\partial y_s}\left(\mu \frac{\partial u}{\partial y_s}\right) , \tag{101}$$

and the energy equation,

$$\rho u \frac{\partial h}{\partial x_s} + \rho v \frac{\partial h}{\partial y_s} = \frac{\partial}{\partial y_s}\left[\kappa \frac{\partial T}{\partial y_s} + \rho D_{12}\left(h_A - h_M\right)\frac{\partial \alpha}{\partial y_s}\right] + \mu\left(\frac{\partial u}{\partial y_s}\right)^2 , \tag{102}$$

where the subscripts A and M denote atomic and molecular species, respectively.

The ideal dissociating gas model, discussed in Appendix A, provides the following relations: the thermal equation of state,

$$p = \rho(1 + \alpha)R_m T , \tag{103}$$

the caloric equation of state,

$$h = R_m\left[(4 + \alpha)T + \alpha\theta_d\right] , \tag{104}$$

the equilibrium relation,

$$\frac{\alpha_e^2}{1-\alpha_e} = \frac{\rho_d}{\rho} e^{-\frac{\theta_d}{T}} , \tag{105}$$

and the rate equation,

$$\omega = C_f T^n \rho\left[\left(1 - \alpha\right)e^{-\frac{\theta_d}{T}} - \frac{\rho}{\rho_d}\alpha^2\right] . \tag{106}$$

The differential of the enthalpy is obtained from equation (104)

and written

$$dh = R_m\{(4 + \alpha)dT + (\theta_d + T)d\alpha\} \tag{107}$$

With this, the energy equation (102) is

$$\rho R_m(4 + \alpha)\left\{u \frac{\partial T}{\partial x_s} + v \frac{\partial T}{\partial y_s}\right\} + \rho R_m(\theta_d + T)\left\{u \frac{\partial \alpha}{\partial x_s} + v \frac{\partial \alpha}{\partial y_s}\right\} \tag{108}$$

$$= \frac{\partial}{\partial y_s}\left(\kappa \frac{\partial T}{\partial y_s}\right) + R_m\left(\theta_d + T\right)\frac{\partial}{\partial y_s}\left(\rho D_{12} \frac{\partial \alpha}{\partial y_s}\right)$$

$$+ \mu\left(\frac{\partial u}{\partial y_s}\right)^2 ,$$

where $\theta_d \gg T$. Substituting equation (100) into equation (108) gives the energy equation for finite rate flow.

$$\rho R_m(4 + \alpha)\left\{u \frac{\partial T}{\partial x_s} + v \frac{\partial T}{\partial y_s}\right\} = \frac{\partial}{\partial y_s}\left(\kappa \frac{\partial T}{\partial y_s}\right) + \mu\left(\frac{\partial u}{\partial y_s}\right)^2 - R_m(\theta_d + T)\rho\omega \tag{109}$$

The species continuity equation and energy equation for frozen flow are obtained from equations (100) and (109) by setting $\omega = 0$.

For equilibrium flow, the species conservation equation (100) is replaced by the equilibrium relation (105). Since the mixing takes place at constant pressure, the enthalpy for equilibrium flow is a function of temperature only, and is written

$$dh = \left[\left(\frac{\partial h}{\partial T}\right)_{p,\alpha} + \left(\frac{\partial h}{\partial \alpha}\right)_{p,T} \frac{d\alpha_e}{dT}\right] dT \ . \tag{110}$$

Substituting equation (110) into equation (102), the energy equation

for equilibrium flow is written:

$$\rho C_{pr}\left(u \frac{\partial T}{\partial x_s} + v \frac{\partial T}{\partial y_s}\right) = \frac{\partial}{\partial y_s}\left(k_r \frac{\partial T}{\partial y_s}\right) + \mu\left(\frac{\partial u}{\partial y_s}\right)^2 , \tag{111}$$

where

$$C_{pr} = \left(\frac{\partial h}{\partial T}\right)_{p,\alpha} + \left(\frac{\partial h}{\partial \alpha}\right)_{p,T} \frac{d\alpha_e}{dT} \tag{112}$$

and

$$k_r = \kappa + \rho D_{12}\left(\frac{\partial h}{\partial \alpha}\right)_{p,T} \frac{d\alpha_e}{dT} . \tag{113}$$

A generalized energy equation, which incorporates the three flow conditions is written

$$\rho C_p\left\{u \frac{\partial T}{\partial x_s} + v \frac{\partial T}{\partial y_s}\right\} = \frac{\partial}{\partial y_s}\left\{k \frac{\partial T}{\partial y_s}\right\} + \mu\left(\frac{\partial u}{\partial y_s}\right)^2 - \rho R_m(\theta_d + T)\omega , \tag{114}$$

subject to the following conditions:

Finite Rate Flow:

$$\left.\begin{aligned} C_p &= (4 + \alpha)R_m \\ k &= \kappa \\ \omega &= C_f T^n \rho\left[(1 - \alpha)e^{-\frac{\theta_d}{T}} - \frac{\rho}{\rho_d}\alpha^2\right] \end{aligned}\right\} \tag{115}$$

Frozen Flow:

$$\left.\begin{aligned} C_p &= (4 + \alpha)R_m \end{aligned}\right\}$$

$$\left.\begin{aligned} k &= \kappa \\ \omega &= 0 \end{aligned}\right\} \qquad (116)$$

Equilibrium Flow:

$$\left.\begin{aligned} C_p &= C_{pr} = R_m\left[(4+\alpha) + \frac{\alpha(1-\alpha^2)}{2}\left(\frac{\theta_d}{T}+1\right)^2\right] \\ k &= k_r = \kappa + pD_{12}\,\frac{\alpha(1-\alpha)}{2T}\left(\frac{\theta_d}{T}+1\right)^2 \\ \omega &= 0\ . \end{aligned}\right\} \qquad (117)$$

Howarth Transformation

Because of the assumption of variable $\rho\mu$, the momentum and continuity equations are coupled to the energy and species conservation equations. It is advantageous, however, to employ a restricted Howarth transformation (only the normal coordinate is transformed), since it reduces the coupling. In addition, the mass flow rate between two streamlines becomes a simple integration of the streamwise velocity in the transformed plane. As before, an arbitrary reference length, ℓ, is introduced, and the coordinates (x_s, y_s) are transformed to the non-dimensional coordinates (s^*, Y^*) defined by

$$s^* = \frac{x_s}{\ell} \qquad (118)$$

$$Y^* = \frac{\sqrt{Rey}}{\ell}\int_0^{y_s} \frac{\rho}{\rho_\infty}\, dy_s\ , \qquad (119)$$

where the Reynolds number is

$$\mathrm{Rey} = \frac{\rho_\infty U_\infty \ell}{\mu_\infty} \quad . \tag{120}$$

Implicit differentiation of equations (118) and (119) gives the transformation relations

$$\left.\begin{aligned} \frac{\partial}{\partial x_s} &= \frac{1}{\ell}\frac{\partial}{\partial s^*} + \frac{\partial Y^*}{\partial x}\frac{\partial}{\partial Y^*} \\ \frac{\partial}{\partial y_s} &= \frac{1}{\ell}\frac{\rho}{\rho_\infty}\sqrt{\mathrm{Rey}}\,\frac{\partial}{\partial Y^*} \end{aligned}\right\} . \tag{121}$$

The stream function is defined by

$$\left.\begin{aligned} \rho u &= \rho_\infty \frac{\partial \Psi}{\partial y_s} \\ \rho v &= -\rho_\infty \frac{\partial \Psi}{\partial x_s} \end{aligned}\right\} . \tag{122}$$

Equations (122) are transformed by equations (121), giving

$$\left.\begin{aligned} \frac{\partial \Psi}{\partial Y^*} &= \frac{\ell}{\sqrt{\mathrm{Rey}}}\,u \\ \frac{\partial \Psi}{\partial s^*} &= \frac{-\ell}{\sqrt{\mathrm{Rey}}}\,V \end{aligned}\right\} , \tag{123}$$

where V is defined by

$$V = \frac{\rho}{\rho_\infty}\sqrt{\mathrm{Rey}}\,v + \frac{\partial Y^*}{\partial x_s}\,\ell u \quad . \tag{124}$$

The continuity equation is now given by

$$\frac{\partial u}{\partial s^*} + \frac{\partial V}{\partial Y^*} = 0 \ . \tag{125}$$

The transformation relations (121) are now used to write two important operators:

$$u \frac{\partial}{\partial x_s} + v \frac{\partial}{\partial y_s} = \frac{u}{\ell} \frac{\partial}{\partial s^*} + \frac{V}{\ell} \frac{\partial}{\partial Y^*} \tag{126}$$

$$\frac{\partial}{\partial y_s}\left(\beta \frac{\partial}{\partial y_s}\right) = \frac{1}{\ell^2} \frac{\rho}{\rho_\infty} \text{Rey} \frac{\partial}{\partial Y}\left(\beta \frac{\rho}{\rho_\infty} \frac{\partial}{\partial Y^*}\right) \ , \tag{127}$$

where β is any variable.

Applying these operators, equations (126) and (127), to the momentum (101), species conservation (100) and generalized energy (114) equations gives:

the momentum equation,

$$u \frac{\partial u}{\partial s^*} + V \frac{\partial u}{\partial Y^*} = \frac{\text{Rey}}{\ell \rho_\infty} \frac{\partial}{\partial Y^*}\left(\frac{\rho \mu}{\rho_\infty} \frac{\partial u}{\partial Y^*}\right) \ , \tag{128}$$

the species conservation equation,

$$u \frac{\partial \alpha}{\partial s^*} + V \frac{\partial \alpha}{\partial Y^*} = \frac{\text{Rey}}{\ell \rho_\infty} \frac{\partial}{\partial Y^*}\left(\frac{\rho^2 D_{12}}{\rho_\infty} \frac{\partial \alpha}{\partial Y^*}\right) + \ell \omega \ , \tag{129}$$

and the generalized energy equation,

$$u \frac{\partial T}{\partial s^*} + V \frac{\partial T}{\partial Y^*} = \frac{\text{Rey}}{C_p \ell \rho_\infty} \frac{\partial}{\partial Y^*}\left(\frac{k \rho}{\rho_\infty} \frac{\partial T}{\partial Y^*}\right) + \frac{\mu \rho \text{Rey}}{C_p \rho_\infty^2 \ell}\left(\frac{\partial u}{\partial Y^*}\right)^2 \tag{130}$$

$$- \frac{\ell \omega R_m (\theta_d + T)}{C_p} \quad .$$

These equations are non-dimensionalized by introducing the following definitions for the dependent variables:

$$\left.\begin{aligned} u^* &= \frac{u}{U_\infty} \qquad & v^* &= \frac{V}{U_\infty} \\ \rho^* &= \frac{\rho}{\rho_\infty} \qquad & T^* &= \frac{T}{T_\infty} \end{aligned}\right\} , \tag{131}$$

the non-dimensional ratios,

$$\left.\begin{aligned} C &= \frac{\rho\mu}{\rho_\infty \mu_\infty} \qquad & R &= \frac{C_p}{C_{p\infty}} \\ Pr &= \frac{\mu C_p}{k} \qquad & Sc &= \frac{\mu}{\rho D_{12}} \\ & & E_\infty &= \frac{U_\infty^2}{C_{p\infty} T_\infty} \end{aligned}\right\} , \tag{132}$$

and the dimensionless form of the rate equation (107),

$$\omega^* = K T^{*n} \rho^* \left[(1 - \alpha) e^{-\frac{\theta_d^*}{T^*}} - \frac{\rho^*}{\rho_d^*} \alpha^2 \right] , \tag{133}$$

where

$$K = \frac{\ell C_f T_\infty^n}{U_\infty} \rho_\infty \tag{134}$$

and

$$\theta_d^* = \frac{\theta_d}{T_\infty} \qquad \rho_d^* = \frac{\rho_d}{\rho_\infty} \tag{135}$$

are dimensionless parameters.

The expressions for the transport properties are derived in Appendix A.

Substitution of equations (131), (132), (133), and (135) into equations (125), (128), (129), and (130) yields the continuity equation,

$$\frac{\partial u^*}{\partial s^*} + \frac{\partial v^*}{\partial Y^*} = 0 \ , \tag{136}$$

the momentum equation,

$$u^* \frac{\partial u^*}{\partial s^*} + v^* \frac{\partial u^*}{\partial Y^*} = \frac{\partial}{\partial Y^*}\left(C \frac{\partial u^*}{\partial Y^*}\right) \ , \tag{137}$$

the species conservation equation,

$$u^* \frac{\partial \alpha}{\partial s^*} + v^* \frac{\partial \alpha}{\partial Y^*} = \frac{\partial}{\partial Y^*}\left(\frac{C}{Sc} \frac{\partial \alpha}{\partial Y^*}\right) + \omega^* \tag{138}$$

and the generalized energy equation,

$$u^* \frac{\partial T^*}{\partial s^*} + v^* \frac{\partial T^*}{\partial Y^*} = \frac{1}{R} \frac{\partial}{\partial Y^*}\left(\frac{CR}{Pr} \frac{\partial T^*}{\partial Y^*}\right) + \frac{CE_\infty}{R}\left(\frac{\partial u^*}{\partial Y^*}\right)^2 \tag{139}$$

$$- \left(\theta_d^* + T^*\right)\frac{R_m}{C_p} \omega^* \ .$$

Finite Interval Transformation

The computations involved in the implicit finite difference method to be used in the solution of this problem are greatly simplified if the interval of the normal coordinate is finite. Therefore, the normal coordinate, Y^*, is transformed by the hyperbolic tangent transformation, as used by Sills[15]. The new normal coordinate, ζ, is defined by

$$\zeta = \tanh(AY^*) \ , \tag{140}$$

where A is a dimensionless constant which is used to control the grid spacing. This transformation transforms the infinite interval $-\infty < Y^* < \infty$ to the finite interval $-1 \leq \zeta \leq 1$.

This transformation succeeds in eliminating some of the arbitrariness involved in defining a boundary layer edge, and offers several additional advantages. Equally spaced grid points in the ζ-direction transform into unequally spaced points on the Y-axis with a closer spacing near $Y = 0$, where the largest gradients occur. This transformation (140) has a closed form inverse given by:

$$Y^* = \frac{1}{2A} \ln\left[\frac{1+\zeta}{1-\zeta}\right] \ . \tag{141}$$

Since ζ is independent of s^*, the coordinate transformation is accomplished with the relations

$$\left.\begin{aligned} \frac{\partial}{\partial Y^*} &= A\left(1 - \zeta^2\right)\frac{\partial}{\partial \zeta} \\ \text{and} \end{aligned}\right\} \tag{142}$$

$$\frac{\partial^2}{\partial Y^{*2}} = A^2\left(1 - \zeta^2\right)\left[-2\zeta\,\frac{\partial}{\partial\zeta} + \left(1 - \zeta^2\right)\frac{\partial^2}{\partial\zeta^2}\right] \Bigg)$$

The transformation equations (142) are applied to equations (136) through (139) to give the continuity equation,

$$\frac{\partial u^*}{\partial s^*} = -A\left(1 - \zeta^2\right)\frac{\partial v^*}{\partial\zeta}\,, \tag{143}$$

the momentum equation,

$$u^*\,\frac{\partial u^*}{\partial s^*} = -A\left(1 - \zeta^2\right)\left[v^* + 2AC\zeta - A\left(1 - \zeta^2\right)\frac{\partial C}{\partial\zeta}\right]\frac{\partial u^*}{\partial\zeta} \tag{144}$$

$$+ A^2\left(1 - \zeta^2\right)^2 C\,\frac{\partial^2 u^*}{\partial\zeta^2}\,,$$

the species conservation equation,

$$u^*\,\frac{\partial\alpha}{\partial s^*} = -A\left(1 - \zeta^2\right)\left[v^* + \frac{2AC\zeta}{Sc} - A\left(1 - \zeta^2\right)\frac{\partial\left(\frac{C}{Sc}\right)}{\partial\zeta}\right]\frac{\partial\alpha}{\partial\zeta} \tag{145}$$

$$+ A^2\left(1 - \zeta^2\right)^2\,\frac{C}{Sc}\,\frac{\partial^2\alpha}{\partial\zeta^2} + \omega^*\,,$$

and the generalized energy equation,

$$u^*\,\frac{\partial T^*}{\partial s^*} = -A\left(1 - \zeta^2\right)\left[v^* + \frac{2A\zeta C}{Pr} - \frac{A(1-\zeta^2)}{R}\,\frac{\partial}{\partial\zeta}\left(\frac{CR}{Pr}\right)\right]\frac{\partial T^*}{\partial\zeta} \tag{146}$$

$$+ A^2\left(1 - \zeta^2\right)^2\,\frac{C}{Pr}\,\frac{\partial^2 T^*}{\partial\zeta^2} + \frac{CE_\infty}{R}\,A^2\left(1 - \zeta^2\right)\left(\frac{\partial u^*}{\partial\zeta}\right)^2$$

$$- \omega^*\,\frac{R_m}{C_p}\left(\theta_d^* + T^*\right)\,.$$

Boundary and Initial Conditions

The boundary conditions in the physical plane are:

$$\left.\begin{array}{llll} u = U_\infty \quad \alpha = \alpha_b(x_s) \quad T = T_b(x_s) & & \text{at} & y = +\infty \\ v = 0 & & \text{at} & y = 0 \\ u = 0 \quad \alpha = \alpha_{es} \quad T = T_s & & \text{at} & y = -\infty \end{array}\right\} \quad (147)$$

The initial conditions are:

$$\left.\begin{array}{l} u = u(y) \\ v = v(y) \\ \alpha = \alpha(y) \\ T = T(y) \end{array}\right\} \quad \text{at} \quad x_s = 0 \quad . \quad (148)$$

The boundary conditions in the transformed plane, appropriate to equations (143) through (146) are:

$$\left.\begin{array}{llll} u^* = 1 \quad \alpha = \alpha_b(s^*) \quad T^* = \dfrac{T_b(s^*)}{T_\infty} & & \text{at} & \zeta = +1 \\ v^* = 0 & & \text{at} & \zeta = 0 \\ u^* = 0 \quad \alpha = \alpha_{es} \quad T^* = \dfrac{T_s}{T_\infty} & & \text{at} & \zeta = -1 \end{array}\right\} \quad (149)$$

and the initial conditions are:

$$u^* = u^*(\zeta)$$

$$\left.\begin{aligned} v^* &= v^*(\zeta) \\ \alpha^* &= \alpha(\zeta) \\ T^* &= T^*(\zeta) \end{aligned}\right\} \quad \text{at } s^* = 0 \quad . \quad (150)$$

The Finite Difference Solution

Because of the complexity of the system of non-linear partial differential equations derived in the previous section, a numerical solution must be employed. A finite difference method will be used, wherein the derivatives are replaced by finite difference approximations.

Two types of finite difference methods are available; implicit and explicit. Explicit methods have been successfully applied to boundary layer problems (see, for example, references[27] and [28]), but often involve very stringent limits on the allowable step size ratios.

Lately, much attention has been directed to the use of an implicit finite difference method known as the "Crank-Nicholson Method" (see, for example, references [29], [30], [15], [28], and [31]). In this method, the normal, ζ, derivatives are approximated by average central differences and the streamwise, s^*, derivatives by forward difference approximations. This method has stability advantages over explicit methods, as shall be discussed later. The Crank-Nicholson method is used in this thesis.

Finite Difference Equations

The finite difference approximations are based on the grid shown in Figure 14. With the mesh points equally spaced in the ζ-direction,

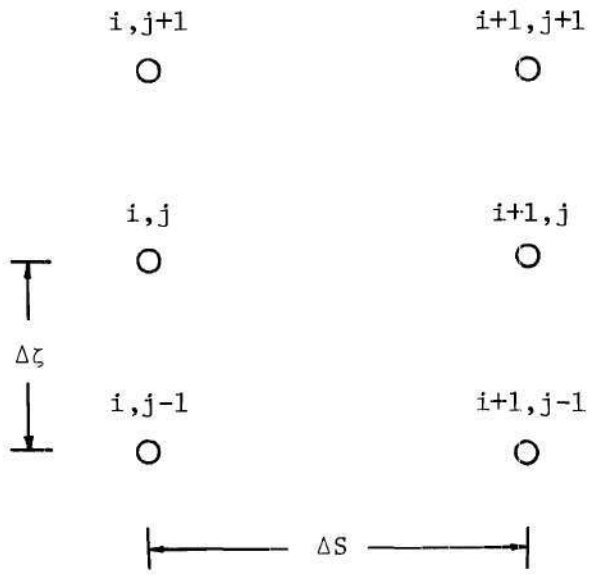

Figure 14. The Finite Difference Grid for the Mixing Region

the approximations are:

$$\left.\begin{aligned}
\frac{\partial g}{\partial s^*} &= \frac{g_{i+1,j}-g_{i,j}}{\Delta s^*} \\
\frac{\partial g}{\partial \zeta} &= \frac{1}{2}\left\{\left(\frac{g_{i+1,j+1}-g_{i+1,j-1}}{2\Delta\zeta}\right)+\left(\frac{g_{i,j+1}-g_{i,j-1}}{2\Delta\zeta}\right)\right\} \\
&= \frac{g_{i+1,j+1}-g_{i+1,j-1}+g_{i,j+1}-g_{i,j-1}}{4\Delta\zeta} \\
\frac{\partial^2 g}{\partial \zeta^2} &= \frac{1}{2(\Delta\zeta)^2}\left[g_{i+1,j-1}-2g_{i+1,j}+g_{i+1,j-1}+g_{i,j+1}-2g_{i,j}+g_{i,j-1}\right]
\end{aligned}\right\} \qquad (151)$$

where g is any of the dependent variables u*, α, or T*; i is the index in the s^*-direction; j is the index in the ζ-direction; Δs^* is the incremental distance between two neighboring streamwise stations; and $\Delta\zeta$ is the distance between two neighboring vertical stations.

Equations (151) are substituted into the momentum equation (144), species conservation equation (145), and generalized energy equation (146) resulting in a set of difference equations relating the unknown variables, u*, α, and T*, at the i + 1st station in terms of the known variables at the ith station.

In the iterative method to be used, all non-linear coefficients are replaced by average quantities and denoted by a bar. For example,

$$\bar{u}^*_j = \frac{u^*_{i+1,j}+u^*_{i,j}}{2} \quad .$$

For the first iteration, $u^*_{i+1,j}$ is assigned the value of $u_{i,j}$. For subsequent iterations, the value of $u^*_{i+1,j}$, obtained from the preceding

iteration, is used. The thermodynamic and transport properties are evaluated at the averaged temperature $\bar{T}^*_j$ and degree of dissociation $\bar{\alpha}_j$.

Introduction of the finite difference approximations (151) into the momentum equation (144) yields:

$$u^*_{i+1,j-1}\left[-A_1(i,j) - A_2(i,j)\right] + u^*_{i+1,j}\left[\frac{\bar{u}^*_j}{2\Delta s^*} + 2A_2(i,j)\right] \qquad (152)$$

$$+ u^*_{i+1,j+1}\left[A_1(i,j) - A_2(i,j)\right]$$

$$= u^*_{i,j-1}\left[A_1(i,j) + A_2(i,j)\right] + u_{i,j}\left[\frac{\bar{u}^*_j}{2\Delta s^*} - 2A_2(i,j)\right]$$

$$+ u^*_{i,j+1}\left[-A_1(i,j) + A_2(i,j)\right]$$

where $A_1(i,j)$ is composed of the coefficients of the first order ζ-derivatives in equation (144), and is given by

$$A_1(i,j) = \frac{A(1-\zeta_j^2)}{4\Delta\zeta}\left\{\bar{v}^*_j + 2A\zeta_j\bar{C}_j\right\} + \frac{A^2(1-\zeta_j^2)^2}{8(\Delta\zeta)^2}\left\{\bar{C}_{j-1} - \bar{C}_{j+1}\right\}, \qquad (153)$$

and $A_2(i,j)$ is the coefficient of the second order ζ-derivative in equation (144);

$$A_2(i,j) = \frac{A^2(1-\zeta_j^2)^2}{2(\Delta\zeta)^2}\bar{C}_j \,. \qquad (154)$$

The finite difference approximation of the species conservation equation (145) is

$$\alpha_{i+1,j-1}\left[-C_1(i,j) - C_2(i,j)\right] + \alpha_{i+1,j}\left[\frac{\bar{u}_j^*}{2\Delta s^*} + 2C_2(i,j)\right] \quad (155)$$

$$+ \alpha_{i+1,j+1}\left[C_1(i,j) - C_2(i,j)\right]$$

$$= \alpha_{i,j-1}\left[C_1(i,j) + C_2(i,j)\right] + \alpha_{i,j}\left[\frac{\bar{u}_j^*}{2\Delta s^*} - 2C_2(i,j)\right]$$

$$+ \alpha_{i,j+1}\left[-C_1(i,j) + C_2(i,j)\right]$$

$$+ \bar{\omega}_j^* \ ,$$

where

$$C_1(i,j) = \frac{A(1-\zeta_j^2)}{4\Delta\zeta}\left\{\bar{v}_j^* + 2A\zeta_j\left(\frac{\bar{C}}{Sc}\right)\right\} + \frac{A^2(1-\zeta_j^2)^2}{8(\Delta\zeta)^2}\left\{\left(\frac{\bar{C}}{Sc}\right)_{j-1} - \left(\frac{\bar{C}}{Sc}\right)_{j+1}\right\} \quad (156)$$

and

$$C_2(i,j) = \frac{A^2(1-\zeta_j^2)^2}{2(\Delta\zeta)^2}\left(\frac{\bar{C}}{Sc}\right)_j \ . \quad (157)$$

The finite difference approximation of the generalized energy equation (146) is

$$T^*_{i+1,j-1}\left[-E_1(i,j) - E_2(i,j)\right] + T^*_{i+1,j}\left[\frac{\bar{u}_j^*}{2\Delta s^*} + 2E_2(i,j)\right] \quad (158)$$

$$+ T^*_{i+1,j+1}\left[E_1(i,j) - E_2(i,j)\right]$$

$$= T^*_{i,j-1}\left[E_1(i,j) + E_2(i,j)\right] + T^*_{i,j}\left[\frac{\bar{u}^*_j}{2\Delta s^*} - 2E_2(i,j)\right]$$

$$+ T^*_{i,j+1}\left[-E_1(i,j) + E_2(i,j)\right]$$

$$- \frac{R_m}{C_p}\left(\theta^*_d + T^*\right)\bar{\omega}^* + \frac{A^2(1-\zeta_j^2)^2}{4(\Delta\zeta)^2}\left(\frac{CE_\infty}{R}\right)\left[(u^*_{i,j+1} - u^*_{i,j-1})\right.$$

$$\left.(u^*_{i+1,j+1} - u^*_{i+1,j-1})\right]$$

where

$$E_1(i,j) = \frac{A(1-\zeta_j^2)}{4\Delta\zeta}\left\{\bar{v}^*_j + 2A\zeta_j\left(\frac{\bar{C}}{Pr}\right)_j\right\} + \frac{A^2(1-\zeta_j^2)^2}{8(\Delta\zeta)^2}\left\{\left(\frac{\bar{CR}}{Pr}\right)_{j-1} - \left(\frac{\bar{CR}}{Pr}\right)_{j+1}\right\} \quad (159)$$

and

$$E_2(i,j) = \frac{A^2(1-\zeta_j^2)^2}{2(\Delta\zeta)^2}\left(\frac{\bar{C}}{Pr}\right)_j . \quad (160)$$

The averaging procedure used in the rate equation, $\bar{\omega}^*$, is very important, due primarily to the exponential dependence of ω^* on the temperature. In order to speed convergence, it is helpful to include the influence of the rate equation in the coefficients of the unknown temperature and degree of dissociation in equations (158) and (155), respectively. This is done by linearly averaging the rate equation as follows:

$$\bar{\omega}^* = \frac{\omega^*_{i+1,j} + \omega^*_{i,j}}{2} . \quad (161)$$

Following the suggestion of Fay and Kaye[31], the rate equation at the

i + 1st station is written as a Taylor's series expansion from the ith station.

$$\omega^*_{i+1,j} = \omega^*_{i,j} + \left(\frac{\partial\omega^*}{\partial\alpha}\right)_{p,T}\Bigg|_{i,j}\left(\alpha_{i+1,j} - \alpha_{i,j}\right) + \left(\frac{\partial\omega^*}{\partial T^*}\right)_{p,\alpha}\Bigg|_{i,j}\left(T^*_{i+1,j} - T^*_{i,j}\right). \tag{162}$$

Substituting equation (162) into equation (161) gives $\bar{\omega}^*$:

$$\bar{\omega}^* = \omega^*_{i,j} + \frac{1}{2}\left(\frac{\partial\omega^*}{\partial\alpha}\right)\Bigg|_{i,j}\left(\alpha_{i+1,j} - \alpha_{i,j}\right) + \frac{1}{2}\left(\frac{\partial\omega^*}{\partial T^*}\right)\Bigg|_{i,j}\left(T^*_{i+1,j} - T^*_{i,j}\right) \tag{163}$$

where the subscripts on the derivatives have been dropped. Substituting equation (163) into the species conservation equation (155) and regrouping terms gives

$$\begin{aligned}
&\alpha_{i+1,j-1}\left[-C_1(i,j) - C_2(i,j)\right] + \alpha_{i+1,j}\left[\frac{\bar{u}^*_j}{2\Delta s^*} + 2C_2(i,j) - \frac{1}{2}\left(\frac{\partial\omega}{\partial\alpha}\right)_{i,j}\right] \\
&\qquad + \alpha_{i+1,j+1}\left[C_1(i,j) - C_2(i,j)\right] \\
&= \alpha_{i,j-1}\left[C_1(i,j) + C_2(i,j)\right] + \alpha_{i,j}\left[\frac{\bar{u}^*_j}{2\Delta s^*} - 2C_2(i,j) - \frac{1}{2}\left(\frac{\partial\omega}{\partial\alpha}\right)_{i,j}\right] \\
&\qquad + \alpha_{i,j+1}\left[-C_1(i,j) + C_2(i,j)\right] \\
&\qquad + \left[\omega^*_{i,j} + \frac{1}{2}\left(\frac{\partial\omega^*}{\partial T^*}\right)_{i,j}\left(T^*_{i+1,j} - T^*_{i,j}\right)\right]
\end{aligned} \tag{164}$$

where $C_1(i,j)$ and $C_2(i,j)$ are given by equations (156) and (157). Similarly, the generalized energy equation (158) becomes

$$T^*_{i+1,j-1}\left[-E_1(i,j) - E_2(i,j)\right] \tag{165}$$

$$+ T^*_{i+1,j}\left[\frac{\bar{u}^*_j}{2\Delta s^*} + 2E_2(i,j) + \frac{R_m}{2C_p}(\theta^*_d + \bar{T}^*)\left(\frac{\partial\omega^*}{\partial T^*}\right)_{i,j}\right]$$

$$+ T^*_{i+1,j+1}\left[E_1(i,j) - E_2(i,j)\right] = T^*_{i,j-1}\left[E_1(i,j) + E_2(i,j)\right]$$

$$+ T^*_{i,j}\left[\frac{\bar{u}^*_j}{2\Delta s^*} - 2E_2(i,j) + \frac{R_m}{2C_p}(\theta^*_d + \bar{T}^*)\left(\frac{\partial\omega^*}{\partial T^*}\right)_{i,j}\right]$$

$$+ T^*_{i,j+1}\left[-E_1(i,j) + E_2(i,j)\right] - \frac{R_m(\theta^*_d+\bar{T}^*)}{C_p}\left[\omega^*_{i,j} +\right.$$

$$\left.\frac{1}{2}\left(\frac{\partial\omega^*}{\partial\alpha}\right)_{i,j}(\alpha_{i+1,j} - \alpha_{i,j})\right]$$

$$+ \frac{A^2(1-\zeta^2)^2}{4(\Delta\zeta)^2}\left(\frac{CE}{R}\right)\left[\left(u^*_{i,j-1} - u^*_{i,j+1}\right)\left(u^*_{i+1,j-1} - u^*_{i+1,j+1}\right)\right]$$

where $E_1(i,j)$ and $E_2(i,j)$ are given by equations (159) and (160).

The derivatives of the rate equation are obtained by differentiating equation (133), yielding:

$$\left(\frac{\partial\omega^*}{\partial\alpha}\right)_{p,T} = -\frac{2KT^{*n}\rho^*}{(1+\alpha)}\left[e^{-\frac{\theta^*_d}{T^*}} + \alpha\frac{\rho^*}{\rho^*_d}\right] \tag{166}$$

and

$$\left(\frac{\partial \omega^*}{\partial T}\right)_{p,\alpha} = KT^{*n-1}\rho^*\left[(1 - \alpha)e^{-\frac{\theta_d^*}{T^*}}\left(\frac{\theta_d^*}{T^*} + n - 1\right)\right. \tag{167}$$

$$\left. + \frac{\rho^*}{\rho_d^*}\alpha^2(2 - n)\right] .$$

The interval $-1 \leq \zeta \leq 1$ is divided into 2N segments with the grid points $j = \pm N$ corresponding to $\zeta = \pm 1$ and $j = 0$ is $\zeta = 0$ (the dividing streamline). Each equation in the set (152), (164), and (165) represents a set of 2N-1 equations, since each equation is valid at the 2N-1($i = -N+1, \ldots -1,0,+1, \ldots i = N-1$) grid points of the finite difference mesh. Therefore, each equation can be represented as a matrix equation. For example, the species conservation equation (164) is written

$$Z_{mn}\,\alpha_n = d_m \tag{168}$$

where α_n represents the unknown quantity $\alpha_{i+1,n}$, Z_{mn} contains the corresponding coefficients of $\alpha_{i+1,n}$, and d_m is the right-hand side of equation (164), also known.

The boundary conditions (149) for the three sets of equations (152), (164), and (165) are specified at $j = N(\zeta = 1)$ and $j = -N(\zeta = -1)$, and are incorporated into the known vector d_m. Due to the choice of finite difference approximations, the resulting form of Z_{mn} is tridiagonal (i.e., the only non-zero elements in the matrix are those along the main diagonal element and the elements to either side of the main

diagonal) and can be rapidly solved using a method of Gaussian elimination known as "line inversion" described in reference [32].

In the finite difference scheme used in this thesis, with the rate equation averaged according to equation (163), the parameter K, given in equation (134), appears in both Z_{mn} and d_n. By Cramer's rule, the solution for α is a quotient of two determinants, each now containing K, so that for near equilibrium flow as K approaches infinity, the solution is bounded. If, on the other hand, $\bar{\omega}^*$ in equations (155) and (156) was calculated based on the linearly averaged $\bar{T}^*$ and $\bar{\alpha}$, i.e.,

$$\bar{\omega}^* = \omega^*(\bar{T}^*, \bar{\alpha}) \ ,$$

then K would appear only in d_n. Actual computing experience using the latter scheme has shown the convergence to be very slow for near equilibrium flow.

The continuity equation (143) is first order and is solved explicitly. The values of u^* are known on the columns i and i+1 from the solution of the momentum equation (152), so that the continuity equation (143) is used to evaluate $\bar{v}^*$ on the line i+1. Following the suggestion of Wu[27], the continuity equation (143) is evaluated by the use of an averaged backward difference approximation for the s^*-derivative,

$$\frac{\partial u^*}{\partial \zeta} = \frac{u_{i+1,j} - u_{i,j} + u_{i+1,j-1} - u_{i,j-1}}{2\Delta s^*} \qquad (169)$$

and a central difference approximation for the ζ-derivative

$$\frac{\partial v^*}{\partial \zeta} = \frac{v^*_{i+1,j} - v^*_{i+1,j-1}}{\Delta\zeta} \quad . \tag{170}$$

For points above the dividing streamline ($\zeta > 0$), the continuity equation is solved explicitly for v* as follows:

$$v^*_{i+1,j} = v^*_{i+1,j-1} - \frac{\Delta\zeta}{2A\Delta s^*}\left[\frac{u^*_{i+1,j} - u^*_{i,j} + u^*_{i+1,j-1} - u^*_{i,j-1}}{\left[1 - \frac{(\zeta_j - \zeta_{j-1})^2}{4}\right]}\right] . \tag{171}$$

The solution begins with the boundary condition v* = 0 on the dividing streamline, $j = 0(\zeta = 0)$, and marches upward to $j = N(\zeta = 1)$.

The solution for the normal velocity below the dividing streamline marches downward from j = 0 by means of the explicit relation

$$v^*_{i+1,j} = v^*_{i+1,j+1} + \frac{\Delta\zeta}{2A\Delta s^*}\left[\frac{u^*_{i+1,j} - u^*_{i,j} + u^*_{i+1,j+1} - u^*_{i,j+1}}{\left[1 - \frac{(\zeta_j - \zeta_{j+1})^2}{4}\right]}\right] , \tag{172}$$

which is simply a convenient rearrangement of equation (171) obtained by replacing j by j + 1 and solving for $v^*_{i+1,j}$.

Initial Profiles

Initial profiles of the Wu[27] type were selected for the free shear layer calculations. For all grid points above the dividing streamline, the initial conditions were given as

$$\left.\begin{aligned} u^* &= 1 \\ \alpha &= \alpha_\infty \\ T^* &= 1 \end{aligned}\right\} \quad \begin{aligned} &0 < \zeta \leq 1 \ , \\ &s^* = 0 \end{aligned} \tag{173}$$

while on and below the dividing streamline, the initial conditions are

given by

$$\left.\begin{aligned} u^* &= 0 \\ \alpha &= \alpha_{es} \\ T^* &= \frac{T_s}{T_\infty} \end{aligned}\right\} \qquad \begin{matrix} -1 \le \zeta \le 0 \ , \\ s^* = 0 \end{matrix} \tag{174}$$

where T_s is the specified stagnation region temperature, and α_{es} is the corresponding equilibrium degree of dissociation. The initial vertical velocity is zero at all grid points.

$$v^* = 0 \qquad \begin{matrix} -1 \le \zeta \le 1 \ . \\ s^* = 0 \end{matrix} \tag{175}$$

Iterative Procedure

The momentum equation is dependent on the temperature and degree of dissociation through the term $\rho^*\mu^*$. This coupling is not strong, and the following procedure, illustrated in Figure 15, is used.

For the first approximation, the product $\overline{\rho^*\mu^*}$ is computed based on the known fluid properties at station i, and the average velocities $\bar{u}^*$ and $\bar{v}^*$ are set equal to the velocities $u^*_{i,j}$ and $v^*_{i,j}$, respectively. The momentum equation (152) is solved by "line inversion," and the resulting values of $u^*_{i+1,j}$ are used in the continuity equations (171) and (172) to find $v^*_{i+1,j}$. New values of $\bar{u}^*$ and $\bar{v}^*$ are computed by linear averaging, and the solutions are iterated until the changes in $\bar{u}^*$ and $\bar{v}^*$ between iterations is less than one tenth of one per cent.

With the above "u-v" iterations completed, the average velocities u^* and v^* are used in the solution of the species conservation (164) and

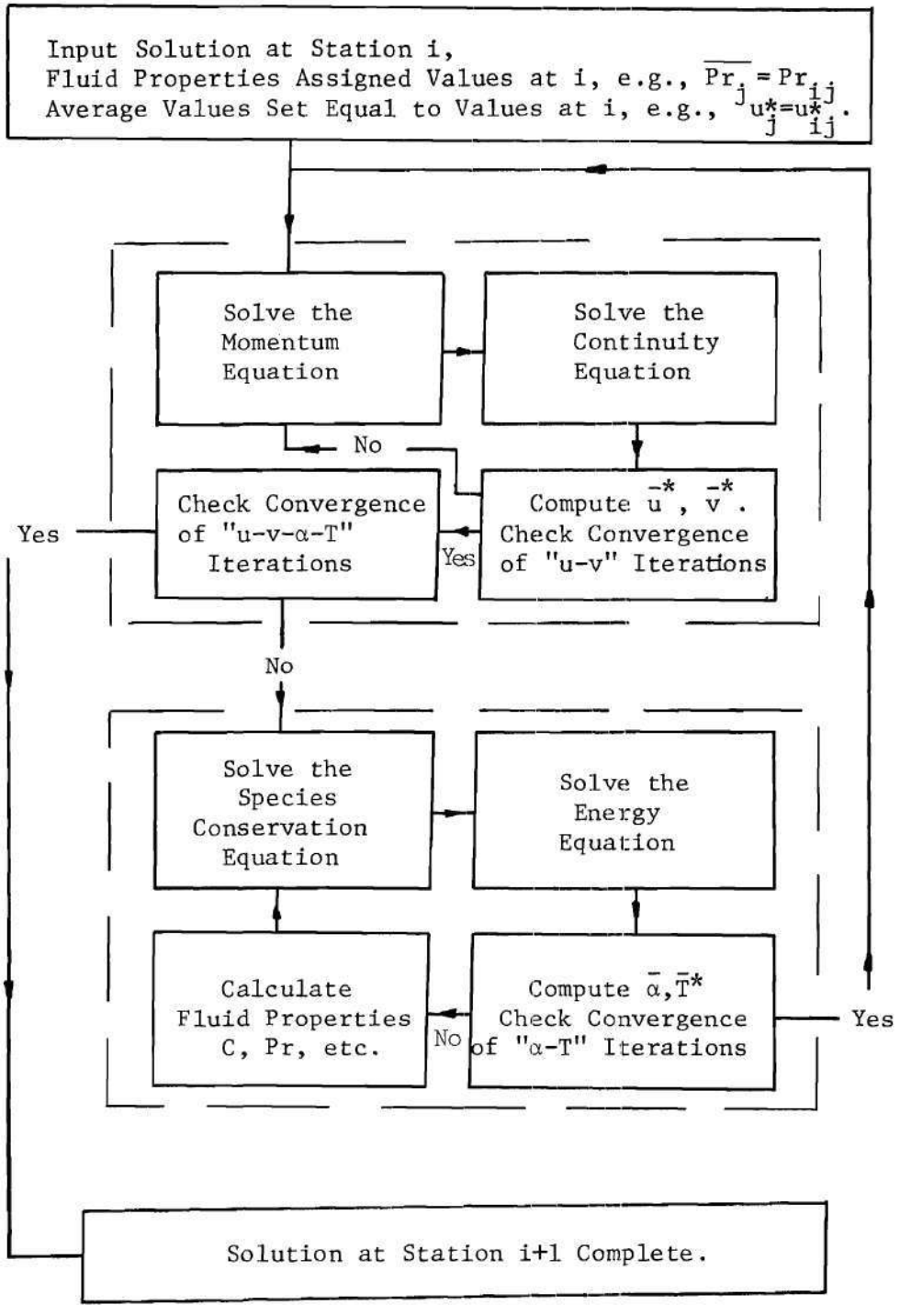

Figure 15. Iteration Procedure for the Finite Difference Solution

energy (165) equations. The rate equation (133) and its derivatives (166) and (167) are computed at station i and remain fixed. For the first iteration, the average degree of dissociation $\bar{\alpha}$ and temperature $\bar{T}^*$ are assumed to be given by $\alpha_{i,j}$ and $T^*_{i,j}$ and the average fluid properties (132) are computed. The species conservation equation (164) and the energy equation (165) are solved by "line inversion." New average values of $\bar{\alpha}$ and $\bar{T}^*$ are computed by linear averaging, and new average fluid properties are calculated. The "α-T" iterations continue until the successive values of $\bar{\alpha}$ and $\bar{T}^*$ change less than one tenth of one per cent.

For subsequent approximations, the last computed values of $\bar{\alpha}$ and $\bar{T}^*$ are used to compute $\overline{\rho^*\mu^*}$. The entire procedure is repeated until all average values vary less than one tenth of one per cent between successive approximations.

Stability and Convergence

The first important consideration which must be given to a finite difference approximation to a partial differential equation is that of stability. If a finite difference equation is stable, then any small error, such as roundoff error, introduced at a point in the calculation decays as the solution proceeds. An unstable solution propagates and magnifies these errors so that the solution becomes invalid. One of the advantages of the implicit type of equation used in this solution is that there is generally no restriction of the ratio of step sizes, Δs^* to $\Delta\zeta$, such as encountered in explicit types of solutions [30]. As will be shown, there are restrictions on the coefficients of certain terms in the equations.

The second consideration is that of "convergence," i.e., does the solution of the finite difference equation converge to the solution of the differential equation as the grid spacings are decreased. Existing evidence indicates that a finite difference approximation which is stable is also convergent (for example, see reference [30]), and thus the question of convergence will not be considered here.

No special consideration need be given to the continuity equations (171) and (172) since they are first order and the random round-off errors are simply added at each station, and thus it is stable.

If the non-linear terms encountered in the remaining three equations (152), (164), and (165) are replaced by average values, which are assumed to be known, a von Neumann stability analysis may be used. This method (see, for example, references [30] and [15]) introduces an error distribution and investigates the propagation of the error. The requirement that the eigenvalue of the resulting matrix be less than unity in magnitude imposes the conditions of stability.

For the momentum equation (152), the requirement is

$$\frac{A^2(1-\zeta_j^2)^2\bar{C}_j\Delta s^*}{2\bar{u}_j^*(\Delta\zeta)^2} \geq 0 \ , \qquad (176)$$

which requires $\bar{u}_j^* \geq 0$, or no regions of reversed flow. Because of this requirement, great care must be exercised in the acceptance of the first profiles of the velocity. Because of the large initial gradient, the first velocity profiles generated tend to have a small negative velocity due to numerical error. The equations must be iterated until this vanishes.

For the species continuity equation (164), the criterion is

$$\frac{A^2(1-\zeta_j^2)^2}{\left[2\ \bar{u}_j^* - \left(\frac{\partial \omega^*}{\partial \alpha}\right)_j\right]}\left(\frac{\bar{C}}{Sc}\right)_j \frac{\Delta s^*}{(\Delta\zeta)^2} \geq 0 \ . \qquad (177)$$

Since $\bar{u}^* > 0$, $\left(\frac{\bar{C}}{Sc}\right) \geq 0$, and $\left.\frac{\partial \omega^*}{\partial \alpha}\right|_{p,T} \leq 0$, there is no new restriction on stability.

The energy equation (165) is stable if

$$\frac{A^2(1-\zeta_j^2)^2}{\left[2\ \bar{u}_j^* + \frac{(\theta_d^*+\bar{T}^*)R_m}{C_p}\left(\frac{\partial \omega^*}{\partial T^*}\right)_j\right]}\left(\frac{\bar{C}}{Pr}\right)_j \frac{\Delta s^*}{(\Delta\zeta)^2} \geq 0 \ . \qquad (178)$$

Since the thermodynamic and transport properties are always positive, the solution is stable, since $\left(\frac{\partial \omega}{\partial T^*}\right)_{p,\alpha} \geq 0$.

The sign of the derivatives of the rate of atom production equations can be obtained from the mathematical expressions (166) and (167) or from physical reasoning. If a volume of partially dissociated gas is disturbed from equilibrium by the sudden addition of atoms, while maintaining a constant temperature, the system will be required to recombine some atoms to molecules in order to return to equilibrium, $(-\omega)$. Similarly, increasing the temperature of a closed system at equilibrium will require a further increase in atoms $(+\omega)$ to reach equilibrium.

Chemical Relaxation Parameter

A chemical relaxation parameter, defined by $\tau^* = \frac{\tau u}{x}$, is introduced to indicate the flow process in the shear layer. Since τ represents the chemical relaxation time and x/u represents the flow time,

the ratio τ^* is indicative of the local relaxation process. For example, frozen flow is approached as τ^* approaches infinity, while τ^* approaching zero, indicates equilibrium flow. Using equation (96), the parameter τ^* is

$$\tau^* = \frac{u}{xC_f T^n \rho} \left\{ e^{-\frac{\theta_d}{T}} \left[1 + \left(\frac{\theta_d}{T} + n \right) \frac{(1-\alpha)}{(1+\alpha)} \right] - \frac{\rho}{\rho_d} \left[\frac{n\alpha^2}{(1+\alpha)} - 2\alpha \right] \right\}^{-1} . \quad (179)$$

This expression is written in terms of the dimensionless variables by use of equations (131) and (134):

$$\tau^* = \frac{u^*}{s^* T^{*n} \rho^* K} \left\{ e^{-\frac{\theta_d^*}{T^*}} \left[1 + \left(\frac{\theta_d^*}{T^*} + n \right) \frac{(1-\alpha)}{(1+\alpha)} \right] - \frac{\rho^*}{\rho_d^*} \left[\frac{n^2}{(1+\alpha)} - 2\alpha \right] \right\}^{-1} .$$

Check of the Solution Method

In Appendix C, the finite difference solutions for laminar mixing are compared with solutions available in the literature. In particular, the velocity profiles for low temperatures are compared with Chapman's[13] similar solution; and the degree of dissociation profiles are compared with the profiles of Kovitz and Hoglund[34] for the case of the mixing of two streams with the same velocity but different degrees of dissociation. For these problems the flow is considered to be frozen and thus, only diffusion and convection are involved. It is shown in Appendix C that the finite difference solutions give results in good agreement with the similar solutions.

Extension of Chapman's Similar Solutions to the Analysis of the Frozen Flow of a Dissociated Gas

Under special circumstances, it is possible to reduce the governing partial differential equations to ordinary differential equations in terms of a single "similarity" variable. The variable boundary conditions, and especially the finite reaction rates, which are essential to this thesis, destroy the possibility of similarity. However, if the flow is considered to be frozen, constant boundary conditions are specified, and the properties are assumed to be constant; flow similarity is assured. The resulting similarity solutions can be used for comparison with the finite difference solution.

Chapman[13,33] has investigated the laminar shear layer for an undissociated gas, and obtained solutions for the velocity and enthalpy profiles. The density-viscosity product and the Prandtl number are considered to be constant.

In Appendix B, similar solutions are obtained for the frozen flow of a dissociated gas. The properties are assumed to be constant and the Lewis number is taken to be unity. In this thesis, the term "constant properties" is used to denote constant values of Pr, Sc, and C.

The momentum, species conservation, and energy equations become ordinary differential equations when written in terms of the similarity variable

$$\eta_c = \frac{\eta_{bl}}{\sqrt{C}} , \tag{180}$$

where

$$\eta_{b1} = \frac{Y^*}{\sqrt{s^*}} \tag{181}$$

is the usual Blasius similarity variable. The resulting momentum equation is uncoupled from the energy and species conservation equations. The momentum equation has been solved by Chapman[13].

The energy equation for the frozen flow of a dissociated gas with constant properties is identical to the energy equation investigated by Chapman[33]. The differential equation is non-homogeneous and the resulting solution is written

$$h^* = 1 + (h_s^* - 1)\, g_1(\eta_c, Pr) + \frac{U_\infty^2}{2h_\infty}\, g_2(\eta_c, Pr) \ . \tag{182}$$

Profiles of the functions g_1 and g_2 are tabulated in Reference [33] for various Prandtl numbers.

When written in similarity form, the species conservation equation for frozen flow is identical to the homogeneous part of the energy equation. The solution is given by

$$\alpha = \alpha_\infty + (\alpha_s - \alpha_\infty)\, g_1(\eta_c, Sc) \ . \tag{183}$$

Thus, Chapman's profiles of g_1 provide the solution of the species conservation equation.

Results and Discussion

Since the laminar free shear layer for a dissociating gas has not been previously analyzed, several cases are presented and discussed.

First, the frozen flow limit is investigated. The recirculation

region temperature is taken to be low, to increase the time ratio τ^*. Finite difference solutions were obtained for finite rate flow with variable properties, frozen flow with variable properties, and frozen flow with constant properties. The finite difference solutions for constant properties are compared with the similar solution (Appendix C) as a further check on the finite difference solution. The variable property profiles are compared with the constant property profiles to evaluate the assumption of constant properties.

The second case considers nearly equilibrium flow. Profiles for frozen, finite rate, and equilibrium flow are compared.

The third case considers a cool freestream mixing with a hot dissociated stagnation region. The conditions are selected to give results controlled by finite rate reactions. Solutions for frozen, finite rate, and equilibrium flow are compared.

Case 1

$M_\infty = 2.0$

$p_\infty = 0.01$ atmosphere

Gas - Oxygen

$T_\infty = 4240^\circ$ K $\qquad$ $T_s = 1950^\circ$ K

$\alpha_\infty = 0.996$ $\qquad$ $\alpha_s = \alpha_{es} = 0.002$

At $x_s = 3$ meters, the freestream τ^* was found to be 15 and on the dividing streamline $\tau^* = 1.88$. The difference in temperature and degree of dissociation profiles for frozen and finite rate flow was found to be small, as indicated by the large values of τ^*.

The finite difference velocity profiles for variable C and constant C are compared with Chapman's[13] similar solution in Figure 16. For the present example, which involves variable C, an average value of C(= 1.544), as obtained using the method mentioned in Appendix C, was used in the finite difference solution with constant C and in the conversion of the similar solution from η_c to η_{b1}. It is seen that the finite difference solution with constant C exhibits very good agreement with Chapman's solution. However, the agreement with the variable property solution appears rather poor.

As shown in Figure 17, however, if the average value of C is taken to be 1.0, the constant C solution gives a better approximation to the variable C solution. Thus, if an appropriate average value of C is chosen, the similar solution does give a fair representation of the velocity profile for variable C. The method of selecting an average value of C as suggested by Eckert and discussed in Appendix C, however, is not adequate for dissociated gases. Furthermore, since the dividing streamline is located at $\eta_c = 0$, the average value of C has no influence on the dividing streamline velocity. This value is required in the evaluation of the base pressure for closed bases.

Degree of dissociation profiles for frozen flow with variable properties and frozen flow with constant properties (Sc = 1.0 and Sc = 0.655) are presented in Figure 18. The conversion from η_c to η_{b1} was accomplished using C = 1.0.

Figure 18 indicates that the effect of variable Schmidt number on the degree of dissociation profile is rather large and the error incurred by assuming a constant value of the Schmidt number is also rather

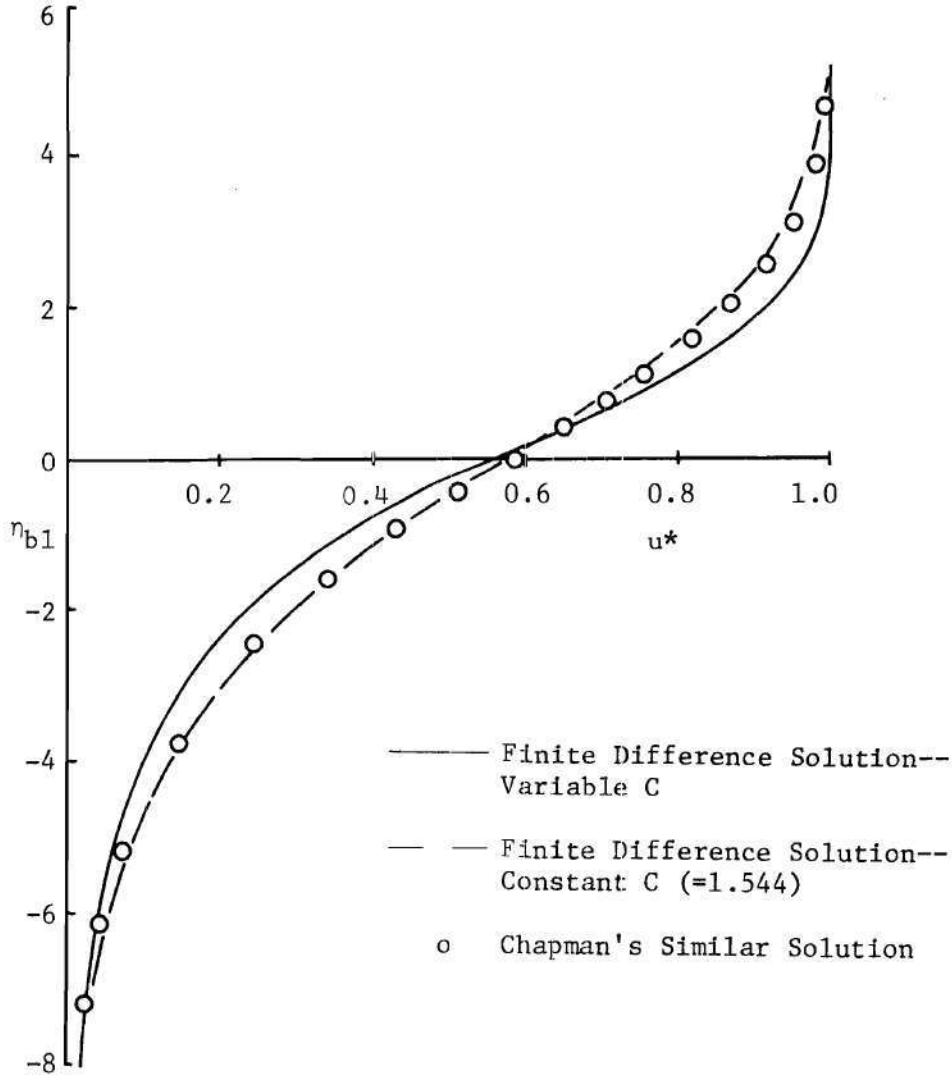

Figure 16. Comparison of Velocity Profiles from the Finite Difference Solution for Variable and Constant C (1.544) with Chapman's Solution

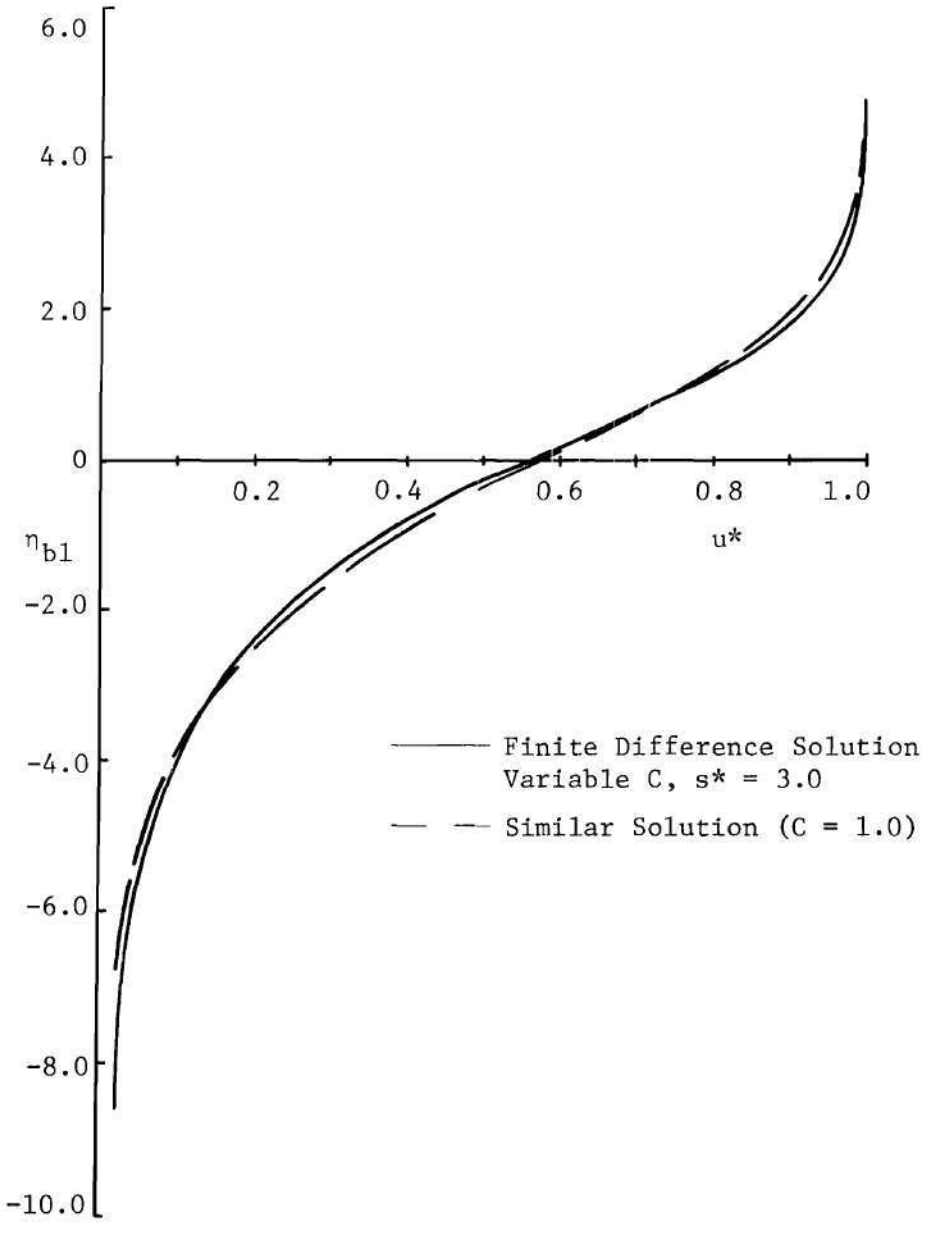

Figure 17. Comparison of the Constant Property "Best Fit" (C = 1.0) Velocity Profile with the Variable Property Solution

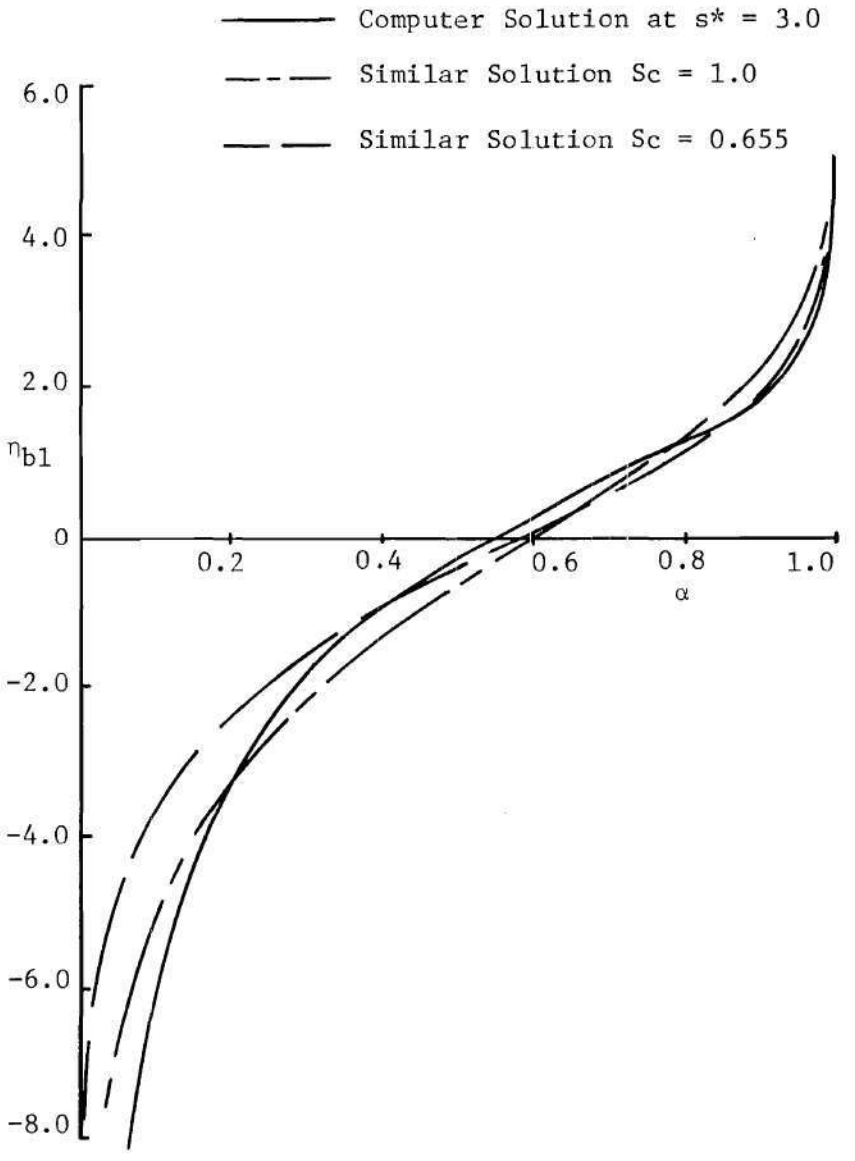

Figure 18. Comparison of the Degree of Dissociation Profiles for Variable and Constant Properties (Frozen Flow)

large. Note that for similar solutions the degree of dissociation on the dividing streamline, as opposed to the velocity, depends on the assumed value of the Schmidt number.

The temperature profiles for frozen flow with variable properties and frozen flow with constant properties (Pr = 1.0 and Pr = 0.655, Le = 1.0) are shown in Figure 19. Although the Prandtl number is nearly constant, the temperature is strongly dependent on the degree of dissociation and the agreement is not good.

The velocity, degree of dissociation, and temperature on the dividing streamline are summarized in Table 1. These values are required in the determination of the base pressure for cases without base bleed.

Table 1. Comparison of the Flow Properties on the Dividing Streamline

Chemical Rate Assumption	Property Assumption	u^*	α	T^*
Finite Rate	Variable	0.557	0.585	0.986
Frozen	Variable	0.558	0.547	1.097
Frozen	Pr = Sc = 0.655	0.587	0.606	1.089
Frozen	Pr = Sc = 1.00	0.587	0.586	1.158

Case 2

$M_\infty = 2.0$

$p_\infty = 1.0$ atmosphere

Gas - Oxygen

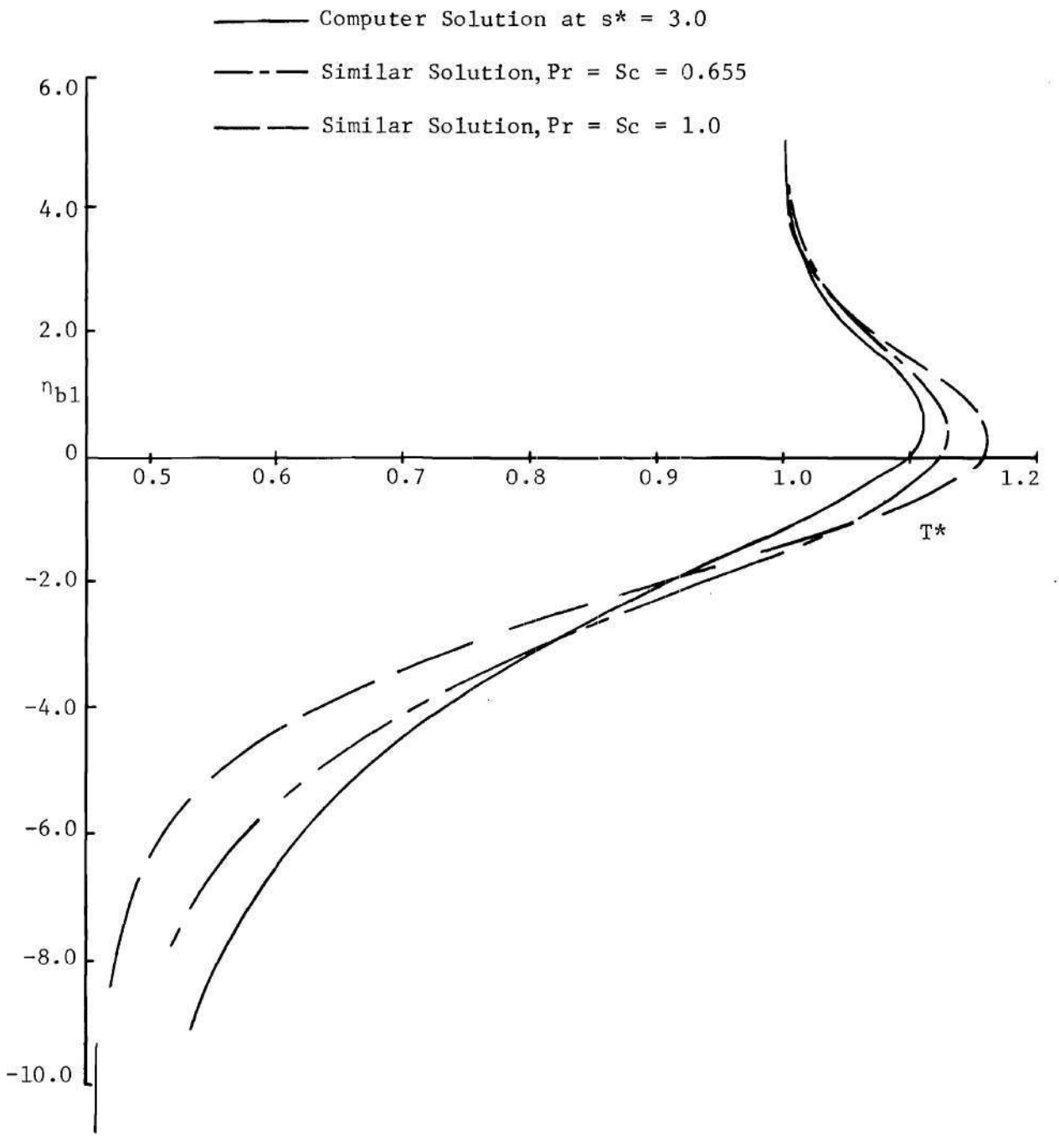

Figure 19. Comparison of the Temperature Profiles for Variable and Constant Properties (Frozen Flow)

$T_\infty = 4240^\circ$ K $\qquad T_s = 1950^\circ$ K

$\alpha_\infty = \alpha_{e\infty} = 0.753 \qquad \alpha_s = \alpha_{es} = 0.000$

Note that the Mach number and temperatures are the same as Case 1, but the pressure is increased and the resulting equilibrium dissociation degrees are lowered. Correspondingly, the time ratio at x_s= 3 meters was found to be 3.6×10^{-2} in the freestream and 3.4×10^{-2} on the dividing streamline.

Variable property solutions were obtained by the finite difference method for frozen, finite rate, and equilibrium flow.

The velocity profiles are shown in Figure 20. The profiles for all three rate considerations are a single curve. This illustrates the weak coupling between the momentum and continuity equations, and the species conservation and energy equations. Note however that the dividing streamline velocity, u*, at x_s= 3 meters in this case is about 0.562 whereas it was about 0.557 with a pressure of 0.01 atmosphere.

The profiles for the temperature and the degree of dissociation at x_s= 3 meters are presented in Figures 21 and 22. As predicted by the small values of τ^*, the curves for finite rate flow and equilibrium flow are indistinguishable. Since the heat of dissociation is very high, the temperature is strongly dependent on the degree of dissociation. The chemical reactions tend to smooth out the temperature profile in this case and lower the temperature of the dividing streamline.

Within the mixing region v* is always greater than or equal to zero. Thus, below the dividing streamline, the convection is always toward the dividing streamline while above the dividing streamline, the

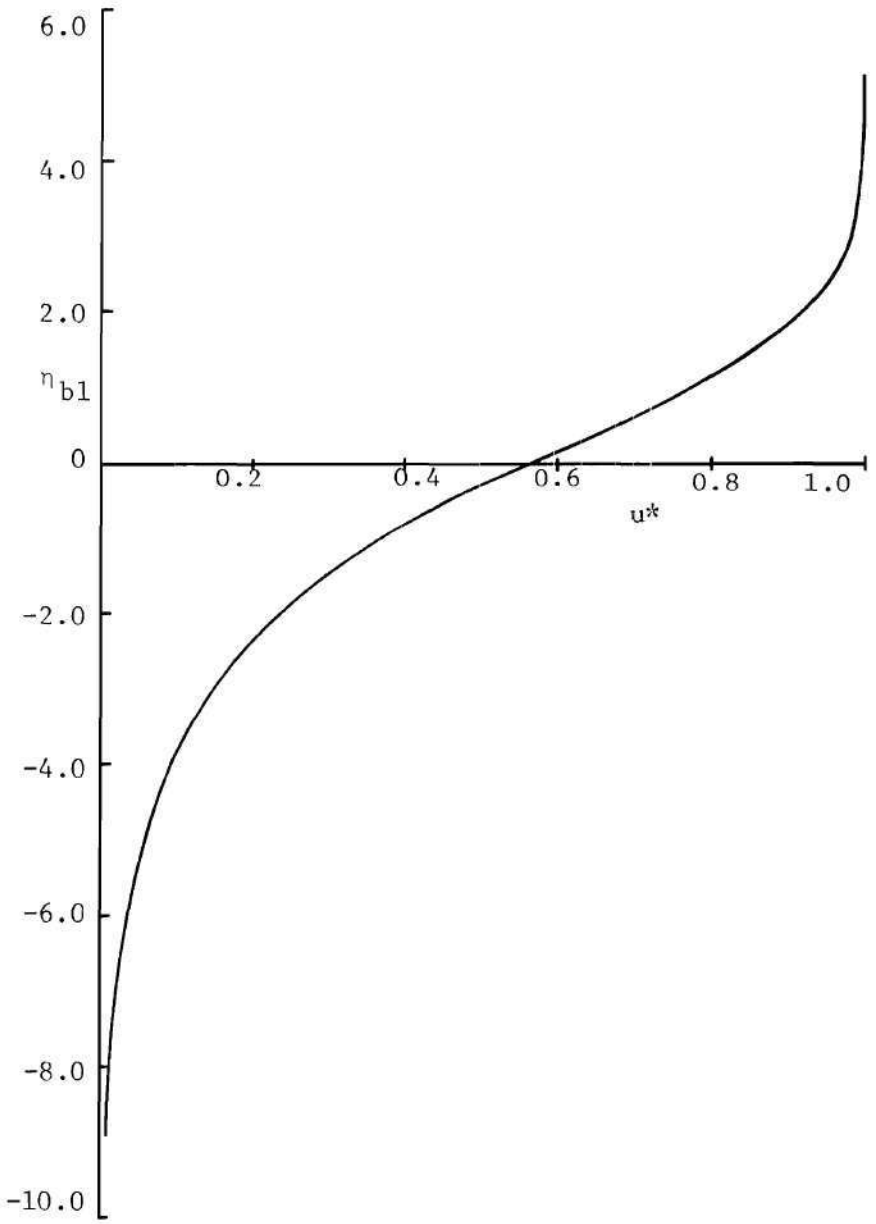

Figure 20. Velocity Profiles at x_s = 3 Meters

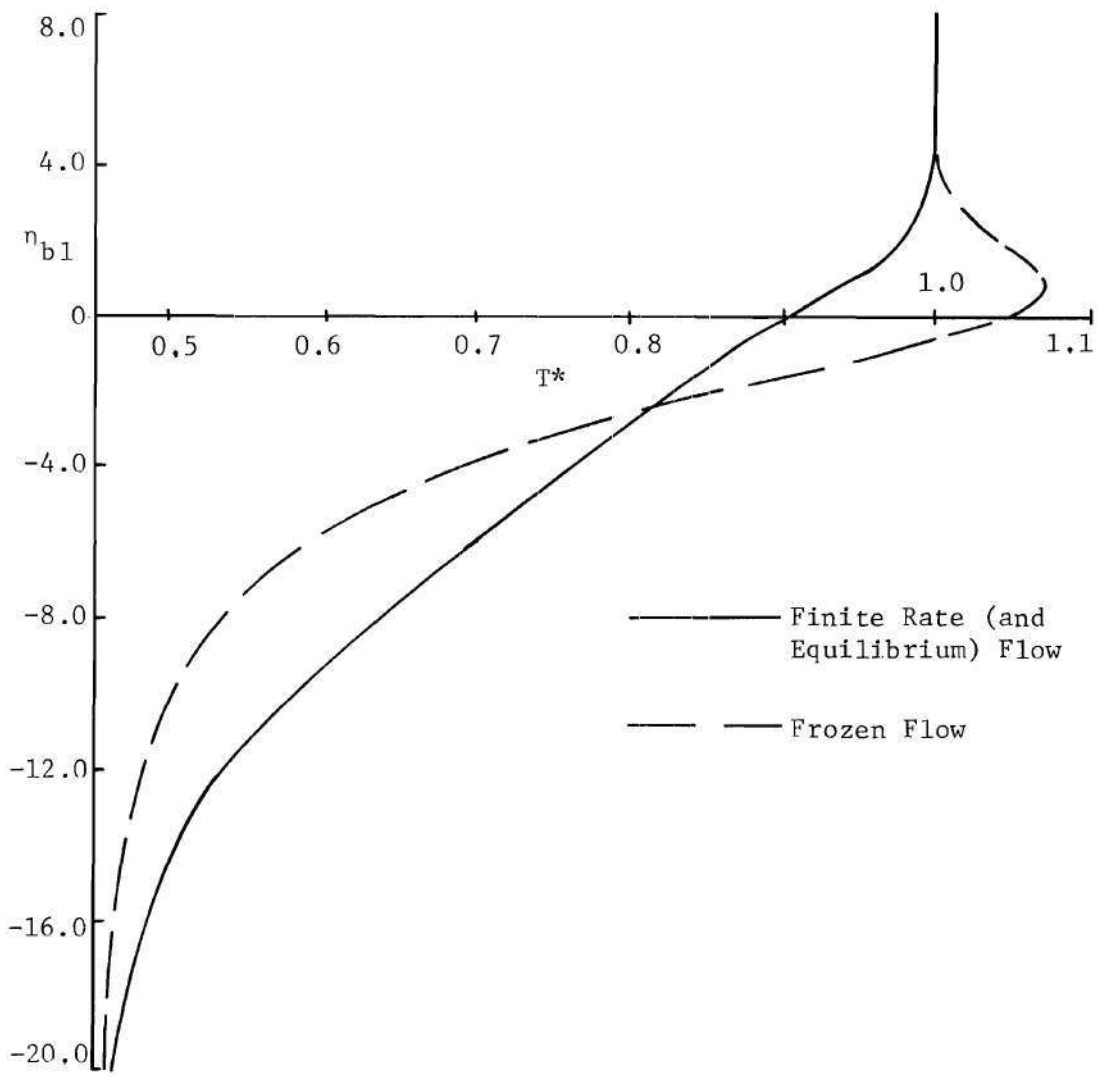

Figure 21. Temperature Profiles at x_s = 3 Meters for Frozen, Finite Rate, and Equilibrium Flow

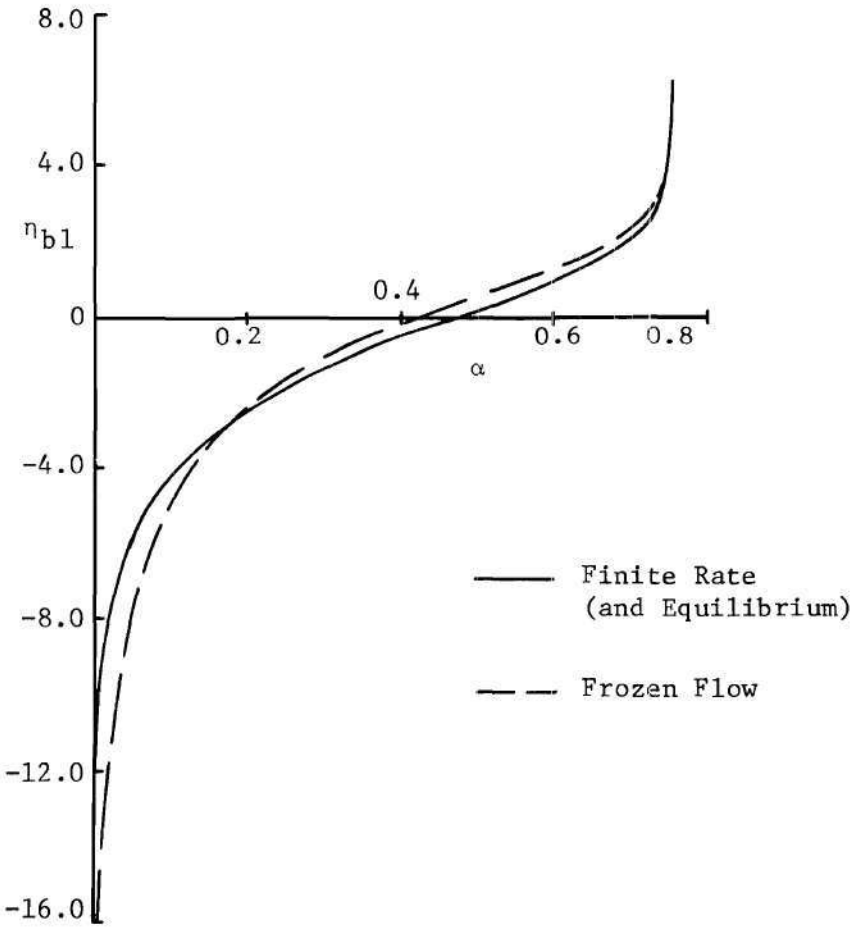

Figure 22. Degree of Dissociation Profiles at $x_s = 3$ Meters for Frozen, Finite Rate, and Equilibrium Flow

the convection is always away from the dividing streamline. By definition, v* is zero on the dividing streamline. Diffusion and heat conduction across the dividing streamline do occur, however, resulting in the transport of species and energy.

In the case under consideration, the atomic species concentration gradient causes the atoms to diffuse toward the stagnant region, i.e., the diffusion opposes the convection. If the flow is considered to be frozen, the atoms can penetrate a large distance below the dividing streamline. As atoms from the hot freestream are being diffused toward the stagnant region, molecules from the cool stagnant region are being diffused and convected toward the freestream.

If the flow is considered to be frozen, atoms entering the cooler region remain dissociated. If chemical reactions are allowed, recombination occurs. The heat of dissociation released during recombination thus increases the temperature of the gas below the dividing streamline. Similarly, molecular dissociation takes place in the high temperature region created by the viscous dissipation, and the temperature decreases.

Case 3

$M_\infty = 2.62$

$p_\infty = 0.0364$

Gas - Oxygen

$T_\infty = 1464^\circ$ K $\qquad$ $T_s = 3142^\circ$ K

$\alpha_\infty = 0.000$ $\qquad$ $\alpha_s = 0.407$

The temperature of the stagnant region is the frozen stagnation temperature of the freestream. At $x_s = 3$ meters, the time ratio τ^* is

about 4×10^6 in the freestream and 6 on the dividing streamline. The cool, high velocity freestream produces a large τ^*, indicating frozen flow, while in the stagnant region, the low velocity and high temperature give a low τ^*, indicating equilibrium flow.

The velocity profiles, shown in Figure 23, for frozen, finite rate, and equilibrium flow with variable properties are indistinguishable, with $u^* = 0.588$ on the dividing streamline. Although the dividing streamline velocity is the same as Chapman's, it is coincidental.

The degree of dissociation and temperature profiles at 3 meters are shown in Figures 24 and 25. In this example, the normal convection, atomic diffusion, and thermal conduction are all toward the freestream. The maximum temperature if found in the stagnant region. The dissociation degree and temperature profiles show that the degree of dissociation corresponding to equilibrium flow is always less than the frozen degree of dissociation and the equilibrium temperature is always greater than the temperature for frozen flow. The finite rate profiles indicate recombination is occurring throughout the shear layer.

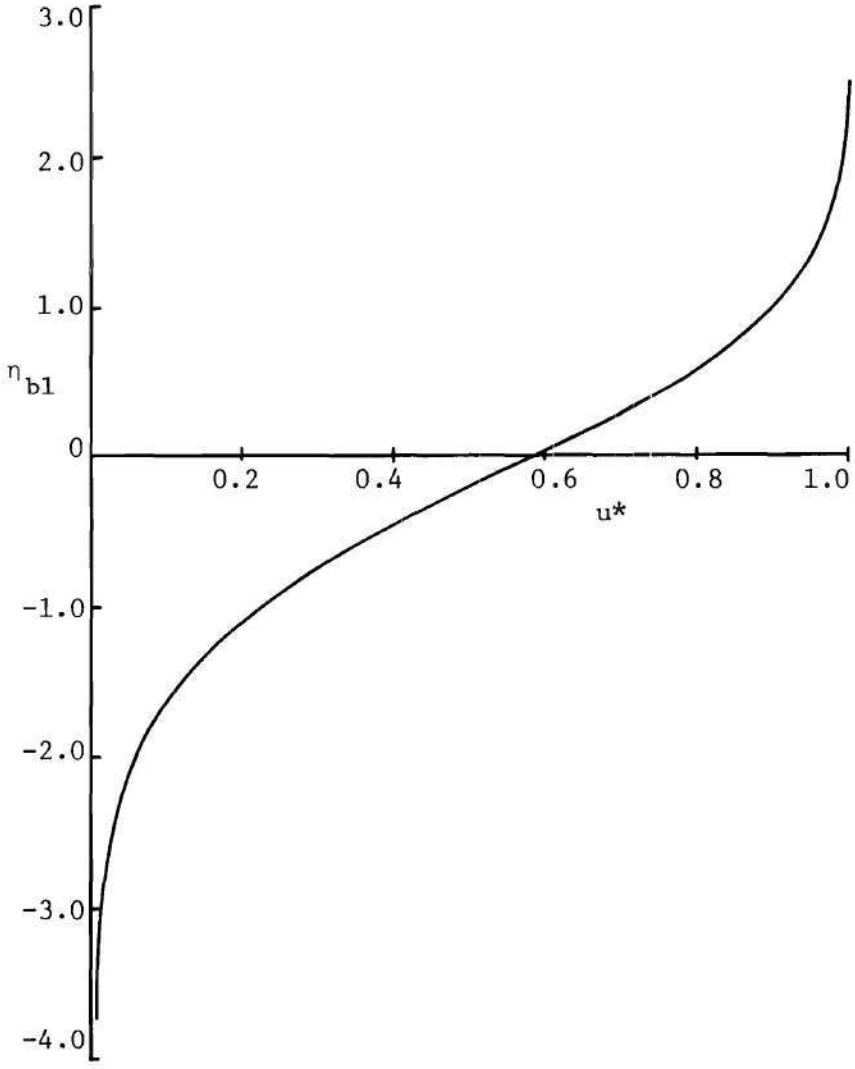

Figure 23. Velocity Profiles at $x_s = 3.0$

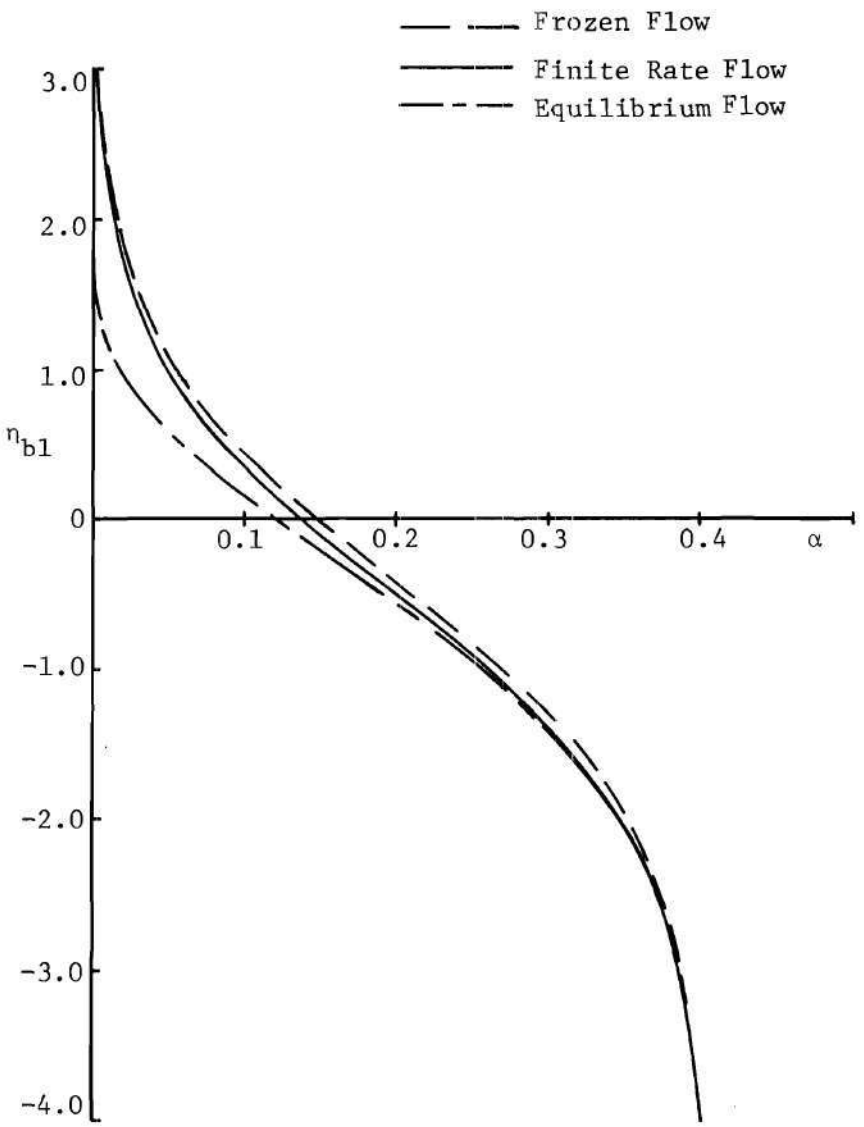

Figure 24. Degree of Dissociation Profiles at $x_s = 3$ Meters for Frozen, Finite Rate, and Equilibrium Flow

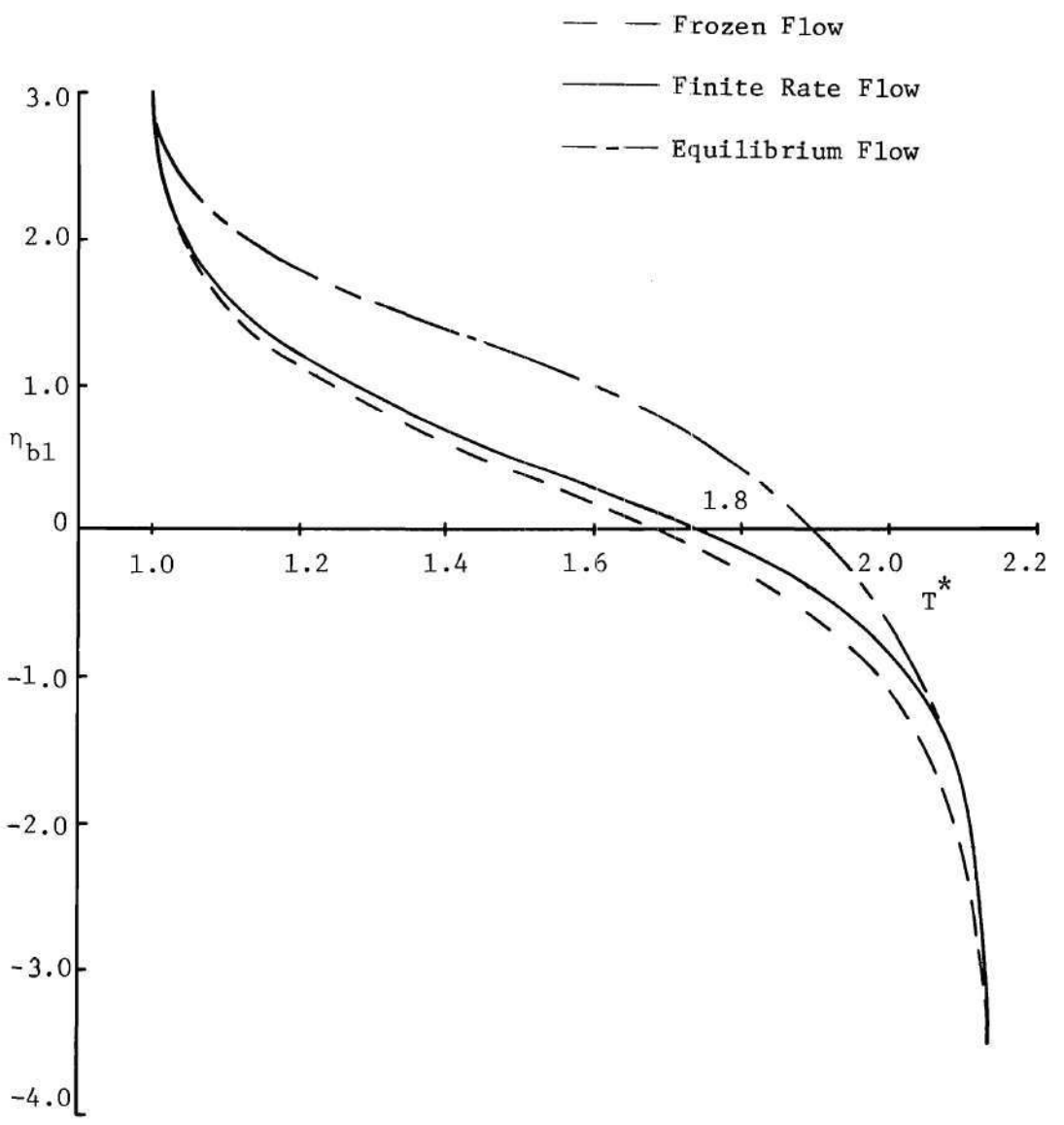

Figure 25. Temperature Profiles at x_s = 3.0 for Frozen, Finite Rate, and Equilibrium Flow

CHAPTER V

EVALUATION OF THE BASE PRESSURE

As discussed in Chapter II, an iterative process is used to obtain the base pressure. For a given set of flow conditions, M_∞, T_∞, p_∞, and T_B, a first guess of the base pressure, p_B, is made. The reference length, ℓ, is taken to be the base half height, H. The inviscid flow region consisting of the flow expansion to the base pressure and the subsequent chemical relaxation is computed by the method of characteristics as described in Chapter III. The computation of the inviscid flow region continues until the boundary of the inviscid flow intersects the base centerline. The frozen shock angle β_f (Figure 26) is obtained from the frozen oblique shock relations

$$\tan \theta_\ell - \frac{2 \cot \beta_f (M_{f_2}^2 \sin^2 \beta_f - 1)}{M_{f_2}^2 (\gamma_2 + \cos 2\beta_f) + 2} = 0 , \tag{184}$$

where

$$\gamma_2 = \frac{4+\alpha_2}{3} .$$

The pressure ratio across the shock, $\frac{p_3}{p_2}$, is obtained from

$$\frac{p_3}{p_2} = \frac{p_3}{p_B} = 1 + \frac{2\gamma_2}{\gamma_2+1}\left[M_2^2 \sin^2 \beta_f - 1\right] . \tag{185}$$

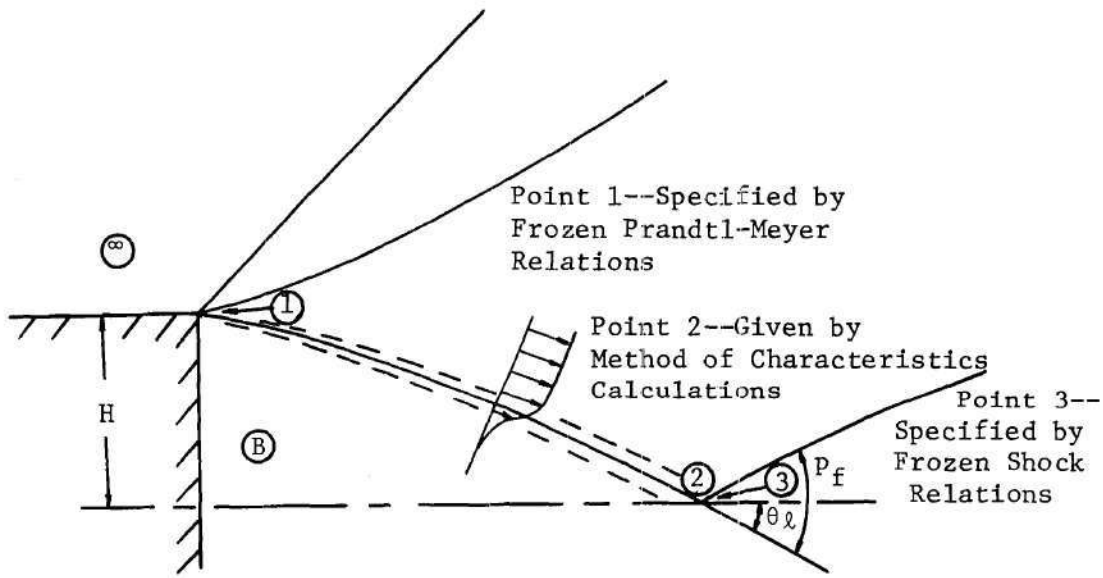

Figure 26. Flow Regions for Base Pressure Calculations

For the shear layer calculations, the initial velocity, temperature, and degree of dissociation profiles are step profiles. The initial values above the dividing streamline correspond to the conditions following the frozen expansion of the inviscid flow. The initial u velocity on and below the dividing streamline is zero and the degree of dissociation is the equilibrium value, α_{eB}, corresponding to the assumed base pressure, p_B, and the specified value of T_B. The vertical velocity is zero at the initial station.

The boundary conditions for temperature and degree of dissociation at $\zeta = +1$, are specified functions of s*, previously obtained from the inviscid solution. The pressure throughout the mixing region is a constant, p_B. The boundary conditions at $\zeta = -1$ are $u = 0$, $T = T_B$, and $\alpha = \alpha_{eB}$.

Using the implicit finite difference method discussed in Chapter IV, the velocity, temperature and species concentration profiles in the mixing region are computed up to the s*-station where the oblique shock in the inviscid flow occurs. At this station, the frozen Mach number, M_{fj}, is computed at each grid point ($j = -N,\ldots,0,\ldots,+N$). The corresponding stagnation to static pressure ratio is computed at each grid point from the relation:

$$\frac{p_{st,j}}{p_j} = \frac{p_{st,j}}{p_B} = \left(1 + \frac{\gamma_j - 1}{2} M_{fj}^2\right)^{\frac{\gamma_j}{\gamma_j - 1}}, \qquad (186)$$

where

$$\gamma_j = \frac{4+\alpha_j}{3} .$$

The relation

$$\frac{p_3}{p_B} = \frac{p_{st,ss\ell}}{p_B} \tag{187}$$

establishes the stagnating streamline as the streamline through grid point $ss\ell$.

Since the flow is steady, the mass in the recirculating region is conserved, and the rate of mass bled into the base region is equal to the mass flow rate between the stagnating streamline and the dividing streamline. If the stagnating streamline is below the dividing streamline, the mass flow will be considered positive, indicating bleeding into the base region. The mass flow is written

$$m = \int_{y_{ss\ell}}^{0} \rho u dy_s , \tag{188}$$

where $y_{ss\ell}$ is the stagnating streamline location. Transforming to the Stewartson coordinate (119), and introducing the non-dimensional variables (131), equation (188) becomes

$$\frac{m\sqrt{Re_y}}{\rho_\infty U_\infty \ell} = \int_{Y^*_{ss\ell}}^{0} u^* dY^* . \tag{189}$$

Application of the finite range transformation (140) gives

$$\frac{\dot{m}_{\ell}\sqrt{Re_{\ell}}}{\rho_{\infty}U_{\infty}\ell} = \frac{1}{A}\int_{\zeta_{ss\ell}}^{0} \frac{u^*}{1-\zeta^2}\, d\zeta \ . \qquad (190)$$

The non-dimensional base bleed is numerically integrated using Newton-Cotes integration formulae.

To summarize then, with specified upstream flow conditions, stagnation region conditions, and base height, a base pressure value is assigned. The external expansion, relaxation and recompression are computed to find the recompression pressure ratio. The viscous mixing is solved to obtain the stagnation pressure profile for the assigned base pressure. The mass flow between the stagnating streamline, which has sufficient kinetic energy to penetrate the recompression rise, and the dividing streamline is computed. The assigned base pressure is thus the solution corresponding to the specified conditions with the calculated amount of base bleed.

In order to obtain a base pressure solution for a closed base (zero bleed), different base pressure values are assigned. Base bleeds corresponding to the assigned base pressures are determined. The closed base solution is determined by plotting p_B/p_∞ versus the base bleed. This procedure gives, in addition to closed base solutions, solutions for cases involving base bleed.

Alternatively, with each assigned base pressure, the dividing streamline stagnation pressure is compared to the pressure after the recompression shock. The closed base solution corresponds to the case where these two pressures are equal. This method allows the exterior inviscid flow and the viscous shear layer to be separated and thus, the effects of dissociation in the two regions are separated.

The Base Pressure for a Gas Without Dissociation

In order to check the computer solution, a case was solved for an ideal dissociating gas with negligible dissociation. Calculations were carried out for the following conditions:

$$M_\infty = 3.55$$

$$p_\infty = 1 \text{ atmosphere}$$

$$T_\infty = 500^\circ \text{ K}$$

$$T_B = 1550^\circ \text{ K}$$

$$\text{Gas - Air } (\hat{M} = 30.0)$$

The recirculation region temperature corresponds to the freestream stagnation temperature. The base bleed as obtained from the computer solution is plotted against the corresponding base pressure in Figure 27.

The computed results are compared with values obtained using the Chapman[5] theory (C = const., Pr = 1.0) and the Chapman[13,33] theory ($C \sim T^{0.24}$, Pr = 0.70) in Table 2.

Table 2. Comparison of the Base Pressures for Closed Bases as Computed from the Finite Difference Solution and Similar Solutions for a Gas with Negligible Dissociation

Method of Solution	Base Pressure (Atmospheres)
Finite difference, C-variable, Pr = 0.70	0.248
Similar [5], C = const, Pr = 1.0	0.286
Similar [13,33]; C-variable for u^*; C = const, Pr = 0.70 for T^*	0.256

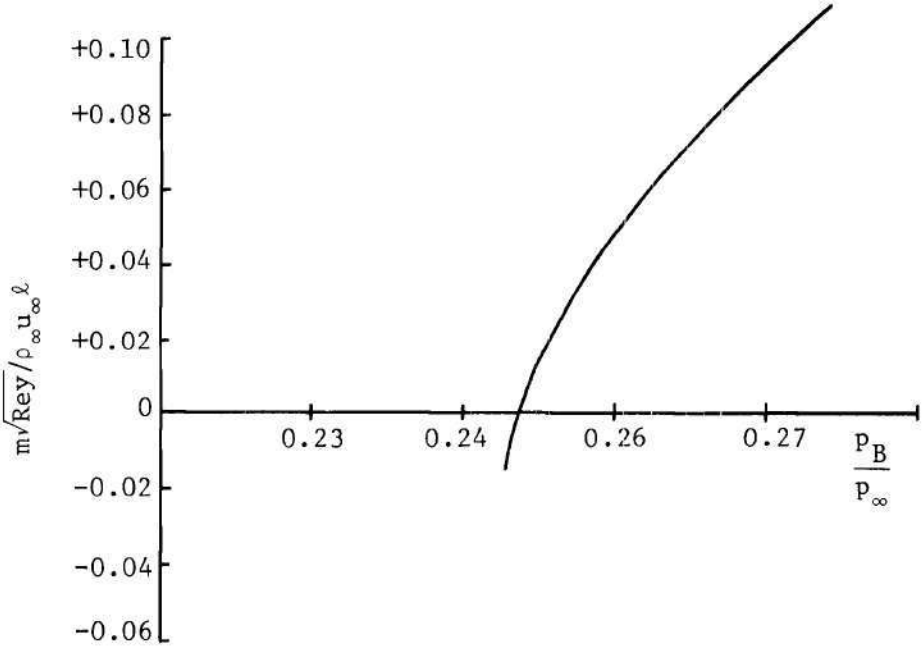

Figure 27. The Dimensionless Base Bleed Rate versus the Base Pressure

The comparison indicates that the computer solution is in reasonable agreement with the Chapman results for Pr = 0.70.

The dividing streamline velocity and temperature as computed by the three theories for $\frac{p_B}{p_\infty} = 0.248$ are compared in Table 3. The dividing streamline velocity as computed by the finite difference method is the same as Chapman's result for variable C. However, the temperature for Chapman's solution with Pr = 0.70 is based on the velocity profiles for constant C, and is slightly high.

Table 3. Comparison of the Velocity and Temperature on the Dividing Streamline at Recompression as Computed by the Finite Difference Solution and the Similar Solutions for $p_B = 0.248$ atm.

Method of Solution	u^*	T^*
Finite Difference, c-variable, Pr = 0.70	0.595	2.974
Similar [5], c = const, Pr = 1.0	0.587	3.225
Similar [13,33]; c-variable for u^*; c = const, Pr = 0.70 for T^*	0.596	3.081

The Base Pressure for a Hot Dissociated Recirculation Region and Negligible Dissociation in the Exterior Flow

In order to investigate the effects of finite rate dissociation in the shear layer on the base pressure, a case with a relatively cool exterior flow and a hot recirculating region was studied. The conditions were

$$M_\infty = 2.0$$

$$p_\infty = 0.1 \text{ atmosphere}$$

$$T_\infty = 1885^\circ \text{ K}$$

$$T_B = 3412^{\circ} \text{ K}$$

$$H = 1.0 \text{ meter}$$

Gas - Oxygen

The base temperature, T_B, corresponds to the frozen stagnation temperature. The degree of dissociation corresponding to the freestream conditions was negligibly small. Thus the entire external flow involved negligible dissociation and the expansion was Prandtl-Meyer. The degree of dissociation in the recirculation region was not negligible. For this case, therefore, the finite rate reaction effects enter only through the shear layer development.

Figure 28 is a plot of the base pressure versus the non-dimensional base bleed for the problem under consideration. The curvature is due primarily to the fact that the mass flow is proportional to the velocity while the kinetic energy is proportional to the velocity squared. As an example, a non-dimensional bleed of 0.25 into the base region would raise the base pressure 17 per cent to 0.590 atmospheres. This bleed rate corresponds to about 3 per cent of the mass flow between the dividing streamline and the shear layer edge. For the same non-dimensional bleed from the base region, the pressure is decreased 21 per cent to 0.40. This mass flow represents about 13 per cent of the mass flow below the dividing streamline.

In Figure 29, the calculated inviscid recompression pressure ratio, p_B/p_3, and the dividing streamline static to stagnation pressure ratio, p_B/p_{st}, are both plotted against the assumed base pressure ratio, $\frac{p_B}{p_\infty}$. The dashed curve represents the inviscid recompression. It is

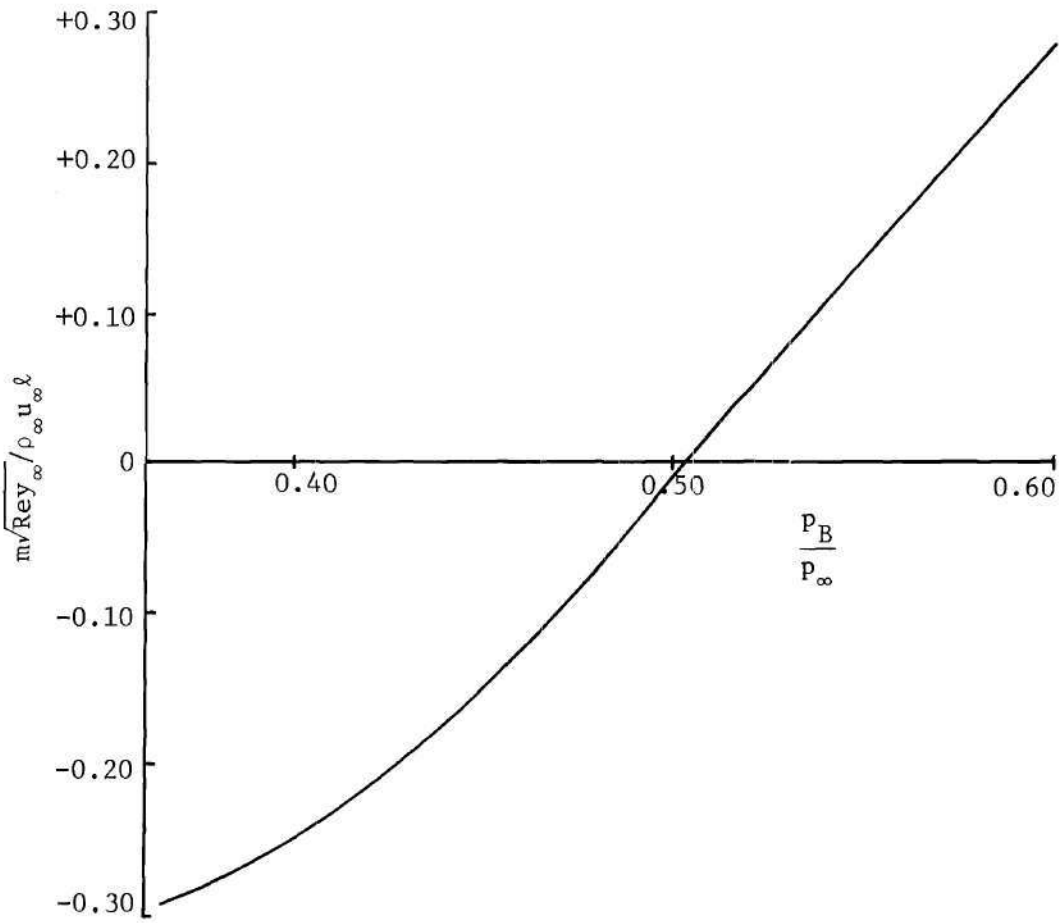

Figure 28. The Dimensionless Base Bleed Rate Versus the Base Pressure. (Dissociation in the Shear Layer.)

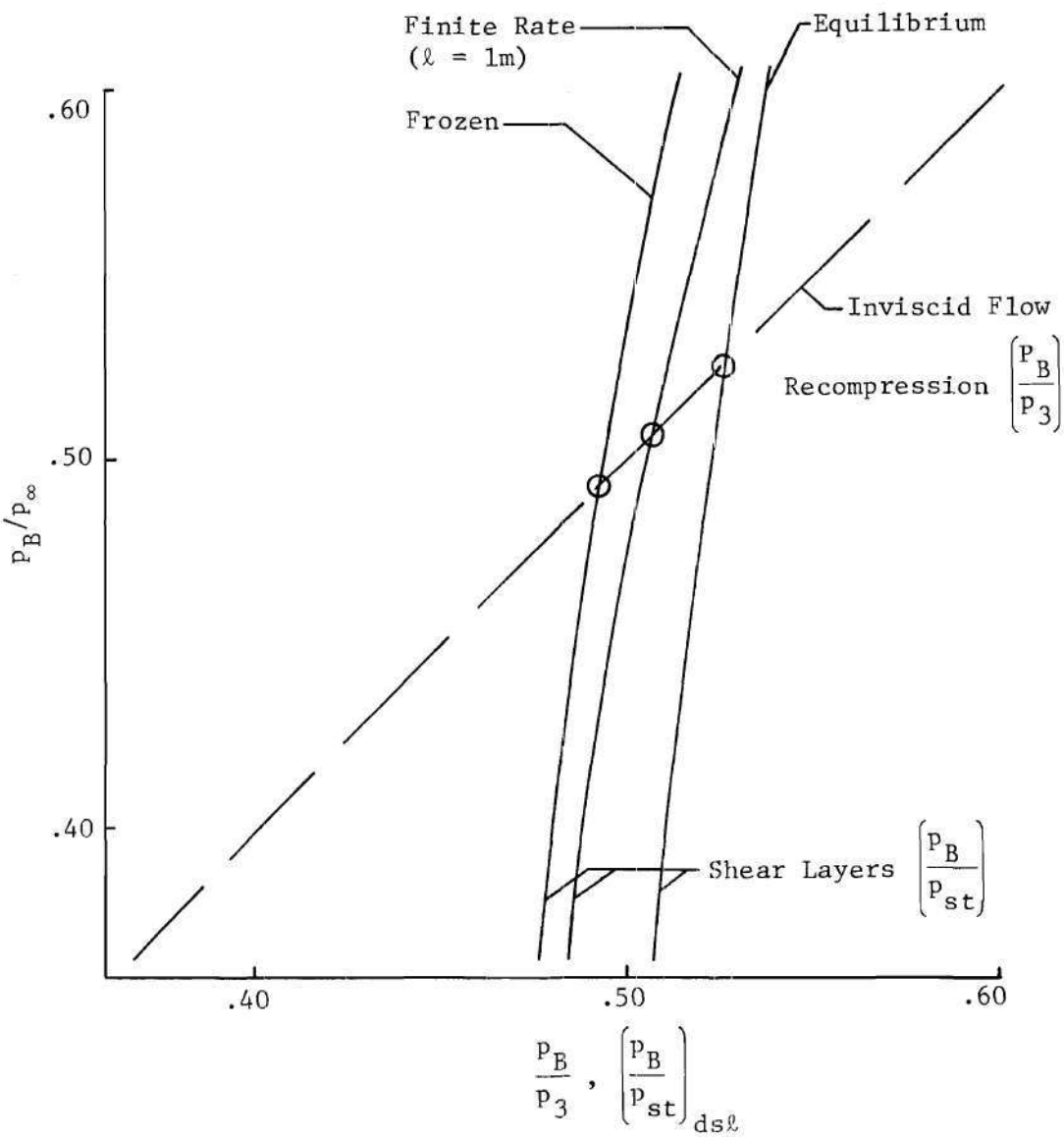

Figure 29. Recompression Pressure Ratios for the Viscid and Inviscid Flow Regions Plotted Against the Base Pressure Ratio

noted that for this example, the exterior flow is frozen and the Mach number is low so that the recompression shock is very weak. As a result, the pressure after the shock, p_3, is nearly equal to the upstream pressure, p_∞. The curves representing the recompression of the shear layer are shown as solid lines. Curves are shown for frozen, finite rate, and equilibrium flow in the shear layer.

The point of intersection of the p_B/p_3 and p_B/p_{st} curves gives the base pressure solution for a closed base. It was found that the finite rate shear layer solution ($p_B = 0.505$) lies between the frozen shear layer solution ($p_B = 0.492$) and the equilibrium solution ($p_B = 0.526$). As discussed in Chapter IV, the dividing streamline velocity ratio, u*, for the frozen, finite rate, and equilibrium cases are nearly identical. The differences in the base pressures for the three rate assumptions are primarily due to the differences in the dividing streamline temperature. The frozen shear layer dividing streamline temperature is lower than that of the equilibrium shear layer (Figure 25). This means that the corresponding density is higher and the kinetic energy available for overcoming the recompression pressure rise is also higher. Thus the base pressure is lower.

Since the computer time required to solve the shear layer is rather large, a simpler approach based on an extension of Chapman's theory (discussed in Appendix B) was attempted.

In Figure 30, the calculated inviscid recompression pressure ratio, p_B/p_3, and the dividing streamline static to stagnation pressure ratio, p_B/p_{st}, are again plotted against the assumed base pressure, $\frac{p_B}{p_\infty}$. In addition to the p_B/p_{st} curve for the shear layer solution with

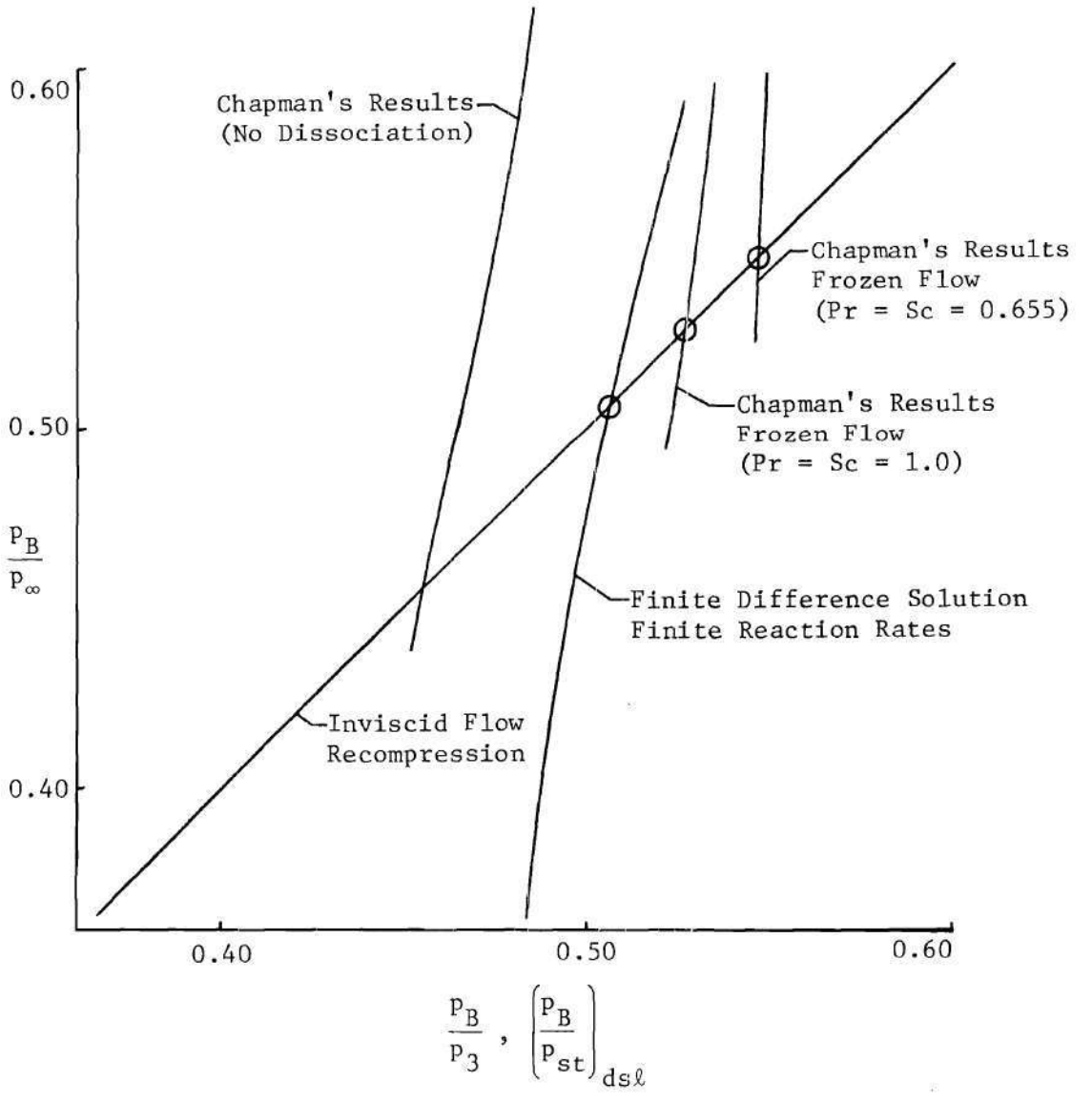

Figure 30. Comparison of Base Pressure Solutions from Chapman's Results by Means of a Recompression Pressure Ratio Plot

finite rate reactions, solutions for frozen flow with Pr = Sc = 1.0 and Pr = Sc = 0.655, as obtained by Chapman's results, are shown. The results are not in good agreement with the present solution.

The Base Pressure for a Cool Recirculation Region with Dissociation Throughout the Flow Field

In order to investigate the effects of finite rate reactions in the exterior inviscid flow and the effects due to cooling the recirculating region, the following case was considered:

$$M_\infty = 3.2$$

$$p_\infty = 0.10 \text{ atmosphere}$$

$$T_\infty = 3221^\circ \text{ K}$$

$$T_B = 3221^\circ \text{ K}$$

$$H = 1 \text{ and } 2 \text{ meters}$$

The degree of dissociation corresponding to the freestream conditions is 0.3245. Calculations for the inviscid expansion and relaxation were carried out by the method of characteristics.

Plots of the base pressure versus the non-dimensional base bleed for finite rate reactions and base half heights of one and two meters are shown in Figure 31. The curves indicate that the closed base pressure decreases as the base half height is increased

In order to investigate the reasons for the decrease, it is helpful to examine Figure 32, which shows the exterior recompression pressure ratio, p_3/p_B, and the dividing streamline static to stagnation pressure ratio, p_B/p_{st}, plotted against the assumed base pressure ratio.

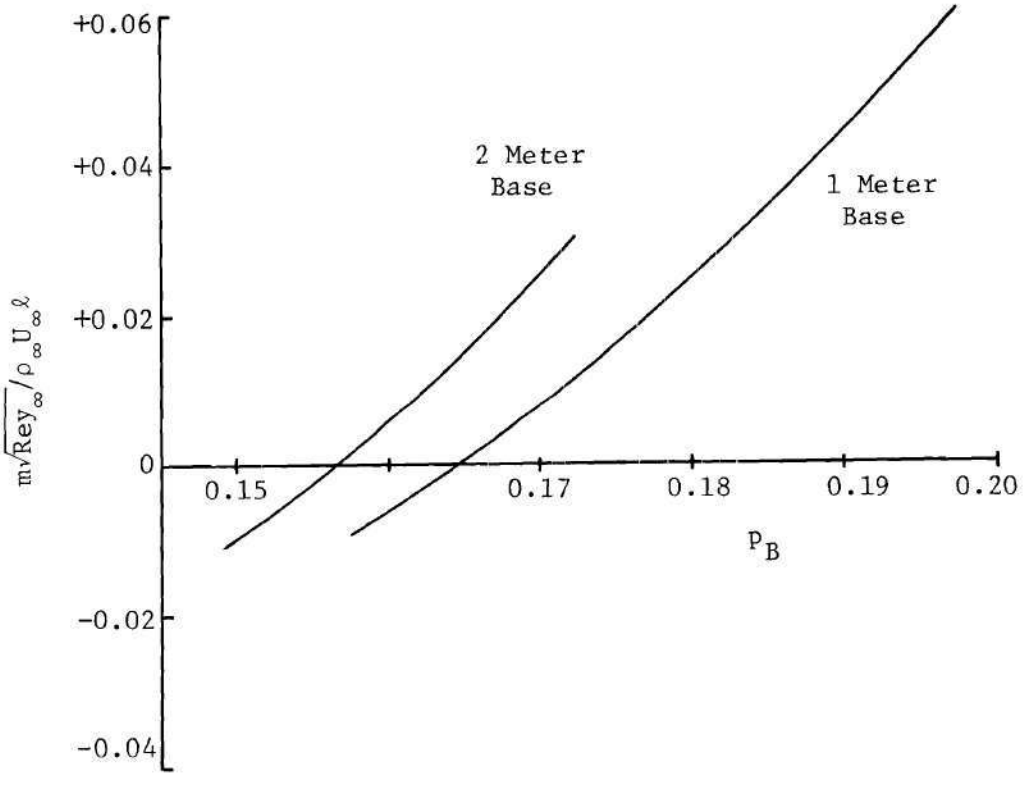

Figure 31. The Dimensionless Base Bleed Rate versus the Base Pressure (Dissociation Throughout the Flow)

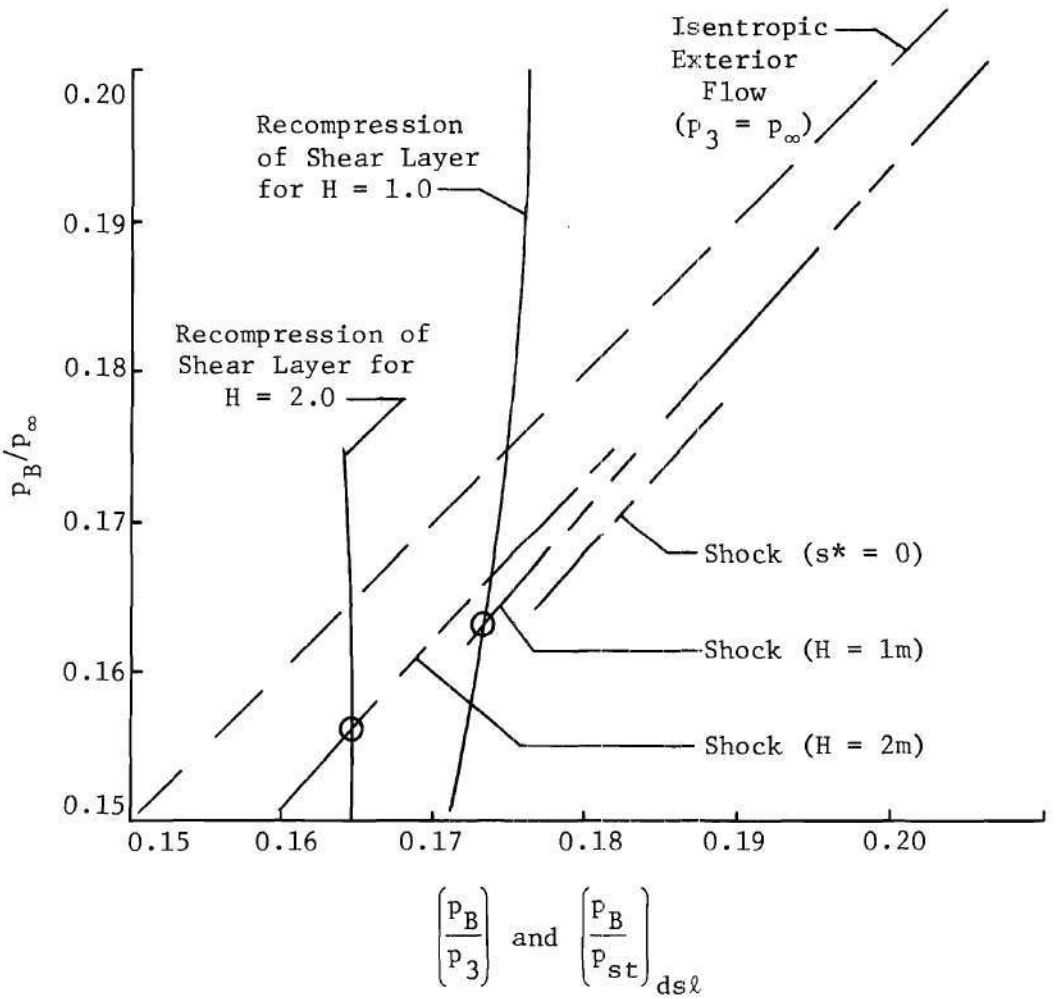

Figure 32. Recompression Pressure Ratios for the Viscid and Inviscid Flow Regions for 1 and 2 Meter Base Half Heights versus the Base Pressure Ratio

The three dashed curves represent the exterior shock recompression pressure ratio, p_3/p_B, for zero (frozen flow), one and two meter base half heights. The equilibrium limit for the inviscid flow was not computed, but certainly the pressure after recompression could not be higher than the freestream pressure. The two shear layer curves (solid lines) represent the recompression for base half heights of one and two meters.

This figure indicates that the finite reaction rates in the exterior flow tend to raise the base pressure. The effect of finite rates in the shear layer is larger, however, so that, at least in this case, the shear layer determines the base pressure change.

The profiles of dissociation degree and temperature in the shear layer are shown in Figures 33 and 34. Since the recirculation region temperature is less than the stagnation temperature, a "hot spot" forms near the dividing streamline.* The dissociation of the gas in this region absorbs this thermal energy and stores it as chemical energy. Thus, in the flow direction, the dividing streamline temperature decreases, while the density and kinetic energy increase. As a result, with a large base height, the dividing streamline can overcome a greater recompression pressure rise and the base pressure is lower.

This indicates that for a case with a cool base, the effect of the finite reaction rates in the shear layer is to reduce the base pressure from the frozen flow value.

In reference [35], Resler considered the base pressure for a body with a specified amount of heat transfer. His qualitative analysis

*Recent experimental results of Batt and Kubota[35] at low temperatures (negligible dissociation) for base pressures on a cooled body have shown the existence of such peaks in the static temperature.

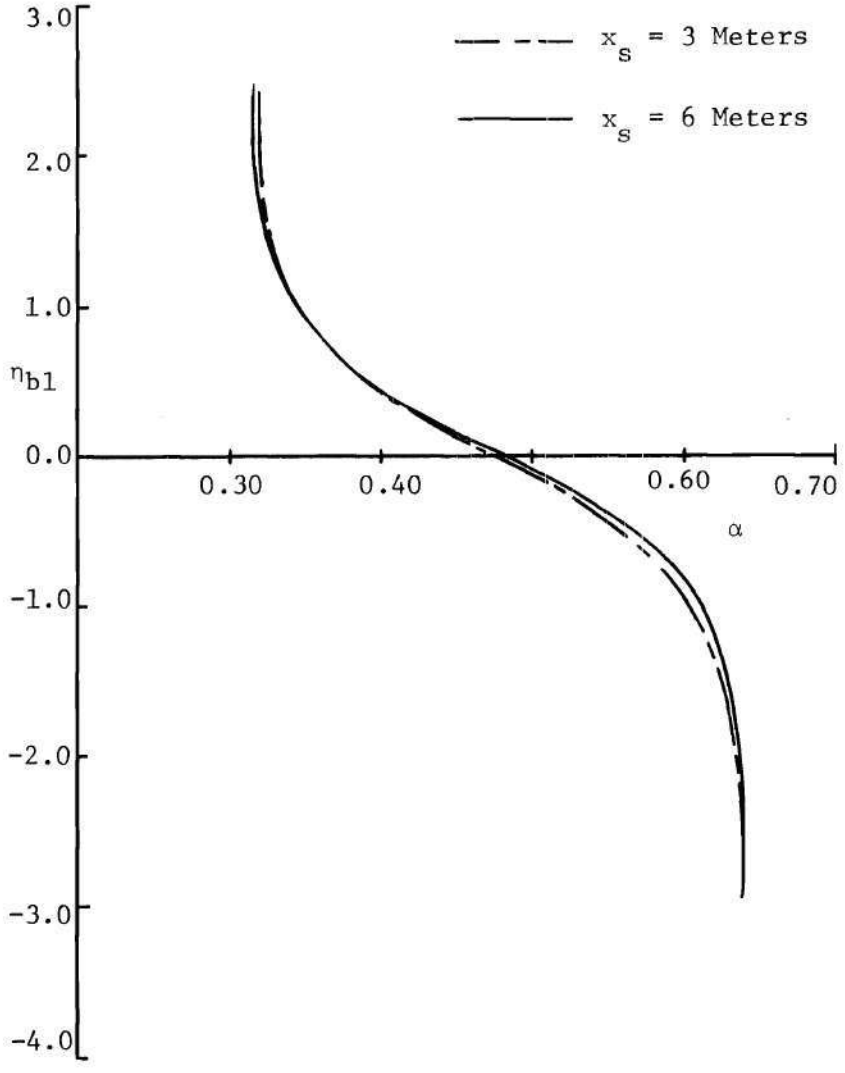

Figure 33. Degree of Dissociation Profiles for Finite Rate Flow at x_s = 3.0 and 6.0 (p_B^* = 0.017)

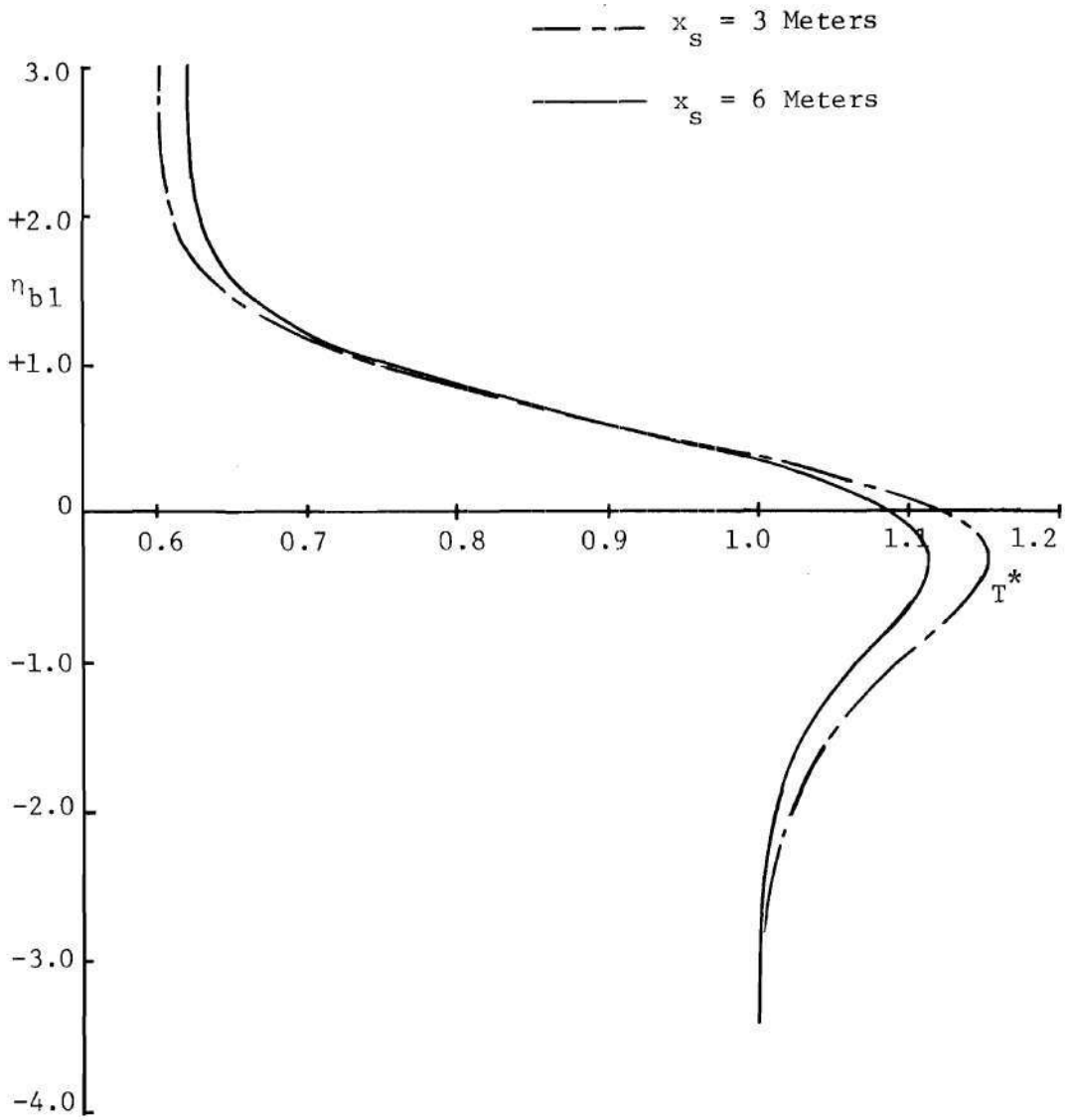

Figure 34. Temperature Profiles for Finite Rate Flow at x_s = 3.0 and 6.0 (p_B^* = 0.017)

indicates that the base pressure value considering the flow to be in equilibrium is higher than that considering the flow to be frozen.

The results for the inviscid (non-heat conducting) flow and the shear layers for hot bases agree with Resler's predictions. However, the results of this thesis indicate that, for the case of a cool base, the trend is opposite to that predicted by Resler.

CHAPTER VI

CONCLUSIONS AND RECOMMENDATIONS

An investigation of the effects of finite rate dissociation-recombination reactions on the base pressure has been made. The exterior inviscid expansion has been treated by the method of characteristics for a reacting gas. A linearized theory for the inviscid expansion into a constant-pressure region has been developed. The laminar mixing region has been investigated by means of an implicit finite difference method. The two regions have been coupled, and several base flow problems have been studied.

The results of the investigation led to the following conclusions:

1. The inviscid expansion of an ideal-dissociating gas into a constant-pressure region represents a simpler flow than the previously reported expansion around a convex corner. Following the frozen expansion, the flow deflection, degree of dissociation, and Mach number along the constant-pressure boundary decrease monotonically, while the temperature increases monotonically. No overshoot of the flow deflection corresponding to the pressure overshoot for the problem of flow around a convex corner was observed. The waves reflecting from the constant-pressure boundary are expansion waves, and thus, a recombination shock is not possible.

2. The linearized theory for the supersonic flow expanding into a constant-pressure region is very useful for small expansions and for

purposes of prediction.

3. The implicit finite difference method with the finite range transformation offers a stable, accurate method of solution to boundary layer types of flows without reverse flow regions. The use of the Taylor series expansion of the rate equation reduces the calculation time by as much as 80 per cent, without any additional restrictions for stability.

4. The velocity profiles in the mixing region are relatively insensitive to the rate process. The finite rate profiles for temperature and degree of dissociation fall between the limits of frozen and equilibrium flow, as expected.

5. Chapman's[33] results are extended to account for dissociation in a frozen flow with constant Pr, Sc, and C. Furthermore, the finite difference results using the same assumptions show excellent agreement with the similar profiles. However, due to the large temperature differences encountered in this problem, the assumption of constant Pr, Sc, and C gives results in poor agreement with the solutions for variable properties.

6. Finite reaction rates in the inviscid exterior flow cause an increase in the base pressure. This result agrees with the predictions of Resler that the drag on a body in equilibrium flow is less than the drag on a body in frozen flow.

7. The effects of finite rate reactions in the mixing region depend on the temperature of the recirculation region.

If the temperature of the recirculation region is on the order of the freestream stagnation temperature, atomic recombination occurs

near the dividing streamline so that the temperature increases and the dividing streamline kinetic energy decreases. This loss in kinetic energy results in an increase in the base pressure. For example, an increase in p_B/p_∞ from 0.492 to 0.526 was computed between the frozen and equilibrium limits.

If the recirculation region is cool, a peak in the static temperature, caused by viscous dissipation, forms near the dividing streamline. The molecular dissociation in this region absorbs thermal energy and causes an increase in the kinetic energy of the dividing streamline. This results in a decrease in the base pressure. In the example for a cool base, presented in this thesis, the effects in the shear layer overpowered the effect of the inviscid flow and the base pressure decreased from 0.163 for a one meter base to 0.156 for a 2 meter base.

In summary, the results of this thesis indicate that the effects of dissociation on the base pressure are important. The recombination in the inviscid flow tends to increase the base pressure. If the base region is hot, recombination occurring near the dividing streamline tends to increase the base pressure. However, if the base region is cool, dissociation occurs near the dividing streamline, which tends to decrease the base pressure.

Although the method of solution used in this thesis is somewhat time consuming (each closed base solution requiring from 1/2 to 3 hours on the Burroughs B 5500 Computer), the simplified approaches have not produced useful results.

Although there is a substantial amount of experimental base pressure data available for lower temperatures, practically no experimental

data for dissociating flows exists in the open literature. Therefore, experimental investigations of the base pressure for dissociating gases are strongly recommended.

A theoretical investigation of the expansion of a dissociating gas with an initial boundary layer appears worthwhile, since the results of this thesis suggest that the decrease in flow deflection on the constant pressure boundary can be of the same order as the initial turning angle underestimation predicted by Weiss and Nelson[7].

Finally, the finite difference method used in this thesis can be applied to attached boundary layers, enabling further investigations into the effects of finite rate reactions on heat transfer and other related problems.

APPENDICES

APPENDIX A

GAS MODEL

In this appendix, a gas model will be presented which accounts for all of the properties of a dissociating gas. All gases of interest in this study will be symmetrical diatomic gases. Attention will first be focused on the determination of the molar concentrations of the individual species. This will involve the specification of an equilibrium relation based on the law of mass action, and a rate equation for non-equilibrium situations. Consideration will then be given to the thermodynamic properties and, finally, the transport properties of the gas.

The equilibrium concentration is determined by the dissociation-recombination reaction of a symmetrical diatomic gas such as oxygen

$$O_2 \rightleftarrows 2O \ . \tag{A-1}$$

Reactions of this kind can be characterized by the degree of dissociation α, where

$$\alpha = \frac{\text{mass of dissociated A-atoms}}{\text{total mass of the gas}}$$

$$= \frac{\rho_A}{\rho} \ , \tag{A-2}$$

and the subscript A denotes atoms. At equilibrium, the degree of dissociation is given by the law of mass action:

$$\frac{\alpha_e^2}{1-\alpha_e} = \frac{\rho_d}{\rho} e^{-\frac{\theta_d}{T}} . \qquad \text{(A-3)}$$

The characteristic density for dissociation, ρ_d, is a mildly varying function of temperature which is small compared to the variation of the exponential term. The widely accepted Lighthill[37] model of an ideal dissociating gas assumes that ρ_d is a constant. Values of the constants ρ_d and θ_d for oxygen are given in Table A-1.

The rate equation for a symmetrical diatomic gas is given by

$$\frac{d\alpha}{dt} = \left(k_{f,A}\alpha + k_{f,M}\frac{(1-\alpha)}{2}\right)\frac{\rho}{\hat{M}_A}\left[(1-\alpha) - \frac{2\rho}{\hat{M}_A K_c}\alpha^2\right] \qquad \text{(A-4)}$$

where the k_f's are forward rate constants and K_c is the equilibrium constant.

Table A-1. Constants for the Gas Used in this Thesis

	Oxygen
ρ_d	150 gm/cm^3
θ_d	59,000^o K
C_f	1.19 X 10^{20}
n	-1.5
ε	100
$\hat{M}_M$	32
$\frac{\sqrt{\hat{M}_M}\varepsilon}{\sigma^2}$	4.62
σ_{12}^2	3.199

Expressing the forward rate constants in terms of the temperature and the equilibrium constant in Lighthill's form, the applicable rate equation becomes:

$$\frac{d\alpha}{dt} = \frac{C_{f_1} T^{n_1}}{\hat{M}_A} \alpha + \frac{C_{f_2} T^{n_2}}{\hat{M}_M} (1 - \alpha) \rho \left[(1 - \alpha) e^{-\frac{\theta_d}{T}} - \frac{\rho}{\rho_d} \alpha^2 \right] . \quad \text{(A-5)}$$

Since there is a substantial amount of uncertainty in the values of C_f, a simplified form of the rate equation, proposed by Freeman[38], is used.

$$\frac{d\alpha}{dt} = C_f T^n \rho \left\{ (1 - \alpha) e^{-\frac{\theta_d}{T}} - \frac{\rho}{\rho_d} \alpha^2 \right\} . \quad \text{(A-6)}$$

The values of C_f and n used in this thesis are also shown in Table A-1.

Assuming that all species in the mixture behave as thermally perfect gases, Dalton's Law is used to write the thermal equation of state in the familiar form

$$p = \rho(1 + \alpha) R_m T . \quad \text{(A-7)}$$

The enthalpy is taken in the form consistent with the ideal dissociating gas based on zero energy in the molecular state at absolute zero.

$$h = R_m [(4 + \alpha) T + \alpha \theta_d] . \quad \text{(A-8)}$$

The corresponding internal energy is given by

$$e = R_m [3T + \alpha \theta_d] . \quad \text{(A-9)}$$

For frozen flow, α is independent of T, and the ratio of specific heats is written

$$\gamma_f = \frac{4+\alpha}{3} \cdot \tag{A-10}$$

Although a more exact formulation for the enthalpy would be proper for the precise numerical technique used in the solution, it is desired to separate the effects of vibration and dissociation. This is effectively done by the ideal dissociating gas model. In the temperature range of interest in this study, 1000 - 5000° K, this model should give good quantitative results. For the cases examined at low temperatures for comparison purposes, the ideal dissociating gas model is only qualitatively correct, since the vibrational excitation term is not included.

In high temperature gas dynamics, the classical thermodynamic state variable known as the speed of sound requires an additional constraint. The pressure is now a function of three variables so that the condition of constant entropy is no longer sufficient to define a sound speed. A study of the "acoustic" equations (references [19] and [20]) results in the discovery of two important sound speeds, frozen and equilibrium. For an ideal dissociating gas, these are

$$a_f^2 = -\frac{\left(\frac{\partial h}{\partial \rho}\right)_{p,\alpha}}{\left(\frac{\partial h}{\partial p}\right)_{\rho,\alpha} - \frac{1}{\rho}} \tag{A-11}$$

$$= \frac{R_m T (4+\alpha)(1+\alpha)}{3}$$

and

$$a_e^2 = -\frac{\left(\frac{\partial h}{\partial \rho}\right)_{p,\alpha} + \left(\frac{\partial h}{\partial \alpha}\right)_{p,\rho}\left(\frac{\partial \alpha_e}{\partial \rho}\right)_p}{\left(\frac{\partial h}{\partial p}\right)_{\rho,\alpha} + \left(\frac{\partial h}{\partial \alpha}\right)_{p,\rho}\left(\frac{\partial \alpha_e}{\partial p}\right)_\rho - \frac{1}{\rho}}$$

$$= R_m T \frac{\alpha_e(1-\alpha_e^2)(1+2T/\theta_d)+(8+3\alpha_e-\alpha_e^3)(T/\theta_d)^2}{\alpha_e(1-\alpha_e)+3(2-\alpha_e)(T/\theta_d)^2} \qquad \text{(A-12)}$$

where the subscript e indicates equilibrium values of α, obtained from equation (A-3).

Although the molecular theory of transport coefficients is well developed within the restrictions of the Chapman-Enskog theory, the interparticle potential for high temperature gases is unknown. Uncertainties exist even in the choice of constants for a particular potential result in uncertainties of 45 per cent or more in transport coefficients.

The coefficients of viscosity and diffusion are written as follows:

$$\mu = 26.693 \left[\frac{\sqrt{\hat{M}\varepsilon}}{\sigma^2}\right]\left[\frac{\sqrt{\frac{T}{\varepsilon}}}{\Omega^{(2,2)*}}\right] \times 10^{-6} \text{ gm/cm-sec} \qquad \text{(A-13)}$$

$$pD_{12} = 0.002628\left[\frac{1}{\sigma_{12}^2}\sqrt{\frac{\hat{M}_A+\hat{M}_M}{2\hat{M}_A\hat{M}_M}}\right]\frac{T^{\frac{3}{2}}}{\Omega^{(1,1)*}}\frac{\text{cm}^2}{\text{sec}} \qquad \text{(A-14)}$$

The values of the parameters ε and σ were taken from Brokaw [39], based on the Leonard-Jones 6-12 potential and are shown in Table A-1. The collision integrals (see, for example, Reference [26], page 296) were approximated by the polynomials

$$\Omega^{(1,1)*} = -0.0611\left[\log\left(\frac{T}{\varepsilon}\right)\right]^3 + 0.3112\left[\log\left(\frac{T}{\varepsilon}\right)\right]^2$$

$$-0.7350\left[\log\left(\frac{T}{\varepsilon}\right)\right] + 1.2266$$

and

$$\Omega^{(2,2)*} = -0.0589\left[\log\left(\frac{T}{\varepsilon}\right)\right]^3 + 0.30726\left[\log\left(\frac{T}{\varepsilon}\right)\right]^2$$

$$-0.7443\left[\log\left(\frac{T}{\varepsilon}\right)\right] + 1.3196$$

For a gas mixture, the viscosity is dependent upon the viscosities of the constituent species. However, for diatomic gases the molecular viscosity is approximately equal to the atomic viscosity.

For a monotomic gas, the Chapman-Enskog theory gives the thermal conductivity as

$$\kappa_A = \frac{15}{4} R_A \mu_A \qquad \text{(A-15)}$$

Using Hirschfelder's improvement to the Eucken correction, the expression for the thermal conductivity of diatomic molecules is [26]

$$\kappa_M = \frac{15}{4} R_M \mu_M \left[0.115 + 0.354 \frac{Cp_M}{R_M} \right] \qquad \text{(A-16)}$$

where the specific heat is obtained from Equation (A-8).

The thermal conductivity of the mixture is given to a first approximation by

$$\kappa = \left(\frac{1-\alpha}{1+\alpha} \right) \kappa_M + \left(\frac{2\alpha}{1+\alpha} \right) \kappa_A$$

Substituting Equations (A-15) and (A-16), the thermal conductivity for the mixture becomes

$$\kappa = 5.7375 \, R_M \mu_M \left(\frac{1 + 1.62\alpha}{1 + \alpha} \right) \qquad \text{(A-17)}$$

Because of the relationship between κ and μ, the Prandtl number is simply

$$Pr = \frac{\mu Cp}{\kappa} = .70 \left[\frac{(1+0.25\alpha)(1+\alpha)}{1 + 1.62\alpha} \right] \qquad \text{(A-18)}$$

APPENDIX B

EXTENSION OF CHAPMAN'S RESULTS TO INCLUDE DISSOCIATION

In reference [33], Chapman presents an analysis of the free shear layer for a thermally perfect gas. The Prandtl number and the product of density and viscosity are assumed to be constant. The resulting momentum equation is independent of the energy equation and is solved numerically. The energy equation is then solved in terms of integrals of the velocity.

It will be shown here that Chapman's analysis can be easily extended to the frozen flow of a dissociated gas, and in fact no additional calculations need be performed.

In addition to the assumptions incorporated in the boundary layer equations (99) through (103), the following additional assumptions will be made

1. $Pr = Sc = \text{constant}$ $(Le = 1.0)$
2. $\rho^* \mu^* = \text{constant}$
3. The flow is frozen $(\omega = 0)$.

The governing differential equations are the continuity equation

$$\frac{\partial(\rho u)}{\partial x} + \frac{\partial(\rho u)}{\partial y} = 0, \tag{B-1}$$

the momentum equation

$$\rho u \frac{\partial u}{\partial x} + \rho u \frac{\partial u}{\partial y} = \frac{\partial}{\partial y}\left(\mu \frac{\partial u}{\partial y}\right), \tag{B-2}$$

the species conservation equation

$$\rho u \frac{\partial \alpha}{\partial x} + \rho v \frac{\partial \alpha}{\partial y} = \frac{\partial}{\partial y}\left(\frac{\mu}{Sc} \frac{\partial \alpha}{\partial y}\right), \tag{B-3}$$

and the energy equation

$$\rho u \frac{\partial h}{\partial x} + \rho v \frac{\partial h}{\partial y} = \frac{\partial}{\partial y}\left(\frac{\mu}{Pr} \frac{\partial h}{\partial y}\right) + \mu\left(\frac{\partial u}{\partial y}\right)^2 . \tag{B-4}$$

The stream function, ψ, defined in equation (122), is used to transform equations (B-1), (B-2), (B-3), and (B-4) to (s,ψ) coordinates. The transformation is accomplished with the aid of the relations

$$\left.\begin{aligned} \left(\frac{\partial}{\partial y}\right)_x &= \frac{\rho u}{\rho_\infty}\left(\frac{\partial}{\partial \psi}\right)_x \\ \left(\frac{\partial}{\partial x}\right)_y &= -\frac{\rho v}{\rho_\infty}\left(\frac{\partial}{\partial \psi}\right)_x + \left(\frac{\partial}{\partial x}\right)_\psi \end{aligned}\right\} \tag{B-5}$$

Due to the choice of coordinates, the continuity equation is automatically satisfied. Applying relations (B-5) and the dimensionless variables (131) to equations (B-2) and (B-4) gives the non-dimensional form of the momentum equation

$$\frac{\partial u^*}{\partial s^*} = \frac{\partial}{\partial \psi^*}\left(u^* \frac{\partial u^*}{\partial \psi^*}\right), \tag{B-6}$$

the species continuity equation

$$\frac{\partial \alpha}{\partial s^*} = \frac{1}{Sc} \frac{\partial}{\partial \psi^*} \left(u^* \frac{\partial \alpha}{\partial \psi^*} \right), \tag{B-7}$$

and the energy equation

$$\frac{\partial h^*}{\partial s^*} = \frac{1}{Pr} \frac{\partial}{\partial \psi^*} \left(u^* \frac{\partial h^*}{\partial \psi^*} \right) + \frac{U_\infty^2}{h_\infty} \left(\frac{\partial u^*}{\partial \psi^*} \right)^2 \tag{B-8}$$

where

$$h^* = \frac{h}{h_\infty}$$

and

$$\psi^* = \frac{\psi}{\sqrt{\frac{\mu_\infty U_\infty LC}{\rho_\infty}}}$$

Since there is no reference length in this problem (the flow is frozen), similar solutions appear possible. The differential equations are transformed from (ψ^*, s^*) to (z, s^*), where

$$z = \frac{\psi^*}{\sqrt{s^*}} \quad . \tag{B-9}$$

The momentum equation (B-6) is thus reduced to the non-linear ordinary differential equation

$$-\frac{z}{2}\frac{du^*}{dz} = \frac{d}{dz}\left(u^*\frac{du^*}{dz}\right) \qquad \text{(B-10)}$$

The numerical solution to this differential equation, subject to the boundary conditions $u^*(+\infty) = 1$ and $u^*(-\infty) = 0$, is discussed in reference [13].

The species conservation equation (B-7) is also transformed to (z,s^*) coordinates:

$$u^*\frac{\partial^2\alpha}{\partial z^2} + \left(Sc\,\frac{z}{2} + \frac{du}{dz}\right)\frac{\partial\alpha}{\partial z} - Sc\;s^*\frac{\partial\alpha}{\partial s^*} = 0 \qquad \text{(B-11)}$$

subject to the boundary conditions

$$\alpha(+\infty) = \alpha_\infty \qquad\qquad \alpha(-\infty) = \alpha_B \ .$$

Since the boundary conditions are not functions of s, and the flow is frozen, the derivative $\frac{\partial\alpha}{\partial s^*}$ is assumed to be zero. Equation (B-11) thus becomes a homogeneous, linear second order ordinary differential equation. The general solution is

$$\alpha = \alpha_\infty + A\int_z^\infty \left(4u^*\frac{du^*}{dz}\right)^{Sc}\frac{dz}{2u^*} \qquad \text{(B-12)}$$

Defining

$$F_1(z) = \int_z^\infty \left(4u^*\frac{du^*}{dz}\right)^{Sc}\frac{dz}{2u^*} \qquad \text{(B-13)}$$

the constant A is determined from the boundary condition

$$\alpha_B = \alpha_\infty + AF_1(z_B)$$

where z_B is the finite value of z corresponding to u* = 0. Thus the solution to the species conservation equation is

$$\alpha = \alpha_\infty + (\alpha_B - \alpha_\infty) g_1(z) \tag{B-14}$$

where

$$g_1(z) = \frac{F_1(z)}{F_1(z_B)} \tag{B-15}$$

The energy equation is transformed to the (z,s*) coordinate system, and $\frac{\partial h}{\partial s^*}$ is assumed to be zero. The resulting form

$$u^* \frac{\partial^2 h^*}{\partial z^2} + \left(Pr \frac{z}{2} + \frac{du^*}{dz} \right) \frac{dh^*}{dz} = - Pr \frac{U_\infty^2}{h_\infty} \left(\frac{du^*}{dz} \right)^2 \tag{B-16}$$

is a linear, second order, ordinary differential equation. The general solution is [33]:

$$h^* = 1 + C_1 F_1(z) + \frac{U_\infty^2}{2h_\infty} F_2(z)$$

where

$$F_1(z) = \int_z^\infty \left(4u^* \frac{du^*}{dz} \right)^{Pr} \frac{dz}{2u^*} \tag{B-17}$$

$$F_2(z) = \frac{Pr}{2} \int_z^\infty \left(4u^* \frac{du^*}{dz}\right)^{Pr} G(z) \frac{dz}{2u^*} , \tag{B-18}$$

and

$$G(z) = \int_o^z \left(4u^* \frac{du^*}{dz}\right)^{2-Pr} \frac{dz}{2u^*} . \tag{B-19}$$

The constant C_1 is determined from the boundary condition

$$h_B^* = 1 + C_1 F_1(z_B) + \frac{U_\infty^2}{2h_\infty} F_2(z_B) .$$

Thus the enthalpy is written:

$$h^* = 1 + (h_B^* - 1) g_1(z) + \frac{U_\infty^2}{2h_\infty} g_2(z) \tag{B-20}$$

where the normalized functions $g_1(z)$ and $g_2(z)$ are defined as

$$g_1(z) = F_1(z)/F_2(z_B) , \tag{B-21}$$

and

$$g_2(z) = F_2(z) - g_1(z) F_2(z_B) . \tag{B-22}$$

Note that the species conservation equation (B-11) is simply the homogeneous form of the energy equation (B-16). The resulting functions F_1 and g_1 are the same for both equations.

Values of the functions $g_1(z)$ and $g_2(z)$ are tabulated in reference [33] for various values of the Prandtl (or Schmidt) number. Since

the dividing streamline is of primary concern in the solution of the base flow problem, the results for the dividing streamline from reference [33] are plotted versus the Prandtl number in Figure B-1.

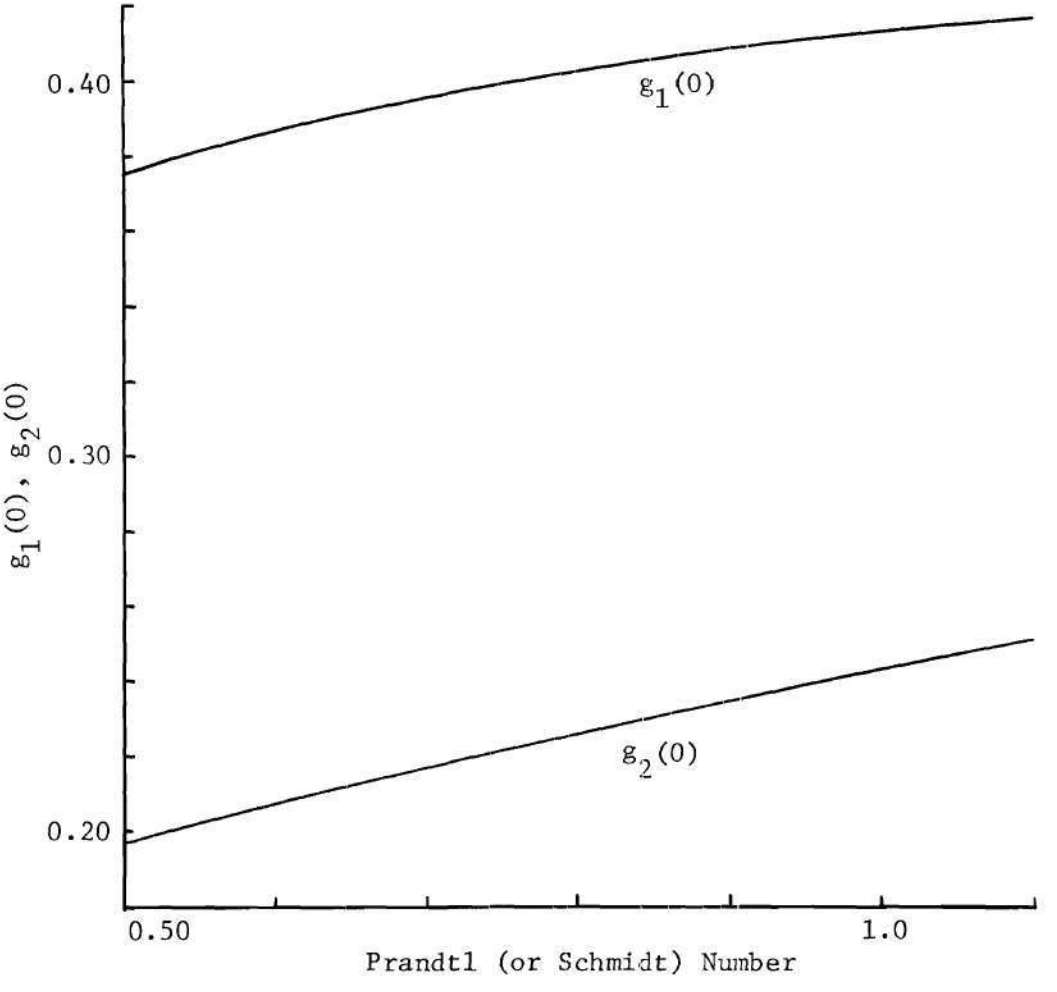

Figure B-1. The Functions $g_1(0)$ and $g_2(0)$ versus the Prandtl (or Schmidt) Number

APPENDIX C

COMPARISON OF THE FINITE DIFFERENCE MIXING SOLUTIONS WITH AVAILABLE SOLUTIONS

In this appendix, the finite difference solutions of the laminar mixing problem are compared with solutions available in the literature. The velocity profiles are compared with Chapman's similar solution. Degree of dissociation profiles for the problem of the constant velocity mixing of two reaching streams having constant fluid properties are compared with the results of Kovitz and Hoglund.

The Laminar Free Shear Layer

The similar solution obtained by Chapman [13] is used as a test of the finite difference solution. For this comparison, the thermodynamic and transport properties obtained in Appendix A are replaced by constant properties (in this case Pr = C = 1) in the solution. The selection of C = 1, transforms the variable η into the variable used by Chapman.

$$\eta_c = \frac{\eta_{bl}}{\sqrt{C}}$$

where the subscript C denotes Chapman's variable. The initial profiles were of the Wu type. A value of N = 25 was chosen, so that there were 51 grid points in the η-direction. Initial step sizes of $\Delta s = 2 \times 10^{-3}$

and 6×10^{-4} were used. The step size was increased as the square root of s.

The velocity profiles are shown in Figure C-1. The agreement is seen to be excellent.

Figure C-2 shows the velocity along the dividing streamline for various s* stations. The scale is enlarged so that the approach to the asymptotic limit can be seen. With the larger initial step size the dividing streamline velocity is at 96 per cent of the asymptotic limit at s* = 0.36, and 98 per cent at s* = 3.00 which is a reasonable distance for a short base.

Under the conditions of constant properties, the finite difference equations reduce to the equations of reference [15]. In this reference the Chapman solution was used as an initial profile, and it was shown that the finite difference scheme preserves these profiles.

The Constant Velocity Mixing of Two Reacting Streams

Kovitz and Hoglund [34] have examined the mixing of two streams at constant velocity. The two streams are separated by a semi-infinite partition along $x \leq 0$ and $y = 0$. Each stream consists initially of the same symmetric diatomic gases but with different enthalpies and therefore different concentrations.

The similarity coordinate can be expressed in terms of the variable z_k used in reference [34] by the transformation

$$\eta_c = \frac{\eta_{bl}}{\sqrt{C}} = \frac{2z_k}{\sqrt{Sc}}$$

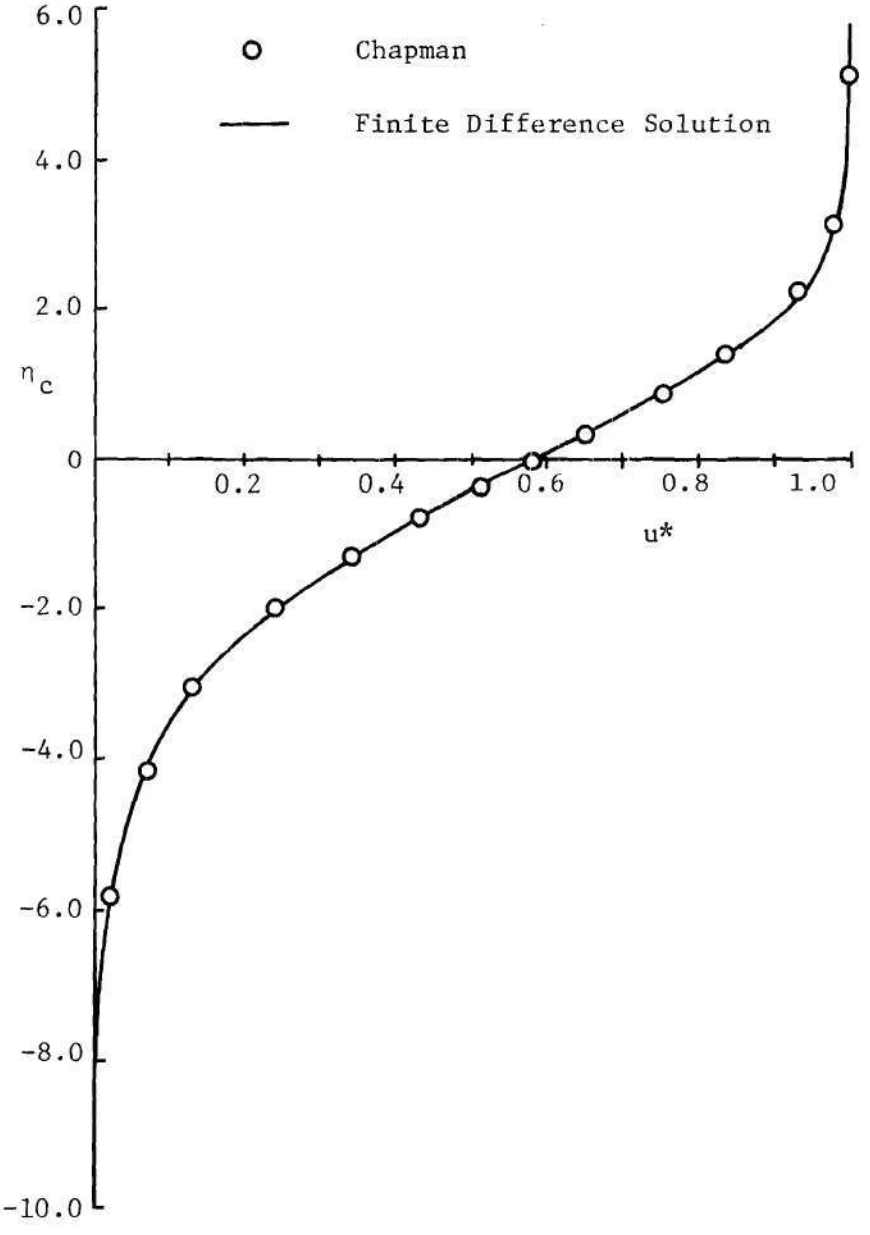

Figure C-1. Comparison of the Velocity Profile from the Finite Difference Solution at s* = 3 with Chapman's Similar Solution

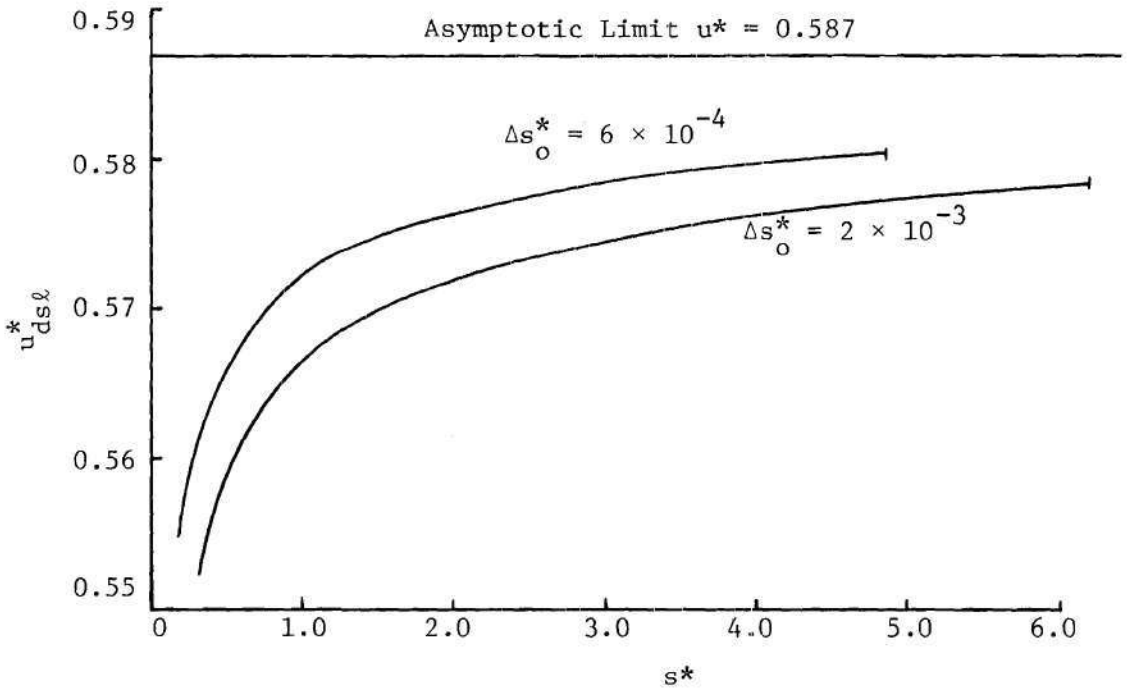

Figure C-2. Influence of the Initial Step Size on the Dividing Streamline Velocity Ratio for Constant Properties

The numerical solution presented by Kovitz and Hoglund was for the mixing of oxygen at a pressure of 0.01 atmosphere. The upper stream consisted entirely of atoms at a temperature of 4240°K, and the lower stream was entirely molecular at T = 1950°K.

Finite difference solutions were obtained for variable and constant properties. For the constant property solution, a reference temperature was obtained by the method suggested by Eckert [39].

$$h_r = \frac{1}{2}(h_\infty + h_B) + 0.0833\ U_\infty^2$$

Assuming equilibrium, the law of mass action (A-3) and the caloric equation of state (A-8) can be iterated to obtain T_r = 2970°K and α_r = 0.42. (In the frozen flow solution the temperature along the dividing streamline was found to be 2900°K, but α = 0.38.)

Following the assumption of Kovitz and Hoglund that the Lewis number is unity, the Prandtl and Scmidt numbers were taken to be 0.655. The value of C was computed to be 1.544.

The three solutions for the degree of dissociation for frozen flow are shown in Figure C-3. The finite difference solution for constant properties converges to the profile presented by Kovitz and Hoglund. The effect of variable properties is immediately evident. The degree of dissociation along the dividing streamline for the flow with variable properties approached the value of 0.43 as compared to the constant value of 0.50 of Kovitz and Hoglund, and 0.49 of the constant property finite difference solution.

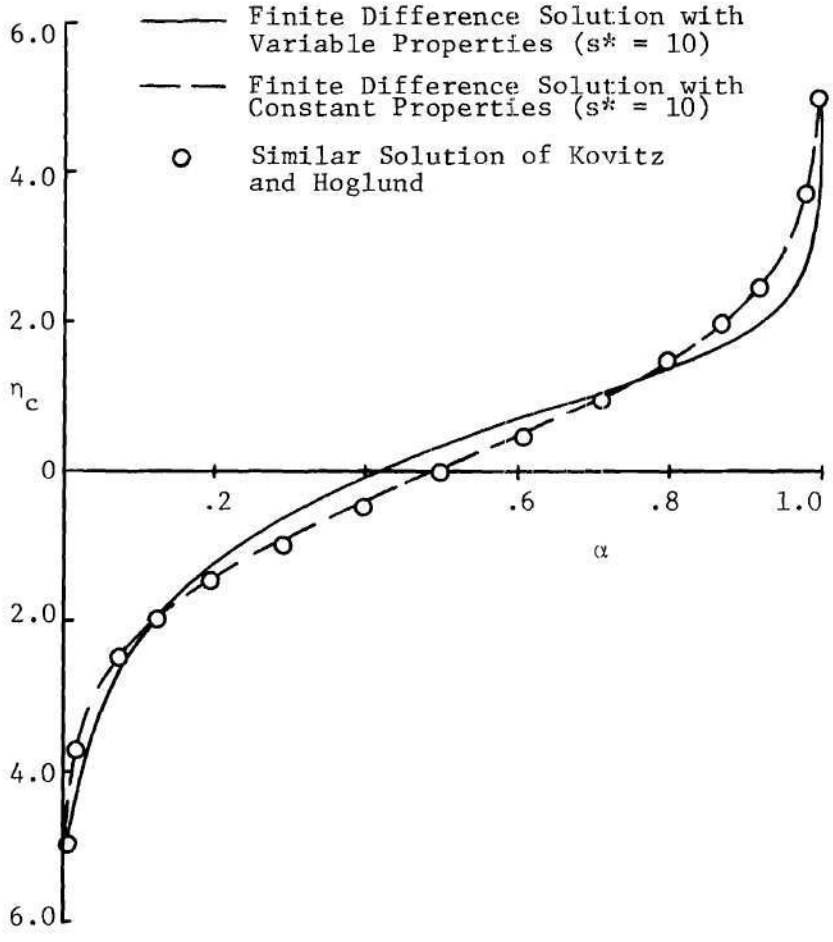

Figure C-3. Comparison of the Degree of Dissociation Profiles for the Frozen Constant Velocity Mixing of Two Streams

LITERATURE CITED

1. Nash, J. F., "A Review of Research on Two Dimensional Base Flow," National Physical Lab., Aero Rept. 1006, A.R.C. 23, 649, F.M. 3171 (1962).

2. Lykoudis, P. S., "A Review of Hypersonic Wake Studies," *AIAA Journal, 4,* pp. 577-590 (1966).

3. Chapman, D. R., "An Analysis of Base Pressure at Supersonic Velocities and Comparison with Experiment," NACA TN-2137 (1951).

4. Crocco, L. and Lees, L., "A Mixing Theory for the Interaction between Dissipative Flows and Nearly Isentropic Streams,"*Journal of the Aerospace Sciences,* 19, 649-676 (1952).

5. Chapman, D. R., Kuehn, D. M., and Larson, H. K., "Investigation of Separated Flows in Supersonic and Subsonic Streams with Emphasis on the Effect of Transition," NACA Report 1356 (1958).

6. Korst, H. H., Page, R. H., and Childs, M. E., "A Theory for Base Pressures in Transonic and Supersonic Flow," Univ. of Illinois, Mech. Engineering Dept., METN-392-2 (1955).

7. Weiss, R. F., and Nelson, W., "Upstream Influence of the Base Pressure," *AIAA JOURNAL, 6,* pp. 466-471 (1968).

8. Hama, F. H., "Experimental Investigations of Wedge Base Pressure and the Lip Shock," TR 32-1033, JPL, California Institute of Technology (1966).

9. Weiss, R. F., and Weinbaum, S., "Hypersonic Boundary-Layer Separation and the Base Flow Problem," *AIAA Journal, 4,* pp. 1321-1330 (1966).

10. Viviand, H., and Berger, S. A., "The Base Flow and Near Wake Problem at Very Low Reynolds Numbers. Part 1. The Stokes Approximation," and "The Base Flow and Near Wake Problem at Very Low Reynolds Numbers. Part 2. The Oseen Approximation," *Journal of Fluid Mechanics, 23,* pp. 417-439 and 439-459 (1965).

11. Weiss, R. F., "The Near Wake of a Wedge," Avco Everett Research Lab., RR-197 (1964).

12. Charwat, A. F., and Yakura, J. K., "An Investigation of Two-Dimensional Supersonic Base Pressures," *Journal of the Aerospace Sciences*, 25, pp. 122-128 (1958).

13. Chapman, D. R., "Laminar Mixing of a Compressible Fluid," NACA R-958 (1950).

14. Denison, M. R., and Baum, E., "Compressible Free Shear Layer with Finite Initial Thickness," *AIAA Journal*, *1*, pp. 342-349 (1963).

15. Sills, J. A., "The Effect of Boundary-Layer Separations on Laminar Heat Transfer," Ph.D. Thesis, Georgia Inst. of Tech. (1967).

16. Lew, H. G., "Nonsimilar Mixing of Chemically Reacting Streams," G. E. Co. Missiles and Space Div. R 66 SD5 (1966).

17. Nash, J. F., "An Analysis of Two-Dimensional Turbulent Base Flow Including the Effect of the Approaching Boundary Layer," National Physical Laboratory Aero Report 1036 (1962).

18. Vincenti, W. G., and Kruger, C. H., *Introduction to Physical Gas Dynamics*, John Wiley and Sons, Inc., New York (1965).

19. Wood, W. W., and Kirkwood, J. G., "Hydrodynamics of a Reacting and Relaxing Fluid," *Journal of Applied Physics*, *28*, pp. 395-398 (1957).

20. Chu, B. T., "Wave Propagation and the Method of Characteristics in Reacting Gas Mixtures with Applications to Hypersonic Flow," Wright Air Development Center TN-57-213 (1957).

21. Appleton, J. P., "Structure of a Prandtl-Meyer Expansion in an Ideal Dissociating Gas," *Physics of Fluids*, *6*, pp. 1057-1062 (1963).

22. Glass, I. I., and Takano, A., "Nonequilibrium Expansion Flow of Dissociated Oxygen Around a Corner," Univ. of Toronto Institute of Aerophysics Rept. No. 91 (1963).

23. Feldman, S., "On the Existence of Recombination Shocks," *Physics of Fluids*, *1*, p. 546, 1958.

24. Clarke, J. F., "The Linearized Flow of a Dissociating Gas," *Journal of Fluid Mechanics*, *7*, pp. 577-595 (1960).

25. Erdelyi, A., Magnus, W., Oberhettinger, F., and Tricomi, F. G., *Tables of Integral Transforms*, Vol. 1. McGraw-Hill Book Co., Inc., New York (1954).

26. Dorrance, W. H., *Viscous Hypersonic Flow*, McGraw-Hill Book Co., Inc., New York (1962).

27. Wu, J. C., "On the Finite Difference Solution of Laminar Boundary Layer Problems," *Proceedings of the Heat Transfer and Fluid Mechanics Institute*, pp. 55-69 (1961).

28. Flügge-Lotz, I., and Blottner, F. G., "Computation of the Compressible Laminar Boundary-Layer Flow Including Displacement-Thickness Interaction Using Finite-Difference Methods," Division of Engineering Mechanics, Stanford Univ. TR 131 (1962).

29. Crank, J., and Nicolson, P., "A Practical Method for Evaluation of Solutions of Partial Differential Equations of the Heat Conduction Type," *Proceedings of the Cambridge Philosophical Society, 43*, pp. 50-67 (1947).

30. Hildebrand, F. B., *Methods of Applied Mathematics*, Prentice-Hall, Inc., Englewood Cliffs, N. J. (1963).

31. Fay, J. A., and Kaye, H., "A Finite Difference Solution of Similar Nonequilibrium Boundary Layers," *AIAA Journal, 5*, pp. 1949-1955 (1967).

32. Ralston, A., and Wilf, H. S., *Mathematical Methods for Digital Computers*, John Wiley and Sons, Inc., New York (1960).

33. Chapman, D. R., "A Theoretical Analysis of Heat Transfer in Regions of Separated Flow," NACA TN-3792 (1956).

34. Kovitz, A. A., and Hoglund, R. F., "Laminar Parallel Stream Mixing with Dissociation and Recombination," *Physics of Fluids, 3*, pp. 436-443 (1960).

35. Batt, Richard G., and Kubota, Toshi, "Experimental Investigation of Laminar Near Wakes Behind 20° Wedges at $M_\infty = 6$," *AIAA Journal, 6*, pp. 2077-2083 (1968).

36. Resler, E. L., "Chemistry in Hypersonics," Institute of Aerospace Sciences Paper No. 63-62 (1963).

37. Lighthill, M. J., "Dynamics of a Dissociating Gas. Part I. Equilibrium Flow," *Journal of Fluid Mechanics, 2*, pp. 1-32 (1957).

38. Freeman, N. C., "Non-equilibrium Flow of an Ideal Dissociating Gas," *Journal of Fluid Mechanics, 4*, pp. 407-425 (1958).

39. Brokaw, Richard S., "Alignment Charts for Transport Properties, Viscosity, Thermal Conductivity, and Diffusion Coefficients for Nonpolar Gases and Gas Mixtures at Low Densities," NASA TR R-81, (1961).

VITA

Robert Kirkland Sigman was born on June 15, 1941, in Coral Gables, Florida. He attended the public schools of that city and was graduated from Coral Gables Senior High School in 1959.

In September, 1959, Mr. Sigman entered the Georgia Institute of Technology and received the degree of Bachelor of Aerospace Engineering in June, 1964. He continued his education at the Georgia Institute of Technology and received NSF and NASA Graduate Traineeships to study under the doctoral program. He received the degree of Master of Science in Aerospace Engineering in June, 1968.

He is a member of Sigma Gamma Tau and Sigma Xi Honor Societies and was a member of the Varsity Swimming Team.

He has been employed part time as a graduate research assistant by the Georgia Institute of Technology.